MIKE 21C

Curvilinear Model

Scientific Documentation

DHI A/S headquarters
Agern Allé 5
DK-2970 Hørsholm
Denmark

+45 4516 9200 Telephone
+45 4516 9333 Support
+45 4516 9292 Telefax

mike@dhigroup.com
www.mikepoweredbydhi.com

PLEASE NOTE

CONTENTS

MIKE 21C
Curvilinear Model
Scientific Documentation

1 Curvilinear Grid Generator

The purpose of this note is to give the user some insight to the mathematical and numerical background applied for the Curvilinear Grid Generator. Basically, it should be thought of as the mathematical/numerical developers guide. It is not the intention to provide detailed mathematical theory. This can easily be obtained from the vast amount of literature on the subject, e.g. Thompson et al. (1985).

The scientific background for the Curvilinear Grid Generator has been divided into two sections covering the mathematical theory and the numerical aspects.

The description of the mathematics is straightforward, and only a very short presentation is needed. The main section covers the numerical aspects, where the solution method is described in detail covering the Stone method for the elliptic equations and the Newton-Raphson method for the boundary conditions. In combination, these form a powerful solution scheme. General attention is given to all the aspects in the grid generation process. These include the discretisation, solution, initial conditions, smoothing methods, and residual evaluation.

1.1 Mathematical Formulation

The grid generator for MIKE 21C is constructed by the following system of partial differential equations

$$\frac{\partial}{\partial \xi}\left(g \frac{\partial x}{\partial \xi} \right) + \frac{\partial}{\partial \eta}\left(g \frac{\partial x}{\partial \eta} \right) = 0 \tag{1.1}$$

$$\frac{\partial}{\partial \xi}\left(g \frac{\partial y}{\partial \xi} \right) + \frac{\partial}{\partial \eta}\left(g \frac{\partial y}{\partial \eta} \right) = 0 \tag{1.2}$$

where x and y are the Cartesian coordinates, and g is a weight factor defined by

$$g = \sqrt{\frac{x_\xi^2 + y_\xi^2}{x_\eta^2 + y_\eta^2}} \tag{1.3}$$

The boundary condition for this system is the non-linear orthogonality condition

$$x_\xi x_\eta + y_\xi y_\eta = 0 \tag{1.4}$$

$$f(x, y) = 0 \tag{1.5}$$

where Eq. (1.4) expressed the condition of orthogonality, and Eq. (1.5) expresses that x and y are located on a specific curve. With this system, the distribution of boundary points cannot in general be known in advance. The system produces an orthogonal grid, and is equivalent to simple potential theory where the ξ and η lines can be though of a streamlines and potential lines. The boundary condition is equivalent to the kinematic boundary condition, i.e. where the streamlines are parallel to a boundary.

A special case occurs when the grid weight (g) is unity. In that case the system is conformal, meaning that

$$\Delta s = \Delta n \tag{1.6}$$

for all cells. In order to add more flexibility to the - otherwise quite restricted (see below) - conformal system, the weight function g has been added to the system.

A river is in fact very good for illustrating the constraint of the conformal mapping. Take a reach of a river, say 50 km, and let the river width be 1 km. Now, one would typically use in the order of magnitude 50 grid points across the river width. If conformal mapping is applied, the amount of grid points in the direction of the river would be 2500. The total amount of grid points in the computational grid would thus be 125.000, and this is an extremely fine grid that would probably not be feasible to use save on very powerful computers. The constraint on the conformal mapping may be expressed mathematically as

$$\frac{N}{M} = \frac{L_x}{L_y} \tag{1.7}$$

where *N* and *M* are the number of grid points in each direction, and L_x and L_y the extend of the geometry.

The advantage of conformal mapping is that the Laplacian operator is invariant to the change of coordinate system. This attribute may be attractive for some purposes, but the price to pay for this is that the grid dimensions are necessarily tied to the overall aspect ratio of the geometry. Furthermore, for complex geometries, it is virtually impossible to find a conformal mapping.

The weight function serves two purposes. First of all the global appearance of the geometry will dictate a weight function, as illustrated by the river example. Secondly the local appearance of the solution found on the grid (water depth, velocity, etc.) may result in a wish for changing the local grid weight to concentrate grid lines.

The first part of the grid weight is purely linked to the geometry, and is therefore normally handled entirely by the program.

1.2 Numerical Aspects

This section serves to present the solution method used in Curvilinear Grid Generator. The order of appearance has been chosen such that it follows the grid generation process. Stone's strongly implicit method is employed for solving the partial differential Eqs. (1.1) and (1.2) with a special Newton-Raphson procedure for the boundary conditions. The elliptic solution method is described thoroughly by Stone (1968).

1.2.1 Discrete equations

The discretisation of the grid equations is straight forward, resulting in

$$x_p = a_N x_N + a_E x_E + a_S x_S + a_W x_W \tag{1.8}$$

$$y_p = a_N y_N + a_E y_E + a_S y_S + a_W y_W \tag{1.9}$$

Note that the source term is identically zero for both equations. The coefficients in these equations are given by

$$a_N = \frac{1}{g_{j,k+½}} \tag{1.10}$$

$$a_E = g_{j+½,k} \tag{1.11}$$

$$a_S = \frac{1}{g_{j,k-½}} \tag{1.12}$$

$$a_W = g_{j-½,k} \tag{1.13}$$

the diagonal coefficient is implicit understood to be unity (achieved by normalisation after the calculation of the coefficients), i.e.

$$\sum a_{nb} = 1 \tag{1.14}$$

At the boundary points, the boundary conditions are treated as Dirichlet conditions that change during the solution process. Thus, at the boundary points the equation can be written

$$x_{j,k} = x_b \tag{1.15}$$

$$y_{j,k} = y_b \tag{1.16}$$

meaning that the transport coefficients (a_N-a_W) are all identically zero, while the source is $S = x_b$. In the Fortran code, there is no need for doing it like that. Instead, the boundary points are not relaxed in the iteration step covering the elliptic equations (the loop go from 1 to N-1), and thus the source term can be taken as being always identically zero.

1.2.2 Initial conditions

The initial conditions for the elliptic system serve two purposes. Obviously, the elliptic system requires initial conditions for the iterative solution. It is, however, not crucial to choose good initial conditions for the Stone's strongly implicit procedure used for the iterative solution of the equations (directly related to the principle of fast short wave error decay in elliptic solution methods).

A much more important purpose of the initial condition is to obtain the grid weights.

NOTE: In simple geometries the grid weight may actually be set to a constant value in the entire domain, but it is generally not possible for complex geometries. It becomes even more pronounced in multiblock structures.

The strategy in Gridgen is to use an algebraic mapping system for the initial conditions, and from this calculate the grid weights, which are then finally run through an adaptive filter (see

Section 1.2.5). The use of algebraic mapping to generate the initial conditions is a general practise in elliptic grid generation.

The algebraic grid generator used for the generation of the initial conditions is the frequently used transfinite interpolation method

$$x_{j,k} = (1-\phi)x_{0,k} + \phi x_{N,k} + (1-\psi)x_{j,0} + \psi x_{j,M} - (1-\phi)(1-\psi)x_{0,0} - (1-\phi)\psi x_{0,M} - \phi(1-\psi)x_{N,0} - \phi\psi x_{N,M} \quad (1.17)$$

The advantage of the algebraic mapping method is that it is extremely fast compared to the elliptic methods. However, the grids are normally not as smooth as those obtained by using the elliptic grid generators. This is part of the reason why the grid weights are smoothed prior to the solution of the elliptic system.

1.2.3 Calculation of the grid weight function

For the present single block version of the grid generator, the grid weights have been located at the cell corners, where the coordinates *x* and *y* are also found.

With the grid weight function located at the cell corner, the grid weight function is calculated by using central differences in the interior and one-sided differences at the boundaries, i.e.

$$\frac{\partial x}{\partial \xi} = \begin{cases} 0.5(x_E - x_W), & 1 \le j \le N-1 \\ x_E - x_P, & j = 0 \\ x_P - x_E, & j = N \end{cases} \quad (1.18)$$

The transport coefficients for the discrete grid equations are thus given by

$$a_N = \frac{2}{g_P + g_N} \quad (1.19)$$

$$a_E = \frac{2}{g_P + g_E} \quad (1.20)$$

After calculating the transport coefficients, normalisation is performed.

1.2.4 Solution of the grid equations

The partial differential equations governing the grid are fully elliptic, and generally anisotropic. These two features automatically call for a strong elliptic equation solution method, especially on fine grids. The grids that are used for MIKE 21C calculations will typically have more than 10000 cells, so the grids are very fine.

The solution method used for the grid generator is Stone's strongly implicit procedure (abbr. SSIP, see Stone, 1968). In all aspects this method is a very good choice for the grid generator. First of all it is extremely fast compared to the point/line implicit methods, and secondly the incomplete factorisation used in the method need be performed only once.

The rest of the grid generation process consists of performing forward/back sweeps and updating boundary conditions. The amount of computational work per iteration is thus in the same order of magnitude as would be the case for a line implicit method, but the rate of convergence is considerably higher.

1.2.5 Adaptive filters

Adaptive filters are important parts of the Curvilinear Grid Generator. The filters are applied for the boundary lines, and for the grid weight function.

For the boundaries, the adaptive filter uses the relative curvature of the boundary line, i.e.

$$\frac{1}{R} = \frac{(x_E - x_W)(y_E - 2y_p + y_W) - (y_E - y_W)(x_E - 2x_p + x_W)}{\left((x_E - x_W)^2 + (y_E - y_W)^2\right)^{3/2}} \tag{1.21}$$

to evaluate the smoothness. If a certain criterion is not fulfilled, the boundary point is subjected to the running average

$$x_p \leftarrow \frac{x_E + x_P + x_W}{3} \tag{1.22}$$

$$y_p \leftarrow \frac{y_E + y_P + y_W}{3} \tag{1.23}$$

The procedure is repeated until all boundary points have a relative curvature below the limit. During the process of smoothing the boundary lines, the corner points are fixed.

For the smoothing of the grid weight function the adaptive filter uses the relative curvature given by

$$c = \frac{\sum g_{nb}}{4g_P} - 1 \tag{1.24}$$

Please note that g is always positive, since g = 0 cannot occur for well-defined grids. If this is larger than a critical value, $|c| > c_{max}$, then the weight in the grid point is recalculated from an average

$$g_P = \frac{g_P + \sum g_{nb}}{5} \tag{1.25}$$

Again, the process is repeated until the criterion is met for every grid point in the domain. During the process the boundary values for the filter are equivalent to the specification of Neuman conditions. Thus, if the maximum allowed curvature is zero, the grid weight will end up becoming a constant in the entire domain (corresponding to the solution of a homogenous von Neumann problem for the Laplacian).

NOTE: It is important to have a smooth weight function. Rapid changes in the weight function are the same as rapid changes in the grid. Such are not desirable, because the

solution found on the grid will be off poorer quality. This is a point of fundamental importance in computational hydrodynamics.

1.2.6 Numerical treatment of the boundary conditions

The Curvilinear Grid Generator uses splines for representing the boundary lines. Before the splines are adapted to the boundary lines, these are smoothed with a curvature adaptive filter (see previous section). The boundary lines can thus be expresses as

$$\mathbf{r} = (x, y) = (f(t), g(t)) \tag{1.26}$$

where t is running along the boundary line (parameter description), and $0 < t < N$, where N is the number of points on the boundary. The tangential vector for the boundary line is thus proportional to the time derivative of **r**, i.e.

$$\mathbf{s} = \frac{d\mathbf{r}}{dt} \tag{1.27}$$

The vector normal to the boundary line is given by

$$\mathbf{n} = \begin{pmatrix} x_0 - f(t) \\ y_0 - g(t) \end{pmatrix} \tag{1.28}$$

where (x_0,y_0) is the first point in the interior seen from the boundary.

The orthogonality condition can now be written as one single equation by demanding that the dot product of the normal vector and the tangent vector is identically zero

$$F(t) = (x_0 - f(t))f'(t) + (y_0 - g(t))g'(t) = 0 \tag{1.29}$$

which gives the t-value for the grid point on the boundary. The equation is non-linear and is solved by using a special version of the Newton-Raphson solution algorithm. The Newton-Raphson algorithm results in

$$F'(t) = (x_0 - f(t))f''(t) + (y_0 - g(t))g''(t) - f'(t)^2 - g'(t)^2 \tag{1.30}$$

$$\Delta t = -\frac{F(t)}{F'(t)} \tag{1.31}$$

$$t_{n+1} = t_n + \Delta t \tag{1.32}$$

The special part of the algorithm is that the iteration is stopped if one of the following occurs

$$|\Delta t| > 1 \tag{1.33}$$

$$t < 0 \tag{1.34}$$

$$t > N \tag{1.35}$$

These situations may occur because the convergence radius of the Newton-Raphson may sometimes be very small. If the Newton-Raphson is stopped, the time-position is set to the position of the boundary nearest point, but the x and y values are not updated. This gives a better chance of getting a converged Newton-Raphson in the next iteration.

The advantage of using Neton-Raphson is obvious for MIKE 21C applications with moving boundaries. As the changes in the grid are small, the iteration will be very efficient. The special treatment ensures that the method is much more robust than would normally be the case for the Newton-Raphson.

1.2.7 Residual evaluation and normalisation

There are two conditions to satisfy for the grid generation system. These are the fulfilment of the elliptic equations, and the satisfaction of the boundary conditions. It is therefore not straightforward to evaluate whether the grid generator has converged.

Instead of using the residuals for the equation involved, the change in the grid between two global iterations is evaluated. The residual field is now introduced as

$$r = \frac{1}{L}\begin{pmatrix} x_P^{new} - x_p^{old} \\ y_P^{new} - y_P^{old} \end{pmatrix} \tag{1.36}$$

where *L* is the linear cell length scale of the geometry, i.e.

$$L = \frac{\sqrt{Area}}{\#cells} \tag{1.37}$$

The residual field can thus be though of as the change in the point position compared to the typical length of the cell vertex.

The stop criterion is defined by the following two conditions

$$|\mathbf{r}|_{\max} < 10\varepsilon \tag{1.38}$$

$$|\mathbf{r}|_{mean} < \varepsilon \tag{1.39}$$

If e.g. $\varepsilon = 10^{-3}$ then the grid generator should stop when both the maximum relative change in the position is less than 1% of the cell linear length scale, and the mean relative change is less than 0.1% of the cell linear length scale.

1.2.8 Relaxation and time-stepping

Considering the nature of the grid generation system, it can be deduced that there is no need for time-stepping or under-relaxation in the elliptic equations as these are linear. For the boundary conditions, the situation is that they are non- linear. This is why the Newton-Raphson method is applied for the boundary conditions. However, the overall treatment of the system is to handle the elliptic equations and the boundary conditions in two individual steps, and therefore it is necessary to slightly under relax the boundary conditions, i.e.

$$x_b \leftarrow (1-\omega)x_b + \omega f(t) \tag{1.40}$$

$$y_b \leftarrow (1-\omega)y_b + \omega g(t) \tag{1.41}$$

2 2D Hydrodynamic Model

The hydrodynamics of meanders and braided channels are characterised by a complex three-dimensional flow pattern. This has to be taken into account when studying channel morphology. However, to apply a fully three-dimensional model for long-term simulations (several months) of river morphology requires unfeasible computational efforts. By introducing simplifications to the Navier-Stokes equations (Section 2.1), the governing hydrodynamic equations can be reduced to two-dimensional equations of conservation of momentum and mass in the two horizontal directions. Three-dimensional (secondary flow) effects are maintained in the depth-averaged model by introducing a separate model of the helical flow component (Section 2.2) and by assuming similarity of the vertical distribution of the flow velocities (Section 2.3).

2.1 Governing Flow Equations

The two horizontal axes (denoted s- and n-axis) are described in a curvilinear orthogonal coordinate system, where one axis can follow the bank lines of the river. This gives a better (more accurate) description of the flow field near the boundaries, which is especially important when computing bank erosion.

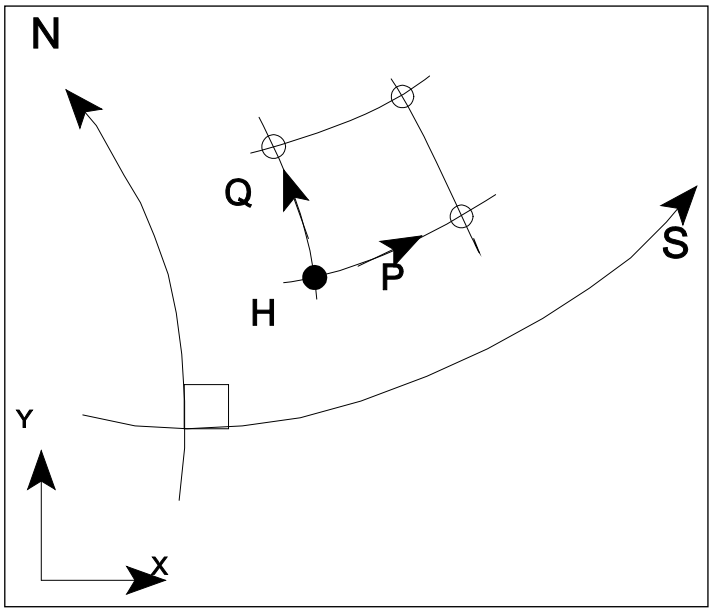

Figure 2.1 Location of flow parameters: fluxes P and Q, and flow depth H in a curvilinear coordinate system (s, n)

Use of an orthogonal coordinate system, where the s- and n-axes are at right angles to each other in every point, makes the mathematical and numerical description substantially simpler. Truncation errors of the finite difference scheme (see below) are smaller and accuracy is higher than in an orthogonal grid. A Cartesian, rectangular coordinate system (x, y) can be applied in the modelling system if required by the user.

Transformations between Cartesian and curvilinear coordinate systems are shown below. Scalar functions such as depth h (denoted H in the curvilinear coordinate system) and

vector functions such as the velocity components (u, v) (denoted U, V in the curvilinear coordinate system) are transformed different between the two coordinate systems. R_s and R_n denote radius of curvature of the s-lines and the n-lines, respectively, at the considered grid point.

$$h = H \text{ and } \frac{\partial h}{\partial x} = \frac{\partial H}{\partial s} \text{ and } \frac{\partial h}{\partial y} = \frac{\partial H}{\partial n} \tag{2.1}$$

$$u = U \text{ and } v = V \tag{2.2}$$

$$\frac{\partial u}{\partial x} = \frac{\partial U}{\partial s} - \frac{V}{R_s} \text{ and } \frac{\partial u}{\partial y} = \frac{\partial U}{\partial n} - \frac{V}{R_n} \tag{2.3}$$

$$\frac{\partial v}{\partial x} = \frac{\partial V}{\partial s} + \frac{U}{R_s} \text{ and } \frac{\partial v}{\partial y} = \frac{\partial V}{\partial n} + \frac{U}{R_n} \tag{2.4}$$

The hydrodynamic model solves the vertically integrated equations of continuity and conservation of momentum (the Saint Venant equations) in two directions. Three main approximations are adopted:

- **Shallow water approximation**
  Lateral exchange of momentum due to friction in the fluid is neglected. The error introduced is a function of the ratio $(h/R)^2$, where h is the water depth and R the radius of curvature of the streamlines. Wall effects along the riverbanks are neglected.

- **Hydrostatic pressure distribution**
  The gradients of the vertical velocity component are neglected. Close to the side walls, the error is of the order of $|h/R|$. In regions with flow over gently varying bed topography the error is much smaller.

- **Rigid lid approximation**
  The rigid lid approximation for the water surface condition implies that the water surface is considered as being a rigid impermeable and shear stress free plate only with normal stresses. The error introduced by the rigid lid approximation will be small when the deviation between the local water surface level and the 'average' water surface level is small. This is the case when the Froude number and the ratio between water depth and radius of curvature (h/R) are small.

To summarise, the flow model is valid for shallow, gently varying topography and mildly curved and wide river channels with small Froude numbers. The following effects are included in the equations when used for river applications:

- Flow acceleration
- Convection and cross-momentum
- Pressure gradients (water surface slopes)
- Bed shear stress
- Momentum dispersion
- Coriolis forces

- Wind forces*
- Flow curvature and helical flow

The equations solved in the curvilinear hydrodynamic model are:

$$\frac{\partial p}{\partial t}+\frac{\partial}{\partial s}\left(\frac{p^2}{h}\right)+\frac{\partial}{\partial n}\left(\frac{pq}{h}\right)-2\frac{pq}{hR_n}+\frac{p^2-q^2}{hR_s}+ gh\frac{\partial H}{\partial s}+\frac{g}{C^2}\frac{p\sqrt{p^2+q^2}}{h^2}=\mathrm{RHS} \quad (2.5)$$

$$\frac{\partial q}{\partial t}+\frac{\partial}{\partial s}\left(\frac{pq}{h}\right)+\frac{\partial}{\partial n}\left(\frac{q^2}{h}\right)+2\frac{pq}{hR_s}-\frac{q^2-p^2}{hR_n}+ gh\frac{\partial H}{\partial n}+\frac{g}{C^2}\frac{q\sqrt{p^2+q^2}}{h^2}=\mathrm{RHS} \quad (2.6)$$

$$\frac{\partial H}{\partial t}+\frac{\partial p}{\partial s}+\frac{\partial q}{\partial n}-\frac{q}{R_s}+\frac{p}{R_n}=0 \quad (2.7)$$

Where

s, *n*	Coordinates in the curvilinear coordinate system
p, *q*	Mass fluxes in the s- and n-direction, respectively
H	Water level
h	Water depth
g	Acceleration of gravity
C	Chezy roughness coefficient
R_s, R_n	Radius of curvature of s- and n-line, respectively
RHS	The right hand side in the force balance, which contains (among others) Reynolds stresses (see below), Coriolis force and atmospheric pressure. See the MIKE 21 Hydrodynamic Module for a more thorough description.

The Reynolds stresses, included in the RHS terms, can be described in a curvilinear grid assuming a smooth grid (R_s and R_n large and slowly varying). For the *p*-direction:

$$\frac{\partial}{\partial x}\left(E\frac{\partial P}{\partial x}\right)+\frac{\partial}{\partial y}\left(E\frac{\partial P}{\partial y}\right)=\frac{\partial}{\partial s}\left(E\frac{\partial p}{\partial s}\right)+\frac{\partial}{\partial n}\left(E\frac{\partial p}{\partial n}\right) -\frac{2E}{R_s}\frac{\partial q}{\partial s}-\frac{\partial E}{\partial s}\frac{q}{R_s}-\frac{2E}{R_n}\frac{\partial q}{\partial n}-\frac{\partial E}{\partial n}\frac{q}{R_n} \quad (2.8)$$

(*P*, *Q*) are fluxes described in a Cartesian (*x*, *y*) system and (*p*, *q*) are fluxes described in curvilinear (*s*, *n*) coordinate system. A similar equation is found for the *q*-direction:

* The wind force is only included in the present version of the modelling system when a rectangular Cartesian computational grid is used. In river applications, where curvilinear computational grids are required, the wind forces are usually not the governing driving forces.

$$\frac{\partial}{\partial x}\left(E\frac{\partial Q}{\partial x}\right)+\frac{\partial}{\partial y}\left(E\frac{\partial Q}{\partial y}\right)=\frac{\partial}{\partial s}\left(E\frac{\partial q}{\partial s}\right)+\frac{\partial}{\partial n}\left(E\frac{\partial q}{\partial n}\right)+\frac{2E}{R_s}\frac{\partial p}{\partial s}+\frac{\partial E}{\partial s}\frac{p}{R_s}+\frac{2E}{R_n}\frac{\partial p}{\partial n}+\frac{\partial E}{\partial n}\frac{p}{R_n} \quad (2.9)$$

The curvature of the coordinate lines gives rise to additional terms in the partial differential equation for flow. The equations are solved by an implicit finite difference technique with variables (water flux density *P* and *Q* in two horizontal directions and water depth *H*) defined on a space staggered computational grid, as shown in Figure 2.2.

The flow variables $P_{j,k}$, $Q_{j,k}$ and $H_{j,k}$ are defined in all grid points and are referred to by the grid coordinates (*j*, *k*). The space steps $\Delta s_{j,k}$ and $\Delta n_{j,k}$ vary in the whole domain due to the curvilinear grid. In comparison, the standard MIKE 21 HD model uses a fixed Δx and Δy. Furthermore, each grid point is characterised by a set of physical coordinates ($x_{j,k}$, $y_{j,k}$) as well as the radius of curvature $R_{s(j,k)}$ of *s*-lines (or *j*-lines) and the radius of curvature $R_{n(j,k)}$ of *n*-lines (or *k*-lines). The time step t_{HD} in the numerical solution of hydrodynamics is constant.

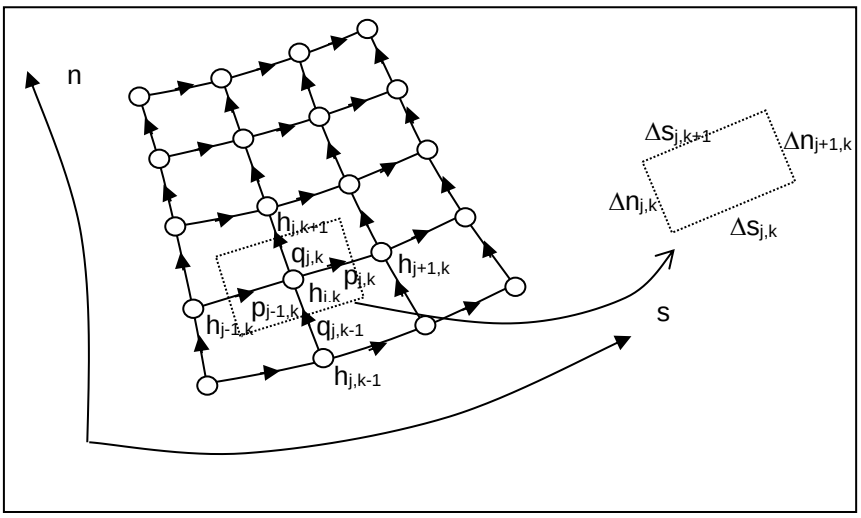

Figure 2.2 Finite Difference Grid in (s, n) space. P and Q are water fluxes in two horizontal directions. H is water depth

Except for the varying space steps Δs and Δn (Δx and Δy in standard MIKE 21) and the additional terms in the equations of motion due to the curving grid lines, the numerical solution of the governing equations is similar to the standard MIKE 21 Hydrodynamic model. Therefore, the reader is referred to the Scientific Background, Appendix A, of the MIKE 21 Hydrodynamics, Users Guide and Reference Manual.

2.2 Helical Flow

Mathematical modelling of flow in a river bend requires insight into the physics of the water motion. For this purpose a physical explanation of the flow distribution in a bend is given below.

When water flows into a river bend, an imbalance of centripetal force starts to generate an outward motion near the free surface and an inward motion near the bed. The reason is that the main stream velocities in the upper part of the flow are greater than velocities in

the lower part of the flow. Therefore, water particles in the upper part of the water column must follow a path with a larger radius of curvature than water particles in the lower part to maintain nearly constant centripetal force over the depth. With velocity v and radius of curvature R, centripetal acceleration is v^2/R.

Simultaneously with generation of helical motion, a lateral free surface slope is created to maintain equilibrium between lateral pressure force, centripetal force and lateral shear force generated from friction along the bed. The classical analytical solution to this flow problem predicts a single helical vortex, which transports fluid downstream in spiral trajectories. This spiral (or helical) flow pattern can be considered as the sum of a longitudinal flow component (main flow) and a circulation in a plane perpendicular to the main flow direction (secondary flow). The secondary flow is directed towards the centre of curvature near the bottom and outwards in the upper part of the cross-section as illustrated in Figure 2.3.

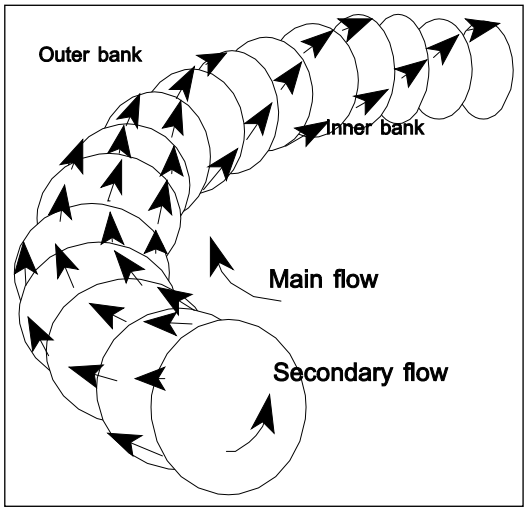

Figure 2.3 Helical flow in river bends

For changing bend curvature and bed topography, the flow distribution will lag slightly behind the change in topography due to the inertia of the main flow. Analytical expressions for helical flow intensity and the length scale for adaptation of secondary flow to changes in topography are discussed below.

The intensity of the helical flow is the magnitude of the transverse velocity component. It is defined by de Vriend (1981) as:

$$i_s = u \cdot \frac{h}{R_s} \tag{2.10}$$

Where

u	Main flow velocity
R_s	Radius of curvature of streamlines
i_s	Helical flow intensity

In Section 2.3 the vertical distribution of the helical flow is described. Secondary flow due to curving streamlines causes a small deviation δs in flow direction near the bed, away from the main stream direction. This also causes deviation in the bed shear stress direction.

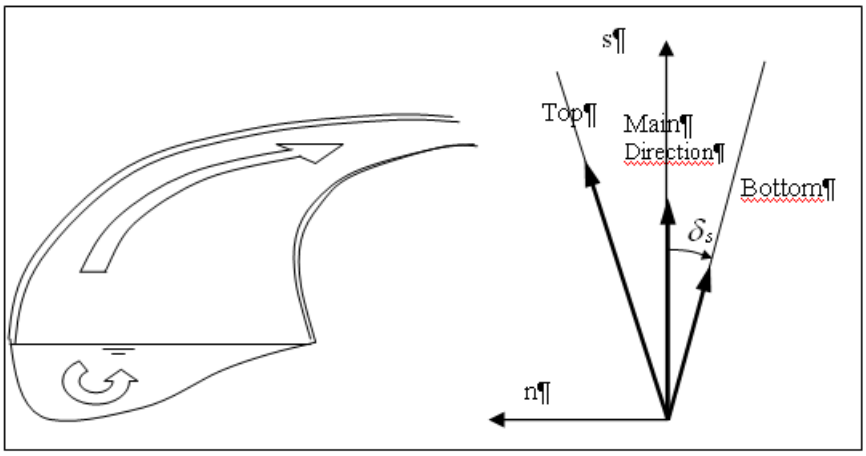

Figure 2.4 Deviation of bed shear stress due to helical flow

The direction of bed shear stress in a curved flow field plays an important role in a bed topography model for river bends. The logarithmic model obtained by Rozovskii (1957) and others yields a bed shear stress direction given by:

$$\tan \delta_s = - \beta \cdot \frac{h}{R_s} \tag{2.11}$$

Where

h	Water depth
R_s	Radius of curvature of flow stream lines
δ_s	Angle between bed shear stress and depth averaged shear stress (or flow)

The parameter β is defined as:

$$\beta = \alpha \cdot \frac{2}{\kappa^2}\left(1 - \frac{\sqrt{g}}{\kappa C}\right) \tag{2.12}$$

Where

κ	Von Kárman's constant, 0.4
g	Acceleration of gravity, 9.81
C	Chezy number
α	Calibration constant

The approximate value of β is 10. Other models of vertical velocity profile, such as the power model, give slightly different values of β. Increasing flow resistance, represented by a decreasing Chezy number, gives a smaller β-value (i.e. less helical flow intensity and a smaller deviation in the direction of bed shear stress), as discussed by Olesen (1987). In the morphological model, α is specified as a calibration parameter (constant or varying in space). The default value is 1.

In regions of changing curvature of streamlines, the secondary flow will adapt gradually. The inertia of the secondary flow has been investigated analytically by (among others) Rozovski (1957) and Nouh & Townsend (1979). De Vriend (1981a), Booij & Kalkwijk (1982) and Kalkwijk & Booij (1986) have carried out numerical investigations of this topic. Further investigations are discussed in Olesen (1987).

Modelling the adaptation of secondary flow is complicated by the fact that (according to numerical experiments) adaptation of the secondary flow profile is considerably faster near the bed (where bed shear stresses act) than compared to higher up in the water column. Strictly speaking, the process of adaptation cannot be characterised by one length scale only. Adaptation length is a function of water depth and friction number. In the present morphological model, the following differential length scale is applied:

$$\lambda_{sf} = \frac{1.2\,h\,C}{\sqrt{g}} \tag{2.13}$$

Where

λ_{sf}	Length scale for secondary flow adaptation
h	Water depth
C	Chezy number
g	Acceleration of gravity

Consequently, the direction of bed shear stress for continuously varying curvature in steady flow conditions can be calculated by:

$$\lambda_{sf}\frac{\partial(\tan\delta_s)}{\partial s_s} + \tan\delta_s = -\beta\cdot\frac{h}{R_s} \tag{2.14}$$

Where

s_s	Stream-wise coordinate along the streamline,
R_s	Radius of curvature of the streamlines
h	Water depth
λ_{sf}	Length scale for secondary flow adaptation

The equation is transformed into a fixed (s, n) coordinate system through the following equations:

$$\frac{\partial s}{\partial s_s}\frac{\partial\tan\delta_s}{\partial s} + \frac{\partial n}{\partial s_s}\frac{\partial\tan\delta_s}{\partial n} + \frac{\tan\delta_s + \beta\dfrac{h}{R_s}}{\lambda_{sf}} = 0 \tag{2.15}$$

Using $\frac{\partial s}{\partial s_s} = \frac{p}{\sqrt{p^2+q^2}}$ and $\frac{\partial n}{\partial s_s} = \frac{q}{\sqrt{p^2+q^2}}$ where p and q are the fluxes in the two horizontal directions as shown in Figure 2.2 we get:

$$\frac{p}{\sqrt{p^2+q^2}}\frac{\partial\tan\delta_s}{\partial s} + \frac{q}{\sqrt{p^2+q^2}}\frac{\partial\tan\delta_s}{\partial n} + \frac{\tan\delta_s + \beta\dfrac{h}{R_s}}{\lambda_{sf}} = 0 \tag{2.16}$$

Which finally leads to:

$$u\frac{\partial\tan\delta_s}{\partial s} + v\frac{\partial\tan\delta_s}{\partial n} + \frac{\sqrt{p^2+q^2}}{h\cdot\lambda_{sf}}\left(\tan\delta_s + \beta\frac{h}{R_s}\right) = 0 \tag{2.17}$$

The equation is solved numerically with the MIKE21 AD (advection-dispersion) model with $\partial(\tan\delta_s)/\partial t = 0$, no dispersion and a source term.

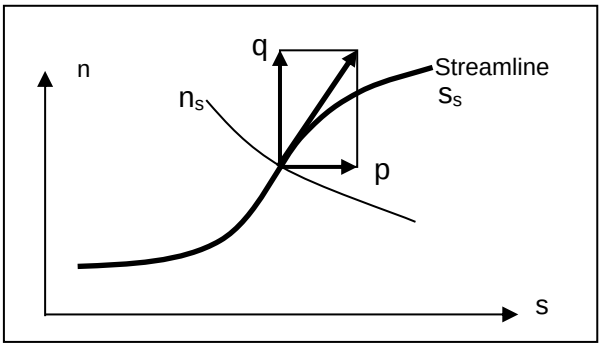

Figure 2.5 Transformation from streamwise coordinates (s_s, n_s) to fixed curvilinear coordinates (s, n)

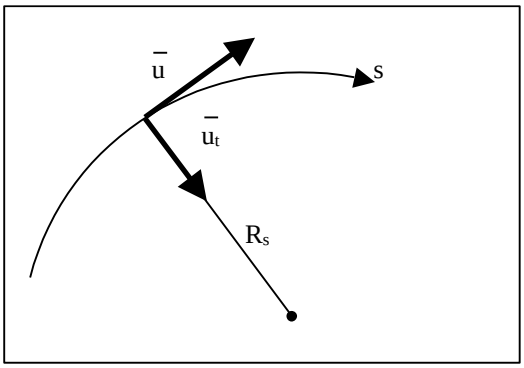

Figure 2.6 Stream line curvature based on velocity vector

The curvature of streamlines is calculated as a cross product between velocity and acceleration vector, as illustrated in Figure 2.6:

$$\frac{1}{R_s} = \frac{|\bar{u} \, x \, \bar{u}_t|}{|\bar{u}|^3} \tag{2.18}$$

In a Cartesian (*x*, *y*) coordinate system, the acceleration vector is:

$$\bar{u}_T = \left(\frac{du}{dt}, \frac{dv}{dt}\right) \tag{2.19}$$

$$\frac{du}{dt} = \frac{\partial u}{\partial x}\frac{\partial x}{\partial t} + \frac{\partial u}{\partial y}\frac{\partial y}{\partial t} + \frac{\partial u}{\partial t} \tag{2.20}$$

Assuming $\frac{\partial u}{\partial t} = 0$, $\frac{\partial x}{\partial t} = u$ and $\frac{\partial u}{\partial t} = v$, respectively, we have:

$$\frac{du}{dt} = u\frac{\partial u}{\partial x} + v\frac{\partial u}{\partial y} \tag{2.21}$$

In a (*s*, *n*) curvilinear coordinate system, the time derivatives become:

$$\frac{du}{dt} = u\left(\frac{\partial u}{\partial s} - \frac{v}{R_s}\right) + v\left(\frac{\partial u}{\partial n} - \frac{v}{R_n}\right) \tag{2.22}$$

$$\frac{dv}{dt} = u\left(\frac{\partial v}{\partial s} + \frac{u}{R_s}\right) + v\left(\frac{\partial v}{\partial n} + \frac{u}{R_n}\right) \tag{2.23}$$

R_s, and R_n are the radius of curvature of the *s*-axis and the *n*-axis, respectively.

Note that the computed deviation in bed shear stress due to helical flow, $\tan\delta_s$, is based on the assumption of quasi-steady hydrodynamic conditions. In rapidly varying flow conditions, the expression does not apply.

Once the deviation in bed shear stress is determined, the corresponding helical flow intensity can be estimated from:

$$i_s = \frac{u \cdot h}{R_s} = \frac{-u}{\beta}\tan\delta_s \tag{2.24}$$

The helical flow intensity is of importance for the analysis and parameterisation of the secondary flow velocity profiles.

2.3 Vertical Velocity Profiles

The hydrodynamic model is based on depth-averaged flow equations. However, information about the vertical velocity profiles is required for determining the bed shear stress and for the suspended sediment transport calculations in the morphological model.

Introducing the Reynolds stress concept and the Prandtl mixing length hypothesis, and assuming that viscous (laminar) friction is much smaller than turbulent friction, the shear stresses in the fluid can be expressed by:

$$\tau_s = \rho E \frac{\partial u}{\partial z} \tag{2.25}$$

Where

ρ	Density of water
u	Velocity in main flow direction
z	Vertical coordinate
E	Turbulent (eddy) viscosity coefficient
τ_s	Shear stress in main flow direction

A similar relation for τ_n applies for the transverse direction. Introducing this into the Navier-Stokes equations (see Olesen, 1987) and assuming steady conditions, the following flow equations for the flow in the longitudinal, *s*, and the transverse direction, *n*, emerge:

$$u\frac{\partial u}{\partial s} + v\frac{\partial u}{\partial n} + w\frac{\partial u}{\partial z} + \frac{uv}{R} + \frac{1}{\rho}\frac{\partial P}{\partial s} = \frac{\partial}{\partial z}\left(E\frac{\partial u}{\partial z}\right) \tag{2.26}$$

$$u\frac{\partial v}{\partial s} + v\frac{\partial v}{\partial n} + w\frac{\partial v}{\partial z} - \frac{u^2}{R} + \frac{1}{\rho}\frac{\partial P}{\partial n} = \frac{\partial}{\partial z}\left(E\frac{\partial v}{\partial z}\right) \tag{2.27}$$

Where

ρ	Density of water
u	Velocity in longitudinal flow direction
v	Velocity in transverse flow direction
w	Velocity in vertical direction
P	Pressure
s	Coordinate in stream wise direction
n	Coordinate in transverse direction
z	Vertical coordinate
R	Radius of curvature of the main streamline
E	Turbulent (eddy) viscosity coefficient

By assuming a hydrostatic pressure distribution P over the vertical, water pressure is simply a function of the water depth.
The vertical distribution of flow velocity can be obtained by asymptotic expansion. First, the zero order approximation of the longitudinal velocity is obtained from Eq. (2.26), assuming v and w and the gradient of the main velocity (du/ds) to be zero (i.e. fully developed flow). Next, the transverse velocity is computed from Eq. (2.27) with the zero-order longitudinal velocity inserted and disregarding $v + dv/dn$ and $w + dv/dz$.

A first order approximation of the longitudinal velocity could be obtained by introducing the first order secondary flow velocity v into Eq. (2.26). De Vriend (1981a) and De Vriend & Struiksma (1983) describe this. The references show that the form of the first order solution differs slightly from the zero order solution.

The boundary conditions for Eq. (2.26) are zero shear stress at the free water surface and no slip at the bottom (z_0, the roughness height).

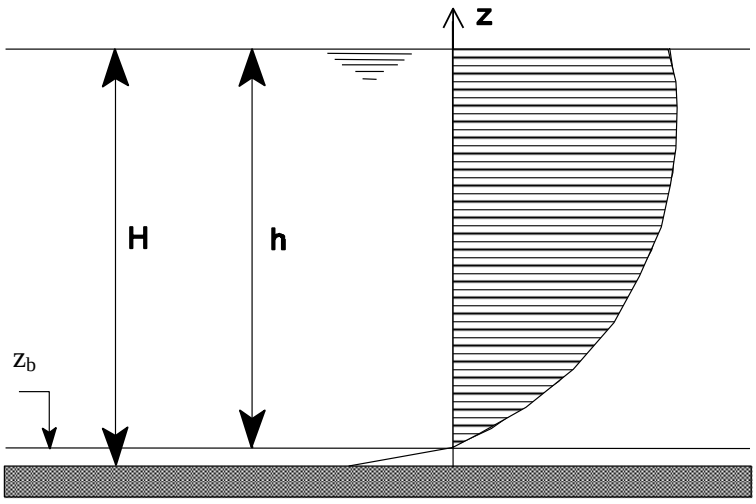

Figure 2.7 Vertical velocity profile, stream wise direction

The reference level z_b shown in Figure 2.7 defines the limit between suspended load and bed load transport. Thus, h is the height at which suspended sediment transport occurs, and H is the total water depth. In the following two non-dimensional vertical coordinates ζ and η are introduced. The ζ-system has its origin at z_b and is defined as $\zeta = z/h$, while the η-system has its origin at the bed and is defined as $\eta = z/H$.

The height of the reference is chosen as $z_b = 0.02H$ in order to fit with the theory of Galapatti (1983), who couples suspended sediment transport to the vertical velocity and concentration profiles.

The velocity profile can be related to the depth-averaged velocity by applying a unit profile function $p_1(\zeta)$, as shown below.

$$u(z) = \bar{u}\, p_1(\eta) \quad , \eta = \frac{z}{H} \tag{2.28}$$

Solution of Eq. (2.26) requires information about the vertical eddy viscosity or the mixing length (using Prandtl's definitions). Applying a logarithmic velocity profile (fully developed rough flow), the unit profile becomes:

$$p_1(\eta) = \frac{u_f}{\kappa \bar{u}} \ln\left(\frac{\eta}{\eta_0}\right) = \frac{\sqrt{g}}{\kappa C} \ln\left(\frac{\eta}{\eta_0}\right) \tag{2.29}$$

The value of η_0 is obtained from the closure criterion:

$$\int_{\eta_0}^{1} p_1(\eta) d\eta = 1 \quad \Rightarrow \quad \eta_0 = Exp\left[\eta_0 - 1 - \frac{\kappa C}{\sqrt{g}}\right] \tag{2.30}$$

The equation is solved by iteration.

As seen from Eq. (2.29) and Eq. (2.30), the velocity profile only depends on vertical coordinate η and resistance number, which is convenient for numerical purposes. Therefore, the mainstream velocity profile for fully developed turbulent flow can be parameterised by the universal function:

$$p_1 = f\left(\eta, \frac{u_f}{\bar{u}}\right) = f\left(\eta, \frac{\sqrt{g}}{C}\right) \tag{2.31}$$

Where u_f is the friction velocity and C the Chezy number.

The profile specified by Eq. (2.29) is evaluated at a number of discrete points located along a logarithmic axis, so that the most intense resolution is obtained near the bottom where the largest velocity gradients occur. In the ζ coordinate system, discrete vertical points are obtained from the relation:

$$\zeta_{j+1} = \zeta_j + \left[\frac{1}{\left(\frac{1-1.05^n}{1-1.05}\right) - 1}\right] 1.05^j \tag{2.32}$$

Where

ζ	Non-dimensional coordinate $\zeta = z/h$
n	Number of numerical points. Default is 200
j	Index for vertical level with $\zeta_1 = 0$ and $\zeta_n = 1$

The coordinates of the ζ-system are transformed to the η-system using:

$$\eta = \zeta + 0.02(1-\zeta) \tag{2.33}$$

It follows that Eq. (2.29) can be used to calculate the velocity profile.

The profile of the secondary flow is illustrated in Figure 2.8 and Figure 2.9:

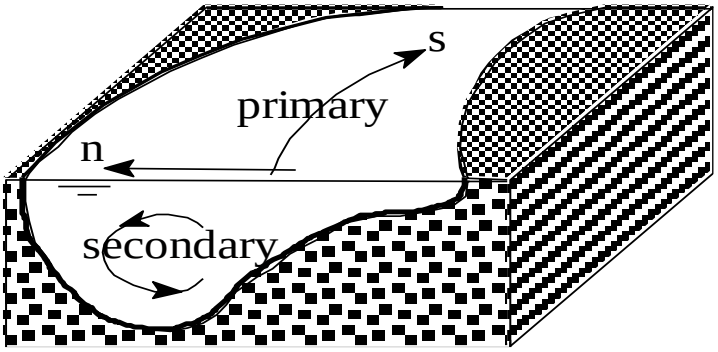

Figure 2.8 Sketch of the river channel

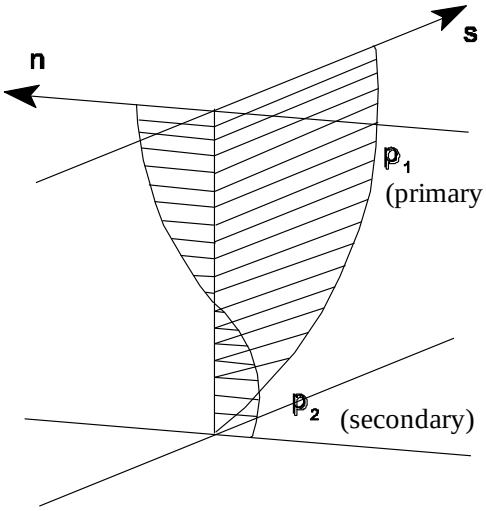

Figure 2.9 Main and secondary velocity profiles

The truncated first order version of the momentum equation in the transverse direction express the equilibrium between pressure forces, friction forces and centripetal forces:

$$\frac{1}{\rho}\frac{\partial P}{\partial n} - \frac{1}{\rho}\frac{\partial \tau_n}{\partial z} - \frac{\bar{u}^2}{R_s} = 0 \tag{2.34}$$

Where the transverse shear stress is given by:

$$\tau_n = \rho E \cdot \frac{\partial v(z)}{\partial z} \tag{2.35}$$

And the symbols represent:

$z = H \cdot \eta$	Vertical coordinate
$P = \rho \cdot g \cdot S$	Hydrostatic water pressure
S	Surface elevation
$\bar{u}$	Depth-averaged velocity
v	Transverse (secondary) velocity
R_s	Radius of curvature of stream line
n	Transverse (horizontal) coordinate

The vertical eddy viscosity coefficient is assumed to be parabolic:

$$E = \kappa H u_f \eta(1-\eta) = \kappa H u_f \varepsilon \tag{2.36}$$

Where

ε	Non-dimensional eddy viscosity
P	Von Kárman's constant (=0.4)

Equilibrium is achieved when the sum of pressure, friction and centripetal force equals zero.

Likewise the primary flow profile, a normalised profile p_2 for the secondary velocity profile *v,* is applied:

$$v = \frac{\bar{u} H}{R_s} p_2(\eta) = i_s \cdot p_2(\eta) \tag{2.37}$$

Where

$\bar{u}$	Depth-averaged velocity
R_s	Radius of curvature of stream line
H	Water depth
i_s	Helical flow intensity

By insertion of Eqs. (2.35) - (2.37) into Eq. (2.34) the following expression is produced:

$$\left(\frac{R_s g}{\kappa u_f \bar{u}}\right)\frac{\partial S}{\partial n} - \frac{\partial}{\partial \zeta}\left(\varepsilon \frac{\partial p_2}{\partial \zeta}\right) = \frac{1}{\kappa}\frac{\bar{u}}{u_f} p_1^2 \tag{2.38}$$

Averaged over the depth, the secondary flow is by definition zero. Near the bottom at $\eta = \eta_0$ the velocity vanishes. Thus, the following two conditions must be fulfilled:

$$\int_{\eta_0}^{1} p_2 d\eta = 0 \tag{2.39}$$

$$p_2(\eta_0) = 0 \tag{2.40}$$

The first term in Eq. (2.38) is constant over the depth. This means that the term can be substituted by a constant denoted A:

$$A = \left(\frac{R_s g}{\kappa u_f \bar{u}} \right) \frac{\partial S}{\partial n} \tag{2.41}$$

Integration of Eq. (2.38) from an arbitrary level in the water column η to the water surface $\eta = 1$ and substituting Eq. (2.41) into Eq. (2.38) results in the following expression:

$$-\varepsilon \frac{\partial p_2(\eta)}{\partial \eta} = -\frac{1}{\kappa} \frac{\bar{u}}{u_f} \int_{\eta}^{1} p_1^2 d\eta + A(1-\eta) \tag{2.42}$$

Where the shear stress term used on the left side is equal to zero at the free surface, which is due to the fact that no shear forces is assumed to act on the free surface.

Eq. (2.42) can be rewritten as:

$$\frac{\partial p_2(\eta)}{\partial \eta} = \frac{1}{\varepsilon} \int_{\eta}^{1} \frac{\bar{u}}{\kappa u_f} p_1^2 d\eta - \frac{A \cdot (1-\eta)}{\varepsilon} \tag{2.43}$$

The secondary velocity profile described by $p_2(\eta)$ can now be obtained by integration of Eq. (2.43) from the level with no slip velocity ($\eta = \eta_0$) at which $p_2(\eta_0) = 0$. This yields:

$$p_2(\eta) = \int_{\eta_0}^{\eta} \left(\frac{1}{\varepsilon} \int_{\eta}^{1} \frac{\bar{u}}{\kappa u_f} p_1^2 d\eta \right) d\eta - A \int_{\eta_0}^{\eta} \frac{1-\eta}{\varepsilon} d\eta \tag{2.44}$$

The function $p_2(\eta)$ is conveniently split up into two functions:

$$p_2 = p_{21}(\eta) - A \cdot p_{22}(\eta) \tag{2.45}$$

Where the function $p_{21}(\eta)$ is given by:

$$p_{21}(\eta) = \int_{\eta_0}^{\eta} \left[\frac{1}{\varepsilon} \int_{\eta}^{1} \left(\frac{\bar{u}}{\kappa u_f} p_1^2 \right) d\eta \right] d\eta \tag{2.46}$$

And the function $p_{22}(\eta)$ is given by:

$$p_{22}(\eta) = \int_{\eta_0}^{\eta} \frac{1-\eta}{\varepsilon} d\eta = \int_{\eta_0}^{\eta} \frac{1-\eta}{\eta(1-\eta)} d\eta = \int_{\eta_0}^{\eta} \frac{1}{\eta} d\eta = \ln\left(\frac{\eta}{\eta_0} \right) \tag{2.47}$$

The integration constant A representing the transverse surface slope is determined by the identity from Eq. (2.41) and results in the following expression:

$$A = \frac{\int_{\eta_0}^{1} p_{21}(\eta) d\eta}{\int_{\eta_0}^{1} p_{22}(\eta) d\eta} \tag{2.48}$$

The function $p_{21}(\eta)$ is singular for $\eta = 1$, which requires special numerical treatment. Furthermore, $p_{21}(\eta)$ consists of integrals with no analytical solution and therefore only can be solved by numerical integration. However, the inner integral in Eq. (2.46) can be solved analytically. This yields:

$$\int_{\eta}^{1} p_1^2(\eta)d\eta = \frac{g}{\kappa^2 C^2}\int_{\eta}^{1} \ln^2\left(\frac{\eta}{\eta_0}\right)d\eta = \frac{g}{\kappa^2 C^2}\cdot\left[(1-\eta)\left(2+2\ln\eta_0+\ln^2\eta_0\right)+\eta\left(2\ln\eta+2\ln\eta_0\ln\eta-\ln^2\eta\right)\right] \tag{2.49}$$

Inserting the right hand side of Eq. (2.49) into Eq. (2.46) yields:

$$p_{21}(\eta) = \frac{\sqrt{g}}{\kappa^3 C}\int_{\eta_0}^{\eta}\frac{2+2\ln\eta_0+\ln^2\eta_0}{\eta}d\eta + \frac{\sqrt{g}}{\kappa^3 C}\left[2(1+\ln\eta_0)\int_{\eta_0}^{\eta}\frac{\ln\eta}{1-\eta}d\eta - \int_{\eta_0}^{\eta}\frac{\ln^2\eta}{1-\eta}d\eta\right] \tag{2.50}$$

The first integral in Eq. (2.50) has the analytical solution:

$$\int_{\eta_0}^{\eta}\frac{2+2\ln\eta_0+\ln^2\eta_0}{\eta}d\eta = \left(2+2\ln\eta_0+\ln^2\eta_0\right)\ln\left(\frac{\eta}{\eta_0}\right) \tag{2.51}$$

The two remaining integrals in Eq. (2.50) do not have any analytical solutions and are evaluated by numerical integration. For $\eta = 1$ some problems can occur due to the singularity. However, by use of the rule of L´Hospital, it can be found that:

$$\frac{\ln^2\eta}{1-\eta}\to 0 \text{ for } \eta\to 1 \text{ and } \frac{\ln\eta}{1-\eta}\to -1 \text{ for } \eta\to 1 \tag{2.52}$$

Due to the fact that only the part of the water column from $\eta_{min} = 0.02$ and up to the free surface is resolved the contribution from the flow below this level is evaluated as:

$$\int_{\eta_0}^{\eta_{\min}}\frac{\ln^2\eta}{1-\eta}d\eta = \frac{2}{2-\eta_{\min}-\eta_0}\int_{\eta_0}^{\eta_{\min}}\ln^2\eta d\eta = \frac{2\eta_{\min}\left(\ln^2\eta_{\min}-\ln\eta_{\min}+1\right)-2\eta_0\left(\ln^2\eta_0-\ln\eta_0+1\right)}{2-\eta_{\min}-\eta_0} \tag{2.53}$$

and

$$\int_{\eta_0}^{\eta_{\min}}\frac{\ln\eta}{1-\eta}d\eta = \frac{2}{2-\eta_{\min}-\eta_0}\int_{\eta_0}^{\eta_{\min}}\ln\eta d\eta = \frac{2\eta_{\min}\left(\ln\eta_{\min}-1\right)-2\eta_0\left(\ln\eta_0-1\right)}{2-\eta_0-\eta_{\min}} \tag{2.54}$$

The shape of the primary and secondary velocity profiles that are used for the evaluation of the suspended sediment transport rates are plotted in Figure 2.10 and Figure 2.11, respectively for four different Chezy numbers.

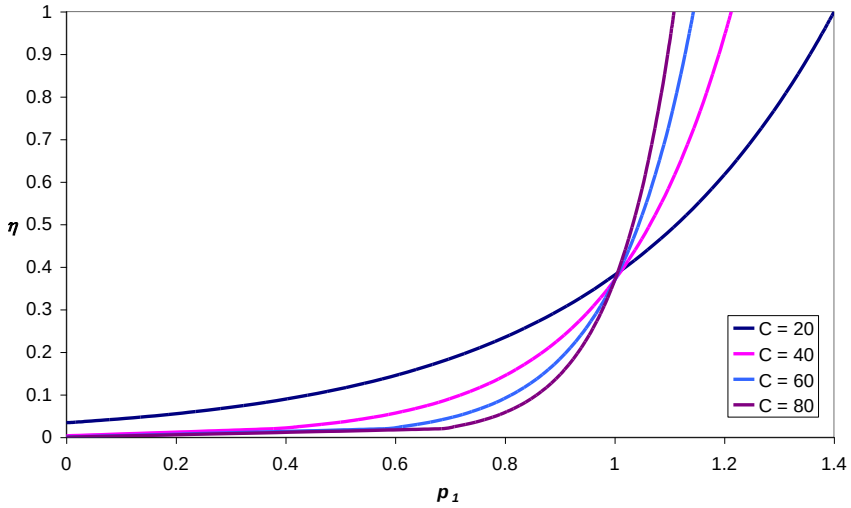

Figure 2.10 Shapes of the primary velocity profile for varying Chezy numbers

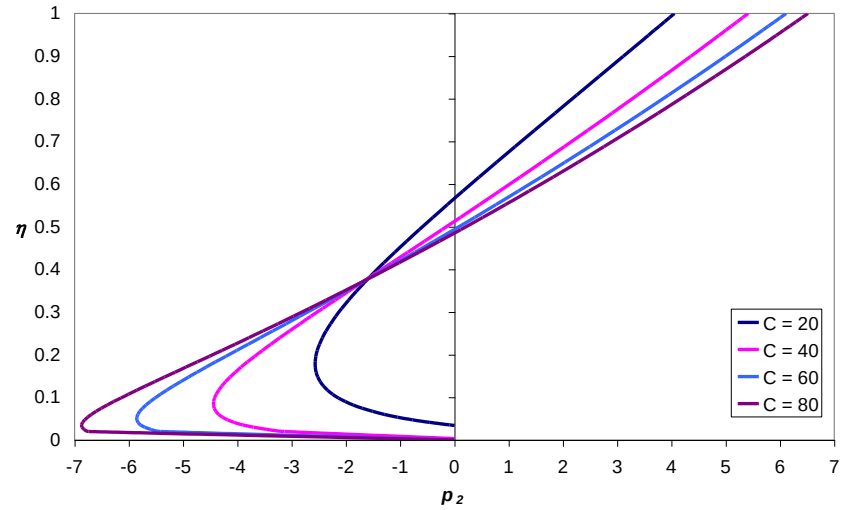

Figure 2.11 Shapes of the secondary velocity profile for varying Chezy numbers

As shown, the absolute value of the profile functions near the bottom increases for increasing Chezy number, i.e. reduced flow resistance.

The shape of the velocity profiles is sketched in Figure 2.12 for two Chezy numbers (from Olesen, 1987) and compared with the profiles obtained using a power assumption on the velocity profile instead. Only slight differences between the flow profiles of the different mixing length models (power profile versus logarithmic velocity profile) can be observed in the figure, although the logarithmic model seems to result in a somewhat larger secondary flow.

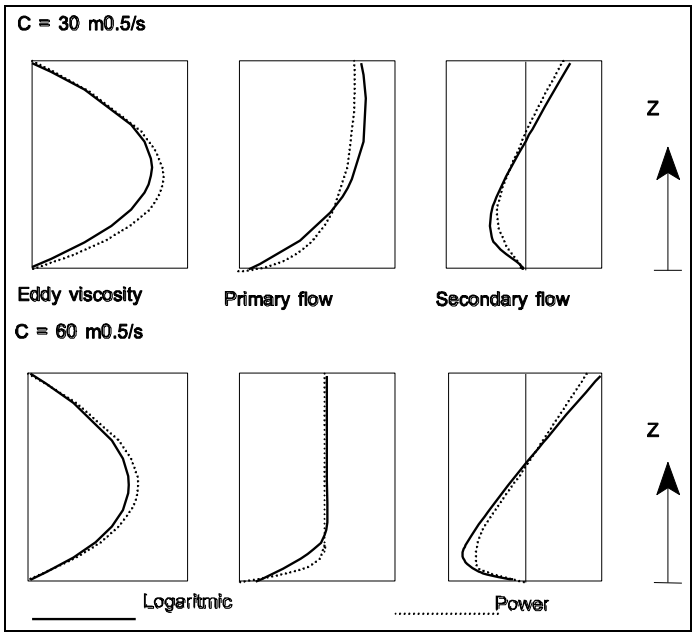

Figure 2.12 Vertical distribution of eddy viscosity and flow velocity (from Olesen, 1987)

The depth integration of the mathematical model is based on an assumption that the horizontal streamlines are approximately parallel through the water column. This means that the secondary velocity component *v* is much smaller than the main flow component *u*. Due to the non-uniform velocity distribution over the depth, some velocity distribution coefficients on the flow convection terms emerge, as discussed by Olesen (1987). Eqs (2.26) and (2.27) are by depth integration transformed into:

$$\frac{1}{\rho}\frac{\partial P}{\partial s} + k_{uu}\left[\bar{u}\frac{\partial \bar{u}}{\partial s} + \bar{v}\frac{\partial \bar{u}}{\partial n} + \frac{\overline{vu}}{R}\right] + \frac{\tau_{bs}}{h} + \frac{k_{sn}}{h}\left[\frac{\partial \bar{u} i_s h}{\partial n} + 2\frac{\bar{u} i_s h}{R}\right] = 0 \tag{2.55}$$

and

$$\frac{1}{\rho}\frac{\partial P}{\partial n} + k_{uu}\left[\bar{u}\frac{\partial \bar{v}}{\partial s} - \frac{\overline{u^2}}{R}\right] + \frac{\tau_{bn}}{h} + \frac{k_{sn}}{h}\cdot\frac{\partial \bar{u} i_s h}{\partial s} = 0 \tag{2.56}$$

In Eq. (2.55) and (2.56) the velocity distribution coefficients are defined as:

$$k_{uu} = \int_{\eta_0}^{1} [p_1(\eta)]^2 \, d\eta \tag{2.57}$$

and

$$k_{sn} = \int_{\eta_0}^{1} p_1(\eta) \cdot p_2(\eta) d\eta \tag{2.58}$$

The coefficient k_{uu} is very close to unity and in most cases can be disregarded (default 1). The k_{sn} coefficient is related to the convection of the main flow momentum by the secondary flow. Kalkwijk et al. (1980) and Olesen (1987) investigated the influence of the

secondary flow convection. The latter also compared velocities from flume tests with numerical experiments using different models of the k_{sn} coefficient. For narrow and smooth channels, the k_{sn} coefficient has some importance, whereas for natural rivers the effect is negligible. Consequently, the convection of momentum by secondary flow is not included in the present model.

3 Sediment Transport

Traditionally, three types of sediment transport are defined: Bed load, suspended load and wash load. Among others, a comprehensive description is given by Engelund & Hansen (1967) and Jansen et al. (1979).

The latter defines bed load transport as the transport of bed material that is rolling and sliding along the bed. Suspended load transport is defined as the transport of sediment, which is suspended in the fluid for some time. According to the mechanism of suspension, suspended sediment may belong to the bed material load and the wash load. Wash load is defined as the transport of material finer than the bed material. It has no relation to the transport capacity of the stream. Usually, a grain diameter of around 0.06 mm divides the region of wash load and bed material load.

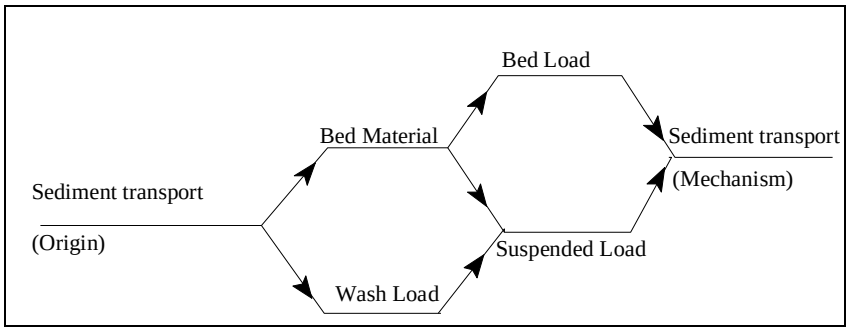

Figure 3.1 Classification of sediment transport. From Jansen et al. (1979)

For morphological development of alluvial rivers with interaction between bed bathymetry and hydrodynamics, only bed material transport is of interest. Thus, only bed load and the part of the suspended load originating from the bed material is considered. The behaviour of suspended load is fundamentally different from that of bed load, which has to be taken into consideration in the sediment transport modelling.

A description of the suspended load transport modelling is provided in Section 3.1. A description of bed load transport modelling is provided in Section 3.2. A number of explicit sediment transport formulas for bed load, suspended load and total load have been developed over the years. The formulas implemented in the present modelling system, at the core of the sediment transport modelling, are described in Section 3.3.

3.1 Suspended Load Transport

The model for suspended sediment transport is based on the theory described by Galappatti (1983). The partial differential equation that governs the transport of suspended sediment by convection and turbulent diffusion is:

$$\frac{\partial c}{\partial t} + u\frac{\partial c}{\partial x} + v\frac{\partial c}{\partial y} + w\frac{\partial c}{\partial z} = w_s\frac{\partial c}{\partial z} + \frac{\partial}{\partial x}\left(\varepsilon\frac{\partial c}{\partial x}\right) + \frac{\partial}{\partial y}\left(\varepsilon\frac{\partial c}{\partial y}\right) + \frac{\partial}{\partial z}\left(\varepsilon\frac{\partial c}{\partial z}\right) \quad (3.1)$$

Where

z	Vertical coordinate
c	Concentration of suspended sediment

ε	Turbulent diffusion coefficient
w_s	Fall velocity of sediment particles in suspension
u, v, w	Flow velocity in x, y and z direction, respectively

If the diffusion terms other than the vertical diffusion term are neglected, then the equation along a streamline is:

$$\frac{\partial c}{\partial t} + u\frac{\partial c}{\partial s} + v\frac{\partial c}{\partial n} + w\frac{\partial c}{\partial z} = w_s\frac{\partial c}{\partial z} + \frac{\partial}{\partial z}\left(\varepsilon\frac{\partial c}{\partial z}\right) \tag{3.2}$$

Where

s	Stream-wise coordinate
n	Transverse coordinate
u	Main flow velocity in stream wise direction
v	Secondary flow velocity in transverse direction

Velocities are represented in the following way as discussed in Section 2.3:

$$u(z) = \bar{u} \cdot p_1(\eta) \tag{3.3}$$

$$v(z) = \frac{\bar{u}H}{R_s} \cdot p_2(\eta) \tag{3.4}$$

Where

$\bar{u}$	Depth-averaged flow velocity
R_s	Radius of curvature of stream line
H	Water depth
p_1	Primary velocity profile (longitudinal)
p_2	Secondary velocity profile (transverse)
η	Non-dimensional vertical coordinate z/H

The surface boundary condition of Eq. (3.2) specifies zero sediment flux across the boundary:

$$w_s \cdot c + \varepsilon\frac{\partial c}{\partial z} = 0 \quad , for \;\; z = z_{surface} \tag{3.5}$$

The boundary condition at the bed is a bottom concentration:

$$c = c_{bed} \quad \text{for} \;\; z = z_A \tag{3.6}$$

Where

z_A	The level just above the river bed, which divides the region of suspended load and bed load.

A special asymptotic approximation technique developed by Galappatti (1983) provides information about the concentration profile. This technique is applicable for conditions where the vertical diffusion coefficient and the fall velocity term are the dominating terms in Eq. (3.1), or that e, defined in Eq. (3.7), is very small:

$$e = \frac{h}{L}\frac{U}{w_s} \tag{3.7}$$

Where

h	The height of the water column at which suspended transport occurs
L	length scale of variations in main flow direction
w_s	fall velocity
U	average flow velocity
e	non-dimensional number

The model developed by Galappatti has been extended in the third dimension. The general solution for slowly varying flow is based on the assumption that the concentration profile is made up of a sum of profiles of increasing orders:

$$c = \sum_{i=0}^{n} c_i \tag{3.8}$$

Where c_0 is the zero-order contribution to c, c_1 is the first order contribution, c_2 the second order contribution, etc.

The concentration of different orders is found by solving Eq. (3.2). First the c_0 concentration is obtained by considering equilibrium between settling of suspended sediment and vertical diffusion:

$$w_s \frac{\partial c_0}{\partial z} + \frac{\partial}{\partial z}\left(\varepsilon \frac{\partial c_0}{\partial z}\right) = 0 \tag{3.9}$$

The zero-order concentration c_0 obtained from the solution of Eq. (3.9) is substituted on the left side of Eq. (3.2):

$$w_s \frac{\partial c_1}{\partial z} + \frac{\partial}{\partial z}\left(\varepsilon \frac{\partial c_1}{\partial z}\right) = \frac{\partial c_0}{\partial t} + u\frac{\partial c_0}{\partial s} + v\frac{\partial c_0}{\partial n} w\frac{\partial c_0}{\partial z} \tag{3.10}$$

This is repeated for the first order concentration c_1, so that the equation for the second order concentration c_2 now becomes:

$$w_s \frac{\partial c_2}{\partial z} + \frac{\partial}{\partial z}\left(\varepsilon \frac{\partial c_2}{\partial z}\right) = \frac{\partial c_1}{\partial t} + u\frac{\partial c_1}{\partial s} + v\frac{\partial c_1}{\partial n} + w\frac{\partial c_1}{\partial z} \tag{3.11}$$

Equations for the higher order concentration profile can be found in the same manner, but usually one stops with the second order contribution.

The following non-dimensional parameters are introduced:
Suspension time scale:

$$\tau = \frac{w_s}{h} \cdot t \tag{3.12}$$

Two horizontal length scales for suspended sediment in the stream-wise and transverse directions, respectively:

$$\xi = \frac{w_s}{uh} \cdot s \tag{3.13}$$

$$\psi = \frac{w_s}{uh} \cdot n \tag{3.14}$$

Vertical length scale:

$$\varsigma = \frac{z}{h} \tag{3.15}$$

A differential operator D is introduced:

$$D = \frac{\partial}{\partial \varsigma} + \frac{\partial}{\partial \varsigma}\left(\varepsilon' \frac{\partial}{\partial \varsigma}\right) \tag{3.16}$$

Where

ε' Non-dimensional turbulent diffusion coefficient $\varepsilon/(w_s h)$

The Eqs. (3.9), (3.10) and (3.11) can now be transformed into a non-dimensional form:

$$D[c_0] = 0 \tag{3.17}$$

$$D[c_i] = \frac{\partial c_{i-1}}{\partial \tau} + p_1(\zeta)\frac{\partial c_{i-1}}{\partial \xi} + p_2(\zeta)\frac{\bar{u}H}{R_s}\frac{\partial c_{i-1}}{\partial \psi} + \frac{w}{w_s}\frac{\partial c_{i-1}}{\partial \zeta} \tag{3.18}$$

Eq. (2.18) is valid for orders of c_i greater than or equal to 1. The last term will be omitted, which implies that the vertical velocity w is much smaller than the fall velocity of the suspended sediment w_s. The boundary condition at the free water surface specified in Eq. (2.5) must be valid for all orders of the concentration, i.e.

$$c_i + \varepsilon' \frac{\partial c_i}{\partial \zeta} = 0 \tag{3.19}$$

Furthermore, it is assumed that higher order concentration profiles do not contribute to the mean (zero order) concentration, i.e.

$$\int_0^1 c_i \, d\zeta = 0 \ , \text{for } i \geq 1 \tag{3.20}$$

As for the velocity profiles, it is convenient to operate with unit concentration profiles for the suspended sediment. Thus, the zero order concentration profile is the product between the depth-averaged concentration and a unit profile function $\Phi_0(\zeta)$:

$$c_0 = \bar{c}(\zeta, \tau) \cdot \Phi_0(\zeta) \tag{3.21}$$

The following discussion considers concentration terms of higher order:

Galappatti (1983) shows that a differential equation of the type $D[F(\zeta)] = G(\zeta)$, with a free surface ($\zeta = 1$) boundary condition $F + \varepsilon' \cdot dF/d\zeta$ and a restriction that F is zero when integrated from $\zeta = 0$ to $\zeta = 1$, has the solution:

$$F(\zeta) = D^{-1}[G(\zeta)] =$$

$$-\int_{\zeta}^{1} G(\zeta)d\zeta + \Phi_0(\zeta) \cdot \int_{\zeta}^{1} \frac{G(\zeta)}{\Phi_0(\zeta)} d\zeta + B \cdot \Phi_0(\zeta) \tag{3.22}$$

Where the constant B is obtained from the requirement:

$$\int_{0}^{1} F(\zeta)d\zeta = 0 \tag{3.23}$$

Higher order concentrations c_i ($i > 0$) can be obtained using this solution technique once the zero order concentration c_0 is known, i.e. from Eq. (3.18):

$$c_1(\zeta) = D^{-1}[\Phi_0(\zeta)] \cdot \frac{\partial \bar{c}}{\partial \tau} + D^{-1}[p_1(\zeta) \cdot \Phi_0(\zeta)] \cdot \frac{\partial \bar{c}}{\partial \xi} \tag{3.24}$$

$$+ D^{-1}[p_2(\zeta) \cdot \frac{\bar{u}H}{R_s} \cdot \Phi_0(\zeta)] \cdot \frac{\partial \bar{c}}{\partial \psi}$$

Thus, if we do not distinguish between H and h, the first order expression for vertical concentration profile based on the asymptotic approximation technique becomes:

$$c(\zeta) = \Phi_o(\zeta) \cdot \bar{c} + \Phi_t(\zeta) \cdot \frac{h}{w_s} \frac{\partial \bar{c}}{\partial t} + \Phi_1(\zeta) \cdot \frac{\bar{u}h}{w_s} \frac{\partial \bar{c}}{\partial s} + \Phi_2(\zeta) \cdot \frac{\bar{u}h^2}{R_s w_s} \frac{\partial \bar{c}}{\partial n} \tag{3.25}$$

Where the higher order concentration profiles Φ_i are solved from Eq. (2.22):

$$\Phi_t(\zeta) = D^{-1}[\Phi_0(\zeta)] \tag{3.26}$$

$$\Phi_1(\zeta) = D^{-1}[p_1(\zeta) \cdot \Phi_0(\zeta)] \tag{3.27}$$

$$\Phi_2(\zeta) = D^{-1}[p_2(\zeta) \cdot \Phi_0(\zeta)] \tag{3.28}$$

The zero order solution to Eqs. (3.9) and (3.17) is based on an exponential profile with modified Rouse parameter (Galappatti 1983, who refers to Delft Hydraulics Laboratory, 1980):

$$\Phi_0(\zeta) = \exp[Z \cdot f(\zeta)] \tag{3.29}$$

Where $f(\zeta)$ can be expressed as a function of ζ or of the non-dimensional vertical coordinate η that was used to obtain the vertical velocity profiles. The function is split into two expressions for the lower and upper part of the fluid:

$$f(\zeta)=(1+\beta_z)\ln\left[\frac{1-\zeta}{\zeta+\beta_z}\right]=(1+\beta_z)\ln\left[\frac{1-\eta}{\eta}\right] \quad \text{for } \zeta<\frac{1-\beta_z}{2} \tag{3.30}$$

$$f(\zeta)=-4\zeta+2\beta+2=-4\eta(1+\beta_z)+2\beta+2 \quad \text{for } \zeta\geq\frac{1-\beta_z}{2} \tag{3.31}$$

The modified Rouse number is defined by:

$$Z=\frac{1}{4\beta_z+4}\cdot\frac{w_s}{u_f}\cdot\frac{1}{0.13+0.20\left(\frac{w_s}{u_f}\right)^{2.12}} \tag{3.32}$$

Where

u_f	Friction velocity
β_z	Non-dimensional concentration reference level over the river bed $(z_b/H)/(1-z_b/H)$

The first term in Eq. (3.25), i.e. the zero order term, describes the equilibrium profile, whereas the first order terms represent the temporal as well as spatial variations in the concentration profile.

The profile functions Φ_0, Φ_1 and Φ_2 are used in the model to transform from depth varying c to the depth averaged. For calculation of the depth-averaged concentration, the bed boundary condition is solved by the following equation system:

$$c(\zeta=0)=c_e(\zeta=0)=\overline{c_e}\,\Phi_o(0) \tag{3.33}$$

Inserting Eq. (3.33) into Eq. (3.25) the following is achieved at the bed boundary:

$$\overline{c_e}\,\Phi_o(0)=\Phi_o(0)\overline{c}+\Phi_t(0)\frac{h}{w_s}\frac{\partial\overline{c}}{\partial t}+\Phi_1(0)\frac{\overline{u}h}{w_s}\frac{\partial\overline{c}}{\partial s}+\Phi_2(0)\frac{\overline{u}\,h^2}{R\,w_s}\frac{\partial\overline{c}}{\partial n} \tag{3.34}$$

Or by introducing the following four coefficients:

$\gamma_0=\Phi_0(0)$, $\gamma_t=\Phi_t(0)$, $\gamma_1=\Phi_1(0)$, $\gamma_2=\Phi_2(0)$

Eq. (3.34) now yields:

$$\gamma_t\frac{\partial\overline{c}}{\partial t}+\gamma_1\overline{u}\frac{\partial\overline{c}}{\partial s}+\gamma_2\overline{u}\frac{h}{R}\frac{\partial\overline{c}}{\partial n}=\gamma_o\frac{w_s}{h}(\overline{c_e}-\overline{c}) \tag{3.35}$$

Until now, the transport equation has referred to a coordinate system (s, n) coinciding with the streamlines. Transformation from stream coordinates to fixed (x, y) coordinates as sketched in Figure 3.2 is determined by:

$$\frac{\partial\overline{c}}{\partial s}=\frac{\partial\overline{c}}{\partial x}\frac{\partial x}{\partial s}+\frac{\partial\overline{c}}{\partial y}\frac{\partial y}{\partial s}=\frac{\partial\overline{c}}{\partial x}\frac{\overline{u}}{\overline{U}}+\frac{\partial\overline{c}}{\partial y}\frac{\overline{v}}{\overline{U}} \tag{3.36}$$

$$\frac{\partial \bar{c}}{\partial n} = \frac{\partial \bar{c}}{\partial x}\frac{\partial x}{\partial n} + \frac{\partial \bar{c}}{\partial y}\frac{\partial y}{\partial n} = -\frac{\partial \bar{c}}{\partial x}\frac{\bar{v}}{\bar{U}} + \frac{\partial \bar{c}}{\partial y}\frac{\bar{u}}{\bar{U}} \tag{3.37}$$

Where $\bar{U}$ is the speed determined by:

$$\bar{U} = \sqrt{\bar{u}^2 + \bar{v}^2} \tag{3.38}$$

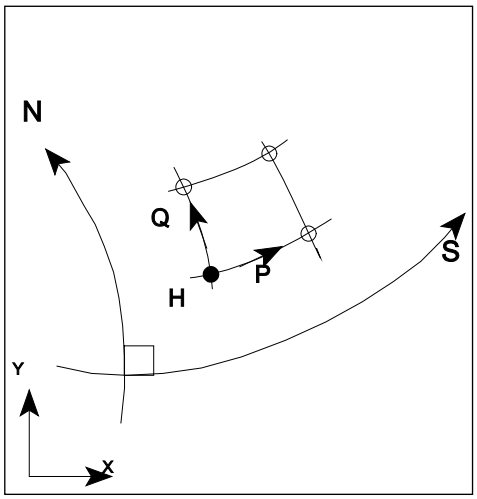

Figure 3.2 Transformation from stream wise (s,n) coordinates to fixed (x,y) coordinate system

Substitution of Eqs. (3.36) and (3.37) Eq. (3.34) yields:

$$\gamma_t \frac{\partial \bar{c}}{\partial t} + \gamma_1 \bar{u}\left(\frac{\partial \bar{c}}{\partial x}\frac{\partial \bar{u}}{\partial \bar{U}} + \frac{\partial \bar{c}}{\partial y}\frac{\bar{v}}{\bar{U}}\right) + \gamma_2 \bar{u}\frac{h}{R}\left(-\frac{\partial \bar{c}}{\partial x}\frac{\bar{v}}{\bar{U}} + \frac{\partial \bar{c}}{\partial y}\frac{\bar{u}}{\bar{U}}\right) = \gamma_o \frac{w_s}{h}\left(\overline{c_e} - \bar{c}\right) \tag{3.39}$$

By further reduction using $\left(\frac{\bar{u}}{\bar{U}} = 1 \text{ and } \frac{\partial \bar{u}}{\partial \bar{U}} = 1\right)$ the final advection-dispersion equation becomes:

$$\frac{\gamma_t}{\gamma_1}\frac{\partial \bar{c}}{\partial t} + \left(\bar{u} - \bar{v}\frac{h}{R}\frac{\gamma_2}{\gamma_1}\right)\frac{\partial \bar{c}}{\partial x} + \left(\bar{v} + \bar{u}\frac{h}{R}\frac{\gamma_2}{\gamma_1}\right)\frac{\partial \bar{c}}{\partial y} + \frac{\gamma_o}{\gamma_1}\frac{w_s}{h}\left(\bar{c} - \overline{c_e}\right) = 0 \tag{3.40}$$

The profile functions change the standard advection-dispersion equation. The time derivative is multiplied by a factor (less than one), which incorporates the time delay due to vertical transport (which corresponds to a distorted time scale according to γ_0).

The convection terms are modified due to secondary flow, which 'disturbs' the concentration profile (represented by γ_2). Numerically, the velocities in the two directions in the advection-dispersion model are modified compared to the hydrodynamic model.

The last term (erosion/deposition) is multiplied by a factor that incorporates differences in the time scale for adaptation to the equilibrium profile. With a high fall velocity (coarse

sediment), the model will respond faster to any changes in the local equilibrium concentration, c_e. This is commonly referred to as the time lag of the sediment model.

The non-uniform vertical profile of concentration implies that the effective fall height of grains will be less than the water depth, due to more suspended grains close to the bed. This is included in the γ_0 term. When the transport is computed by integrating velocity and concentration, the non-uniform profiles in general cause less advection and more dispersion, which is determined by the γ_1 term.

Additional dispersion (which may be necessary during calibration) can be specified using normal dispersion coefficients in the model input specification. Note that the coefficients should not include dispersion due to non-uniform vertical profile, which is included implicitly.

For a uniform distribution of sediment over the vertical (wash load), all γ coefficients are 1 except γ_2 (net convection over the vertical due to helical flow), which is zero. The adaptation to changes in equilibrium concentration would be very slow due to the reduced erosion-deposition term.

As discussed later, a quasi-steady approach can be adopted in the sediment transport model to perform long-term simulations. Therefore, the first coefficient on the temporal term *dc/dt* is not implemented in the present model. It is still possible to simulate either the quasi-steady profile (by iteration of Eq. (2.40) or the actual profile by neglecting the modification of concentration profile due to temporal variations.
The suspended sediment transport in the streamwise direction is found by integrating:

$$S_s = \int_o^h c(z)\cdot u(z)\,dz = h\int_o^1 c(\zeta)\cdot u(\zeta)\,d\zeta = h\,\bar{u}\int_0^1 c(\zeta)\,p_1(\zeta)d\zeta \tag{3.41}$$

Substituting the concentration in Eq. (3.24) into Eq. (3.41) gives:

$$S_s = h\bar{u}\int_0^1 \bar{c}\,\Phi_o(\zeta)\,p_1(\zeta)d\zeta + h\bar{u}\int_0^1 \frac{h}{w_s}\frac{\partial\bar{c}}{\partial t}\phi_t(\zeta)\,p_1(\zeta)d\zeta + \tag{3.42}$$

$$h\bar{u}\int_0^1 \frac{\bar{u}h}{w_s}\frac{\partial\bar{c}}{\partial\zeta}\Phi_1(\zeta)\,p_1(\zeta)d\zeta + h\bar{u}\int_0^1 \frac{\bar{u}h^2}{R_s w_s}\frac{\partial\bar{c}}{\partial n}\phi_2(\zeta)\,p_1(\zeta)d\zeta$$

Eq. (3.42) can be rewritten in a more compact form:

$$S_s = \alpha_{01}\cdot\bar{u}\,h\,\bar{c} + \alpha_{t1}\cdot\frac{\bar{u}\,h^2}{w_s}\frac{\partial\bar{c}}{\partial t} + \alpha_{11}\cdot\frac{\overline{u^2}\,h^2}{w_s}\frac{\partial\bar{c}}{\partial\zeta} + \alpha_{21}\cdot\frac{\overline{u^2}\,h^3}{R_s w_s}\frac{\partial\bar{c}}{\partial\psi} \tag{3.43}$$

Where:

$$\alpha_{01} = \int_o^1 \Phi_0(\zeta)\,p_1(\zeta)\,d\zeta \tag{3.44}$$

$$\alpha_{t1} = \int_o^1 \Phi_t(\zeta)\,p_1(\zeta)\,d\zeta \tag{3.45}$$

$$\alpha_{11} = \int_o^1 \Phi_1(\zeta)\, p_1(\zeta)\, d\zeta \tag{3.46}$$

$$\alpha_{21} = \int_i^1 \Phi_2(\zeta)\, p_1(\zeta)\, d\zeta \tag{3.47}$$

Due to helical flow there is also suspended sediment transport in the transverse direction (across the depth-averaged streamline). This transport can be found by:

$$S_n = \int_o^h c(z) \cdot v(z) dz = h \cdot \int_o^1 c(\zeta) \frac{\bar{u}\, h}{R_s}\, p_2(\zeta)\, d\zeta = \frac{\bar{u}\, h^2}{R_s} \int_o^1 c(\zeta)\, p_2(\zeta)\, d\zeta \tag{3.48}$$

Where *v(z)* represents the helical velocity profile. Substitution of Eq. (3.25)into Eq. (3.48), yields:

$$S_n = \frac{\bar{u}\, h^2}{R_s} \int_o^1 \Phi_t(\zeta) \frac{h}{w_s} \frac{\partial \bar{c}}{\partial t}\, p_2(\zeta) d\zeta +$$

$$\frac{\bar{u}\, h^2}{R_s} \left[\int_o^1 \Phi_o(\zeta)\, \bar{c}\, p_2(\zeta) \cdot d\zeta + \int_0^1 p_2(\zeta)\, \Phi_1(\zeta) \frac{\bar{u}\, h}{w_s} \frac{\partial \bar{c}}{\partial s} d\zeta \right] \tag{3.49}$$

$$+ \frac{\bar{u}\, h^2}{R_s} \int_o^1 \Phi_2(\zeta) \frac{\bar{u}\, h}{R_s\, w_s} \frac{\partial \bar{c}}{\partial n}\, p_2(\zeta) d\zeta$$

Eq. (3.49) can also be written as:

$$S_n = \alpha_{02} \frac{\bar{u}\, h^2}{R} \bar{c} + \alpha_{t2} \frac{\bar{u}\, h^3}{R_s\, w_s} \frac{\partial \bar{c}}{\partial t} + \alpha_{12} \frac{\bar{u}^2\, h^3}{R_s\, w_s} \frac{\partial \bar{c}}{\partial \zeta} + \alpha_{22} \frac{\bar{u}^2\, h^4}{R_s^2\, w_s} \frac{\partial \bar{c}}{\partial \psi} \tag{3.50}$$

Where

$$\alpha_{02} = \int_o^1 \Phi_o(\zeta)\, p_2(\zeta)\, d\zeta \tag{3.51}$$

$$\alpha_{t2} = \int_o^1 \Phi_2(\zeta)\, p_2(\zeta)\, d\zeta \tag{3.52}$$

$$\alpha_{12} = \int_o^1 \Phi_1(\zeta)\, p_2(\zeta)\, d\zeta \tag{3.53}$$

$$\alpha_{22} = \int_o^1 \Phi_2(\zeta)\, p_2(\zeta)\, d\zeta \tag{3.54}$$

Transformation of stream wise S_s and transverse S_n sediment transport rates into a fixed (x, y) coordinate system gives:

$$\frac{\partial \bar{c}}{\partial s} = \frac{\partial \bar{c}}{\partial x} \cdot \frac{\bar{u}}{\bar{U}} + \frac{\partial \bar{c}}{\partial y} \cdot \frac{\bar{v}}{\bar{U}} \tag{3.55}$$

$$\frac{\partial \bar{c}}{\partial n} = -\frac{\partial \bar{c}}{\partial x} \cdot \frac{\bar{v}}{\bar{U}} + \frac{\partial \bar{c}}{\partial y} \cdot \frac{\bar{u}}{\bar{U}} \tag{3.56}$$

$$S_x = S_s \cdot \frac{\bar{u}}{\bar{U}} - S_n \cdot \frac{\bar{v}}{\bar{U}} \tag{3.57}$$

$$S_y = S_s \cdot \frac{\bar{v}}{\bar{U}} + S_n \cdot \frac{\bar{u}}{\bar{U}} \tag{3.58}$$

Which by substitution gives:

$$\begin{aligned} S_x = & \left(\alpha_{01} \bar{U} h \frac{\bar{u}}{\bar{U}} - \alpha_{02} \frac{\bar{U} h^2}{R} \frac{\bar{v}}{\bar{U}} \right) \bar{c} + \left(\alpha_{t1} \frac{\bar{U} h^2}{w_s} \frac{\bar{u}}{\bar{U}} - \alpha_{t2} \frac{\bar{U} h^3}{R w_s} \frac{\bar{v}}{\bar{U}} \right) \frac{\partial \bar{c}}{\partial t} \\ & + \left(\alpha_{11} \frac{\bar{U}^2 h^2}{w_s} \frac{\bar{u}}{\bar{U}} - \alpha_{12} \frac{\bar{U}^2 h^3}{R w_s} \frac{\bar{v}}{\bar{u}} \right) \left(\frac{\partial \bar{c}}{\partial x} \frac{\bar{u}}{\bar{U}} + \frac{\partial \bar{c}}{\partial y} \frac{\bar{v}}{\bar{U}} \right) \\ & + \left(\alpha_{21} \frac{\bar{U}^2 h^3}{w_s} \frac{\bar{u}}{\bar{U}} - \alpha_{22} \frac{\bar{U}^2 h^4}{R^2 w_s} \frac{\bar{v}}{\bar{u}} \right) \left(-\frac{\partial \bar{c}}{\partial x} \frac{\bar{v}}{\bar{U}} + \frac{\partial \bar{c}}{\partial y} \frac{\bar{u}}{\bar{U}} \right) \end{aligned} \tag{3.59}$$

and

$$\begin{aligned} S_y = & \left(\alpha_{01} \bar{u} h \frac{\bar{v}}{\bar{U}} + \alpha_{02} \frac{\bar{U} h^2}{R} \frac{\bar{u}}{\bar{U}} \right) \bar{c} + \left(\alpha_{t1} \frac{\bar{U} h^2}{w_s} \frac{\bar{v}}{\bar{U}} + \alpha_{t2} \frac{\bar{U} h^3}{R w_s} \frac{\bar{u}}{\bar{U}} \right) \frac{\partial \bar{c}}{\partial t} \\ & + \left(\alpha_{11} \frac{\bar{U}^2 h^2}{w_s} \frac{\bar{v}}{\bar{U}} + \alpha_{12} \frac{\bar{U}^2 h^3}{R w_s} \frac{\bar{u}}{\bar{U}} \right) \left(\frac{\partial \bar{c}}{\partial x} \frac{\bar{u}}{\bar{U}} + \frac{\partial \bar{c}}{\partial y} \frac{\bar{v}}{\bar{U}} \right) \\ & + \left(\alpha_{21} \frac{\bar{U}^2 h^3}{R w_s} \frac{\bar{v}}{\bar{U}} + \alpha_{22} \frac{\bar{U}^2 h^4}{R^2 w_s} \frac{\bar{u}}{\bar{U}} \right) \left(-\frac{\partial \bar{c}}{\partial x} \frac{\bar{v}}{\bar{U}} + \frac{\partial \bar{c}}{\partial y} \frac{\bar{u}}{\bar{U}} \right) \end{aligned} \tag{3.60}$$

Rearrangement and substituting $p = \bar{u} h$ and $q = \bar{v} h$ into Eqs. (3.59) and (3.60) gives the equations used in the sediment model:

$$S_x = \left(\alpha_{01}\, p - \alpha_{02}\, q\, \frac{h}{R}\right)\bar{c} + \left(\alpha_{t1}\, p\, \frac{h}{w_s} - \alpha_{t2}\, q\, \frac{h}{R}\, \frac{h}{w_s}\right)\frac{\partial \bar{c}}{\partial t}$$

$$+\left(\alpha_{11}\frac{p^2}{w_s} - \alpha_{12}\frac{p\,q}{w_s}\frac{h}{R} - \alpha_{21}\frac{p\,q}{w_s}\frac{h}{R} + \alpha_{22}\frac{q^2}{w_s}\frac{h^2}{R^2}\right)\frac{\partial \bar{c}}{\partial x} \qquad (3.61)$$

$$+\left(\alpha_{11}\frac{p\,q}{w_s} - \alpha_{12}\frac{q^2}{w_s}\frac{h}{R} + \alpha_{21}\frac{p^2}{w_s}\frac{h}{R} - \alpha_{22}\frac{p\,q}{w_s}\frac{h^2}{R^2}\right)\frac{\partial \bar{c}}{\partial y}$$

$$S_y = \left(\alpha_{01}\, q + \alpha_{02}\, p\, \frac{h}{R}\right)\bar{c} + \left(\alpha_{t1}\, q\, \frac{h}{w_s} + \alpha_{t2}\, p\, \frac{h}{R}\, \frac{h}{w_s}\right)\frac{\partial \bar{c}}{\partial t}$$

$$+\left(\alpha_{11}\frac{p\,q}{w_s} + \alpha_{12}\frac{p^2}{w_s}\frac{h}{R} - \alpha_{21}\frac{q^2}{w_s}\frac{h}{R} - \alpha_{22}\frac{p\,q}{w_s}\frac{h^2}{R^2}\right)\frac{\partial \bar{c}}{\partial x} \qquad (3.62)$$

$$+\left(\alpha_{11}\frac{q^2}{w_s} + \alpha_{12}\frac{p\,q}{w_s}\frac{h}{R} + \alpha_{21}\frac{p\,q}{w_s}\frac{h}{R} + \alpha_{22}\frac{p^2}{w_s}\frac{h^2}{R^2}\right)\frac{\partial \bar{c}}{\partial y}$$

The coefficients γ_i in the advection-dispersion Eq. (3.40) and the α_{ij} coefficients in Eqs. (3.59) and (3.60) are integrals, which are solved numerically. The distribution of vertical discrete points is similar to the approach described for the velocity profiles. Instead of computing the coefficients at all time steps and all grid points in the modelling area (which would require substantial computer power), the coefficients are solved once at the beginning of the simulation for a certain number (and combination) of input parameters. The obtained values are stored in tables from which interpolated values can be extracted during the simulation.

3.2 Bed Load Transport

The interaction between the bed load and the alluvial bed is one of the most fundamental aspects of the morphological behaviour of a river bend (see Engelund, 1974 and Struiksma et al., 1985).

In contrast to the suspended load, it is assumed that the bed load responds immediately to changes in local hydraulic conditions. Thus, there is no need for advection-dispersion modelling in connection with bed load. However, two important effects must be taken into account:

1. The deviation of the direction of the bed shear stress from the mean flow direction due to helical flow; and
2. The effect of a sloping river bed.

The first issue requires separate modelling of helical flow prior to bed load computations (see Section 2.2).

When discussing the local bed load sediment transport capacity of a flow it is convenient only to consider sediment transport in uniform shear flow. For this schematised case numerous transport relations have been presented during past decades. For a review of this topic, suggested references are Vanoni (1975 and 1984). The transport relations implemented in the present modelling system are presented in Section 3.3.

The bed load sediment transport is assumed to be the same as the sediment transport capacity mentioned above, except for bed slope effect and helical flow effect. This is illustrated in Figure 3.3.

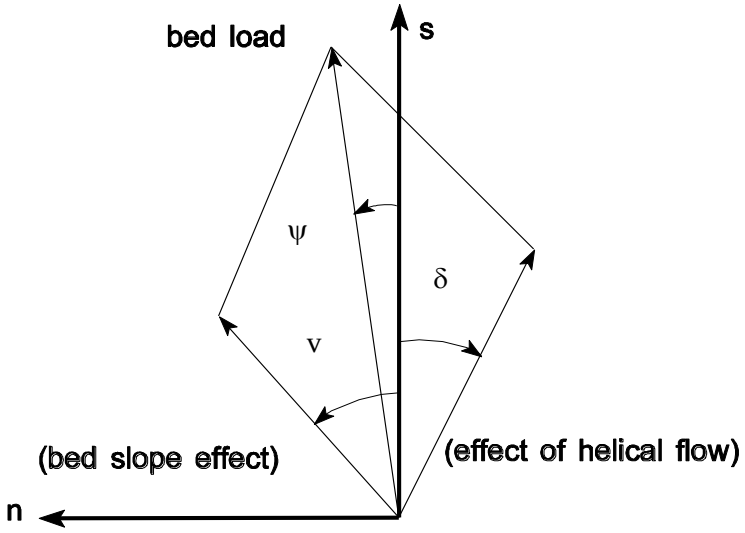

Figure 3.3 Direction of bed load transport influenced by helical flow and transverse bed slope

Bed slope influences the sediment transport rate and direction (the latter being the most important for morphological modelling). Only a few models of the influence of bed slopes on sediment transport rate have been proposed, see Lane (1953), Luque (1976), Koch (1980), Ikeda (1980), and Olesen (1987). In principle, two approaches have been adopted. The first modifies the critical shear stress for initiation of motion:

$$\theta_c = \theta_{c0} \cdot (1 + \frac{\partial z_b}{\partial s}) \tag{3.63}$$

Where

θ_c	Modified critical Shields parameter
θ_{c0}	Critical Shields parameter in uniform shear flow
z_b	Bed level
s	Stream-wise (horizontal) coordinate

The slope effect on sediment transport rate given by Eq. (3.63) cannot be directly incorporated into a model that does not assume zero bed load transport at a critical shear stress (e.g. the Engelund and Hansen formula). For this kind of formula, the following correction can be applied:

$$S_s = \left(1 - \alpha \cdot \frac{\partial z^*}{\partial s}\right) S_{bl} \tag{3.64}$$

Where

α	Model calibration parameter
S_{bl}	Bed load as calculated from sediment transport formula
S_s	Bed load along streamline, s

The Eq. (3.64) is implemented in the present modelling system. The coefficient α has to be specified. An estimate of the coefficient can be obtained by estimating the velocity exponent *b* in the generalised sediment transport formula $\Phi = a \cdot u^b$ (*u*, is flow velocity, *a*, a constant factor, and Φ, the non-dimensional sediment transport) by comparison with the Meyer-Peter & Muller (1948) formula $\Phi = 8 \cdot (\theta' - \theta_c)^{1.5}$. This gives:

$$b = \frac{3 \cdot \theta'}{\theta' - \theta_c} \tag{3.65}$$

Where

θ'	Effective skin friction
θ_c	Critical Shields parameter
b	Velocity exponent in $\Phi = a \cdot u^b$
a	Constant factor
u	Flow velocity
Φ	Non-dimensional sediment transport rate

Using the total load formula of Engelund and Hansen (1967) the velocity exponent *b* is 5 (constant). Using Eq. (3.65), *b* varies from infinity at the threshold of motion to 3 for very high shear stresses.

Secondly, the modified critical Shields parameter from Eq. (3.63) is substituted into the Meyer-Peter & Muller (1947) formula. If Eq. (3.63) is linearised with respect to the bed slope *dz/ds*, the following expression for the α coefficient is obtained:

$$\alpha = \frac{b}{2} \cdot \frac{\theta_{c0}}{\theta'} \tag{3.66}$$

The coefficient varies from around $\alpha = 1.5$ for $\theta' = 2\theta_{c0}$ down to $\alpha \approx 0.2$ for $\theta' = 9\theta_{c0}$. In the present modelling system however, the α coefficient is specified as a constant throughout the modelling period.

The prediction of transverse depth distribution in alluvial channel bends has had considerable attention from river engineers, as it is essential in investigations of navigability improvement in river bends and in design of optimal channel bank protection. Since the pioneering work of van Bendegom (1947), many models of transverse bed slope have been proposed. Most of these can be reformulated so that they also predict the direction of sediment transport. Olesen (1987) gives an exhaustive description of the proposed models. Talmon et al. (1995) has carried out extensive bed levelling experiments for verification of mathematical models of the transverse bed slope effect, which in line with Kikkawa et al. (1976), Parker (1982), Odgaard (1981), and Ikeda (1981) suggested the following suitable formula:

$$S_n = \left(\tan \delta_s - G \cdot \theta^{-a} \cdot \frac{\partial z^*}{\partial n} \right) S_{bl} \tag{3.67}$$

Where

G	Transverse bed slope factor (calibration coefficient)

a	Transverse bed slope exponent (calibration parameter)
$\tan\delta_s$	Bed shear direction change due to helical flow strength, see Section 2.2.

The values of the transverse bed slope factor G and the exponent a, differs somewhat between the various authors. Especially, when results from laboratory flumes are compared with the results from prototypes. For the laboratory flume case the best fit seems to be obtained by:

G = 0.6 and a = 0.5

Talmon et al. (1995) concludes from their experiments that a distinction should be made between laboratory conditions and natural rivers. The magnitude of the transverse slope effect (G) and the direction coefficient (β) of the secondary flow seem to differ by a factor of two. Also, the distribution between suspended and bed load transport is important. The G factor is at least a factor 2 stronger for conditions with prevailing suspended load, indicating that either the transverse slope effect is also acting on the suspended load part or the transverse slope effect is simply stronger. This means that the following values should be used for natural rivers:

G = 1.25 and a = 0.5

If the angle between flow direction and the x-axis is ϕ in a fixed (x, y) coordinate system, bed slopes are computed as:

$$\frac{\partial z^*}{\partial s} = \frac{\partial z}{\partial x}\cos\phi + \frac{\partial z}{\partial y}\sin\phi \tag{3.68}$$

Where

z^*	Bed level at the centre point in the numerical scheme
s	The horizontal coordinate along the streamline
n	The horizontal coordinate in the transverse direction
x	The first horizontal coordinate
y	The other horizontal coordinate
z	The bed level as computed by the morphological model
ϕ	Angle of stream line compared to (x, y) coordinate system

The bed slope calculation in the stream wise direction is fully centred in the considered grid point. The bed slope in the transverse direction, which is upstream centred, is:

$$\frac{\partial z^*}{\partial n} = \frac{\partial z}{\partial y}\cos\phi - \frac{\partial z}{\partial x}\sin\phi \tag{3.69}$$

Transformation from streamline coordinates to fixed coordinates gives the following expression for the transport in x- and y-direction:

$$S_x = S_s\cos\phi + S_n\sin\phi \tag{3.70}$$

$$S_y = S_n\cos\phi - S_s\sin\phi \tag{3.71}$$

3.3 Sediment Transport Formulae

Sediment transport capacity in uniform shear flow has been extensively investigated over the years. For instance, reviews are given in Vanoni (1984). This section discusses the sediment transport formulas used for calculation of bed load and suspended load transport capacity (equilibrium concentration at the riverbed) which are implemented in the present modelling system.

The following symbols are applied.

Symbols

S_{bl}	:	Bed load	<m^2/s>
k_b	:	Bed load calibration factor	< - >
S_{sl}	:	Suspended load	<m^2/s>
k_s	:	Suspended load calibration factor	< - >
t_s	:	Time scale	< s >
s	:	Relative density of the sediment	< - >
S_{tl}	:	Total load	<m^2/s>
c_e	:	Equilibrium mass concentration	<g/m^3>
C	:	Chezy number	<$m^{½}/s$>
u	:	Velocity	<m/s>

All sediment transport formulas described herein exclude the effect of riverbed porosity, which is included in the continuity equation for update of bed level instead.

Some of the formulas only predict total load (bed load + suspended load), whereas information about both bed load and suspended load is required. The total load formulas can still be applied by using the calibration factors k_b and k_s for bed load and suspended load, respectively, in order to differentiate between the two modes of transport. Assume for instance a total load formula. By specifying $k_b = 0.1$ and $k_s = 0.9$, it is understood that 10% of the transport is bed load.

Due to the non-uniform vertical distribution of the suspended sediment concentration, the effective fall height of grains will be different from the mean fall height $h/2$ (where h is water depth). For a uniform vertical concentration profile, the time scale for settling is defined as h/w_s (w_s is the settling velocity). With information about the Rouse number Z, the actual concentration profile can be predicted and therefore a better estimate for the time scale t_s can be obtained. It should, however, be noted that in the suspended load transport model described in Section 3.1, the time scale is automatically accounted for by using the described profile functions, i.e. $t_s = (h/w_s)\cdot(\gamma_1/\gamma_0)$. In that case the time scale t_s, as predicted from the formulas below, are not used.

The Shields parameter θ is defined as:

$$\theta = \frac{\tau}{\rho g (s-1) d_{50}} \tag{3.72}$$

Where

τ	The flow shear stress
ρ	Density of water, approx. 1000 kg/m^3
g	Acceleration of gravity, 9.81 m/s^2
s	ρ/ρ_s relative density of the sediment
ρ_s	Density of sediment, for normal sand 2650 kg/m^3

Flow shear stress is divided into form drag τ'' and skin friction τ'. The total shear stress $\tau = \tau' + \tau''$ is estimated from the local flow velocity u and the local Chezy number C:

$$\tau = \rho g \frac{u^2}{C^2} \tag{3.73}$$

For skin friction, the following approximate friction formula (Engelund & Hansen, 1967) is applied unless otherwise calculated (i.e. in the model of van Rijn or the model of Engelund and Fredsøe, where more sophisticated models are used to describe the physical processes):

$$\theta' = 0.06 + 0.4 \cdot \theta^2 \tag{3.74}$$

The non-dimensional sediment transport rate is defined as:

$$\Phi = \frac{S}{\sqrt{(s-1) g\, d^3}} \tag{3.75}$$

Where

S	Sediment transport (bed load, total or suspended load)
d	Characteristic grain size
Φ	Non-dimensional sediment transport

3.3.1 Engelund and Hansen model

The model by Engelund and Hansen (1967) is a total load model that divides the sediment transport into bed load and suspended load by the relations:

$$S_{bl} = k_b \cdot S_{tl} \tag{3.76}$$

$$S_{sl} = k_s \cdot S_{tl} \tag{3.77}$$

Where the total sediment transport is obtained by:

$$S_{tl} = 0.05 \frac{C^2}{g} \theta^{\frac{5}{2}} \sqrt{(s-1)\, g\, d_{50}^3} \tag{3.78}$$

The time scale t_s for adaptation to the equilibrium concentration profile is determined by:

$$t_s = \frac{h}{2 w_s} \tag{3.79}$$

The equilibrium concentration is simply specified as the suspended load divided by the water flux and converted from volumetric concentration to mass concentration:

$$c_e = \frac{S_{sl}}{u \cdot h} \cdot s \cdot 10^6 \tag{3.80}$$

3.3.2 Van Rijn model

Van Rijn (1984) proposed the following models for sediment transport of bed load and suspended load:

$$S_{bl} = 0.053 \frac{T^{2.1}}{D_*^{0.3}} \sqrt{(s-1)g \cdot d_{50}{}^3} \tag{3.81}$$

Where T is the non-dimensional transport stage parameter and given by:

$$T = \left(\frac{u_{f'}}{u_{f,c}} \right)^2 - 1 \tag{3.82}$$

In Eq. (3.82) the critical friction velocity $u_{f,c}$ is determined as:

$$u_{f,c} = \sqrt{\theta_c (s-1)\, g\, d_{50}} \tag{3.83}$$

The effective friction velocity is estimated from:

$$u'_f = u \frac{\sqrt{g}}{C'} \tag{3.84}$$

Where the resistance (Chezy number) originating from skin friction is based on a logarithmic velocity profile assuming a certain bed roughness:

$$C' = 18 \log \left(\frac{4h}{d_{90}} \right) \tag{3.85}$$

The non-dimensional particle parameter D_* in the bed load transport formula specified in Eq. (3.81) is defined as:

$$D_* = d_{50} \left(\frac{(s-1)\, g}{\nu^2} \right)^{\frac{1}{3}} \tag{3.86}$$

Where ν, is the kinematic viscosity and approximately equal to 10^{-6} m^2/s for water.

Instead of using a constant critical Shields parameter θ_c (approximately equal to 0.06), van Rijn assumes the following variation as a function of D_*, see Table 3.1.

Table 3.1 Relations for determination of critical Shields stress

Range of D_*	θ_c
$D_* < 4$	$0.24/D_*$
$4 < D_* < 10$	$0.14\ D_*^{-0.64}$
$10 < D_* < 20$	$0.04\ D_*^{-0.1}$
$20 < D_* < 150$	$0.013\ D_*^{0.29}$
$D_* > 150$	0.055

Suspended sediment transport occurs only if one of the following criteria below is fulfilled.

$$u_f > \frac{4w_s}{D_*} \quad \text{for} \quad D_* < 10 \tag{3.87}$$

$$u_f > 0.4w_s \quad \text{for} \quad D_* > 10 \tag{3.88}$$

The reference level, at which the bed concentration is determined, is expressed as:

$$a = \max\begin{pmatrix} 0.01\,h \\ 2\,d_{50} \end{pmatrix} \tag{3.89}$$

The volumetric bed concentration is obtained from the relation:

$$c_a = 0.015 \cdot \frac{d_{50}\,T^{1.5}}{a\,D_*^{0.3}} \left[m^3 / m^3\right] \tag{3.90}$$

In Figure 3.4 the reference level and the bed concentration are sketched.

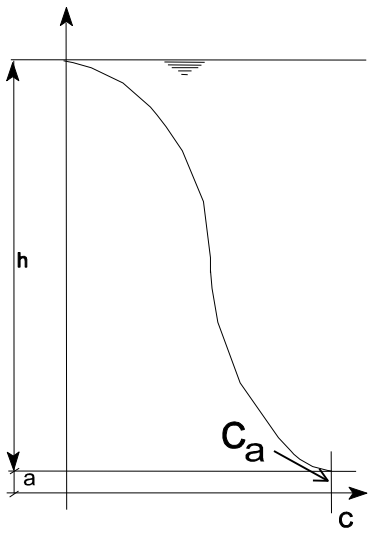

Figure 3.4 Definition of the reference level a for the bed concentration C_a

A correction coefficient, denoted β is applied to the hydrodynamic diffusion coefficient in order to transform the coefficient into a diffusion coefficient for the suspended sediment:

$$\beta = 1 + 2\left(\frac{w_s}{u_f}\right)^2 \tag{3.91}$$

Van Rijn defines a correction factor φ for the concentration profile, which is determined by:

$$\varphi = \frac{5}{2}\left(\frac{w_s}{u_f}\right)^{0.8}\left(\frac{c_a}{c_o}\right)^{0.4} \tag{3.92}$$

Where c_0 (if expressed as volumetric concentration) is the concentration corresponding to firm packing of the sediment, i.e.:

$$c_o = 0.65\ m^3/m^3 \tag{3.93}$$

Applying the correction coefficients defined above a Rouse suspension parameter Z, can be obtained by:

$$Z = \frac{w_s}{\beta\,\kappa\,u_f} + \varphi \tag{3.94}$$

Finally, the depth-integrated transport of suspended load is computed as:

$$S_{sl} = f \cdot c_a \cdot u \cdot h \tag{3.95}$$

Where the correction factor for suspended load is obtained from:

$$f = \frac{\left(\frac{a}{h}\right)^Z - \left(\frac{a}{h}\right)^{1.2}}{\left(1 - \frac{a}{h}\right)^Z (1.2 - Z)} \tag{3.96}$$

The equilibrium concentration c_e and the height above the bed of the centroid of the concentration profile are calculated from the approximations formulas given in the Table 3.2 below:

Table 3.2 Polynomial approximations for determination of the equilibrium concentration and centroid height

Condition	Corresponding value of C_e and h_*
$Z \leq 1$	$C_e = C_a[[(2.21Z - 6.41)Z + 7.21)Z - 3.95]Z + 0.97]$ $h_* = h[(0.119Z - 0.085)Z - 0.400)Z + 0.505]$
$1 \leq Z \leq 3$	$C_e = C_a[[(0.007Z - 0.06)Z + 0.220)Z - 0.347]Z + 0.22]$ $h_* = h[(-0.027Z + 0.208)Z - 0.536)Z + 0.493]$
$Z > 3$	$C_e = C_a[[(4 \cdot 10^{-6} Z - 1.2 \cdot 10^{-4})Z + 1.4 \cdot 10^{-3})Z - 7.67 \cdot 10^{-3}]Z + 0.018]$ $h_* = h[(-4.87 \cdot 10^{-5} Z + 0.0011)Z - 0.0091)Z + 0.0361]$

The time scale for adaptation to the equilibrium profile is:

$$t_s = \frac{h_*}{w_s} \tag{3.97}$$

3.3.3 Engelund, Fredsøe and Zyserman model

The probability of a moving sediment grain can, according to Engelund and Fredsøe (1976), be determined by the expression:

$$p = \left[1 + \left(\frac{\frac{\pi}{6}\mu_d}{\theta' - \theta_c}\right)^4\right]^{-\frac{1}{4}}, \theta' > \theta_c \tag{3.98}$$

The dynamic friction coefficient μ_d is assumed to be equal to: μ_d = 0.51 = tan27°. The non-dimensional skin shear stress is defined by:

$$\theta' = \frac{u_f'^{\,2}}{(s-1)\, g\, d_{50}} \tag{3.99}$$

Where the friction velocity related to skin friction is calculated from the assumption of a logarithmic velocity profile:

$$u_f' = \frac{\bar{u}}{6 + 2.5 \ln\left(\frac{h}{2.5 d_{50}}\right)} \tag{3.100}$$

The bed load transport rate is estimated from:

$$S_{bl} = 5\, p \cdot (\sqrt{\theta'} - 0.7\sqrt{\theta_c})\sqrt{(s-1)\, g\, d_{50}^3} \tag{3.101}$$

The reference concentration near the bed is calculated from an empirical relation obtained by Zyserman and Fredsøe (1994):

$$c_b = \frac{0.331(\theta - \theta_c)^{1.75}}{1 + \frac{0.331}{0.46}(\theta - \theta_c)^{1.75}} \tag{3.102}$$

The empirical relation was established from analysis of the experimental data sets of Guy et al. (1966) and covers a range from pure bed load to dominant suspended transport. The influence of lateral bed slope is included in the relation through a reduced critical Shields stress for onset of motion.

Numerical integration is performed along a logarithmic vertical scale, because a greater density of computational points is required close to the bottom, where the largest velocity gradients occur. The non-dimensional vertical coordinate is obtained from the relation:

$$\eta_j = \eta_{j-1} + \Delta \cdot 1.08^{j-1} \tag{3.103}$$

Where the step height Δ is determined by:

$$\Delta = \frac{1}{\left(\frac{1 - 1.08^{99}}{1 - 1.08}\right) - 1} \tag{3.104}$$

Due to the specific value of the exponent in Eq. (3.104), it is seen that the depth is divided into 99 segments. The velocity profile is assumed to be:

$$u(\eta) = \frac{\sqrt{g}}{0.4C} \ln\left(\frac{\eta}{\eta_0}\right) \tag{3.105}$$

Where the no slip level η_0, is obtained from:

$$\eta_o = \exp\left(\eta_o - 1 - \frac{0.4\,C}{\sqrt{g}}\right) \tag{3.106}$$

Eq. (3.106) is solved by iteration.

The normalised vertical concentration profile is specified in the following way:

$$c(\eta) = \left(\frac{1-\eta}{\eta} \cdot \frac{a}{1-a}\right)^Z \tag{3.107}$$

Where the reference level *a,* is defined by:

$$a = \frac{2 \cdot d_{50}}{h} \tag{3.108}$$

The Rouse suspension parameter is defined as:

$$Z = \frac{w_s}{\kappa u_f} \tag{3.109}$$

The suspended load transport rate is obtained from:

$$S_{sl} = c_b u h \cdot \int_{\eta_0}^{1} u(\eta) \cdot c(\eta) d\zeta \tag{3.110}$$

The equilibrium mass concentration c_e, is determined from:

$$c_e = \frac{S_{sl}}{u h} s \cdot 10^6 \quad \left[g / m^3\right] \tag{3.111}$$

The time scale t_s, is defined as:

$$t_s = \frac{h_*}{w_s} \tag{3.112}$$

In Eq. (3.112) the height of the centroid h_* of the concentration profile above the bed is determined, as suggested by van Rijn.

3.3.4 Meyer-Peter and Müller model

The Meyer-Peter and Müller model (1948) relates the non-dimensional bed load transport Φ to the dimensionless shear stress acting on the grains through the relation:

$$\Phi_{bl} = 8\left(\theta' - \theta_c\right)^{1.5} \tag{3.113}$$

or expressed as a transport rate:

$$S_{bl} = 8\left(\theta' - \theta_c\right)^{1.5} \sqrt{(s-1) g d_{50}^3} \tag{3.114}$$

where θ' is the part of the Shields stress related to skin friction. The relation is only valid for fluvial systems with dominating bed load and slopes ranging from 0.0004 to 0.02.

3.3.5 Empirical relations (Smart and Jaeggi model)

Based on fluvial laboratory experiments Smart and Jaeggi obtained that the Meyer-Peter and Müller formula underestimates the sediment transport rates significantly for slopes steeper than 0.03. Smart and Jaeggi (1983) therefore proposed a new transport relation based on Eq. (3.113) that includes effects of non-uniformity of the sediment as well as the slope induced effect on the sediment transport. The model yields:

$$\Phi = 4\left(\frac{d_{90}}{d_{30}}\right)^{0.2} I^{0.6} C\sqrt{\theta} \cdot \left(\theta - \theta_c\right) \tag{3.115}$$

Where

d_{90} 90 % fractile of the sediment

d_{30}	30 % fractile of the sediment
I	Slope (water surface or bottom level)
C	Chezy number

The model is only recommended for fluvial systems with a median grain diameter greater than 0.4 mm and sediment non-uniformity d_{90}/d_{30} less than 8.5. The application range with regards to slopes is from 0.0004 and up to 0.2, i.e. it is the best approach for mountainous rivers. The model is the default choice when selecting the empirical relation.

The empirical relation is a general extended relation of the Smart and Jaeggi model that is specified by eight coefficients and exponents. The allowance of flexible coefficients and exponents makes it possible for the modeller to use special sediment transport formulas, which have been established for a specific location. The empirical model is made so flexible that different relations can be used for the bed load and the suspended load and for each specified fraction. The general empirical bed load formulation yields:

$$\Phi_{bl} = a_1 \cdot \left[\left(\frac{d_{90}}{d_{30}} \right)^{a_2} I^{a_3} C^{a_4} \theta^{a_5} \cdot [\, a_6 \theta^{a_7} - \theta_c \,]^{a_8} \right] \tag{3.116}$$

Where a_1 - a_8 are user specified coefficients.

For the Smart and Jaeggi model the coefficients and exponents should be given as:

a_1 = 4.00, a_2 = 0.20, a_3 = 0.60, a_4 = 1.00,
a_5 = 0.50, a_6 = 1.00, a_7 = 1.00, a_8 = 1.00

The Meyer-Peter and Müller model can be established if the coefficients and exponents are chosen as:

a_1 = 8.00, a_2 = 0.00, a_3 = 0.00, a_4 = 0.00
a_5 = 0.00, a_6 = 1.00, a_7 = 1.00, a_8 = 1.50

Two additional parameters should be specified when using the empirical model or Smart and Jaeggi model. The first specifies whether the slope is should be related to bed slope or water surface slope, and the second specifies whether θ should be related to the total Shields stress or only the skin friction θ'. Normally, skin friction is applied for bed load formulas only.

The empirical relation for the suspended load formula is similar to the bed load formula, but can be specified with different coefficients:

$$\Phi_{sl} = a_1 \cdot \left[\left(\frac{d_{90}}{d_{30}} \right)^{a_2} I^{a_3} C^{a_4} \theta^{a_5} \cdot [\, a_6 \theta^{a_7} - \theta_c \,]^{a_8} \right] \tag{3.117}$$

The equilibrium concentration for the suspended sediment is determined by:

$$c_e = \frac{S_{sl}}{u\, h} \cdot s \cdot 10^6 \tag{3.118}$$

Where

s	Relative density of sediment, approximately 2.65 for sand
h	Water depth

u Flow velocity

The time scale is obtained from:

$$t_s = \frac{h_*}{w_s} \tag{3.119}$$

Where the height of the centroid above the bed is given by:

$$h_* = \frac{h}{2} \tag{3.120}$$

3.3.6 Yang's model for sand transport

Yang (1983) observed that most published sediment transport formulas for bed load or total load correlates the sediment transport to a single hydraulic variable in a form like:

$$q_s = a\left(X - X_{cr}\right)^n \tag{3.121}$$

Where a is a coefficient, n is an exponent and X is either water discharge, mean velocity, energy or surface slope, bed shear stress, stream power per unit bed area, or unit stream power defined as the product between the mean velocity V and the slope I. X_{cr} represents a critical value for one of the mentioned hydraulic parameters. Based on laboratory flume test with 0.93 mm. sand, Yang observed that the water discharge and surface slope are poor predictors for the sediment transport rate, because that more than one sediment transport rate can occur for a single value of water discharge or water surface slope. For both the mean velocity and the shear stress a single value relationship for the sediment transport rate exists. However, Yang found that the resulting curves based on these two parameters are quite steep, and thereby sensitive to the predicted rates. Yang found that the best correlations were achieved by using the stream power. However, the unit stream power was found to be a better predictor. Based on this analysis suggested a general transport formula of the form:

$$\log_{10}\left(c_{ppm}\right) = A + B\log_{10}\left(\frac{VI}{w_s} - \frac{V_{cr}I}{w_s}\right) \tag{3.122}$$

Where c_{ppm} is the bed material concentration, excluding wash load (in ppm by weight), w_s is the settling velocity and A, B dimensionless variables related to flow and sediment characteristics. The coefficient values were determined by regression analysis of 463 data sets of laboratory data, and resulted in the following formula:

$$\log_{10}\left(c_{ppm}\right) = 5.435 - 0.286\log_{10}\left(\frac{w_s d_{50}}{\nu}\right) - 0.457\log_{10}\left(\frac{u_f}{w_s}\right) + \left(1.799 - 0.409\log_{10}\left(\frac{w_s d_{50}}{\nu}\right) - 0.314\log_{10}\left(\frac{u_f}{w_s}\right)\right)\log_{10}\left(\frac{VI - V_{cr}I}{w_s}\right) \tag{3.123}$$

Where ν is the kinematic viscosity, d_{50} the median grain size, and u_f the friction velocity. The product $V_{cr}I$ is the critical unit stream power at incipient motion. The ratio V_{cr}/w_s is obtained from:

$$\frac{V_{cr}}{w_s} = \frac{2.05}{\log_{10}\left(\frac{u_f d_{50}}{\nu}\right) - 0.06} + 0.66 \quad \text{for} \quad \frac{u_f d_{50}}{\nu} < 70 \tag{3.124}$$

and

$$\frac{V_{cr}}{w_s} = 2.05 \quad \text{for} \quad \frac{u_f d_{50}}{\nu} \geq 70 \tag{3.125}$$

Which shows that it is related to the grain shear Reynolds number.

The total load is obtained from the relation:

$$S_{tl} = \frac{Vhc_{ppm}}{s \cdot 10^6} \tag{3.126}$$

Where *h* is the flow depth and *s* the relative density of the sediment. The total load is divided into bed load and suspended load through the user-specified weight coefficients:

$$S_{bl} = k_b S_{tl} \tag{3.127}$$

$$S_{sl} = k_s S_{tl} \tag{3.128}$$

Likewise is the equilibrium concentration obtained as:

$$c_e = k_s c_{ppm} \tag{3.129}$$

The time scale for the adaptation to the equilibrium concentration profile is obtained from:

$$t_s = \frac{h}{2w_s} \tag{3.130}$$

Even though Yang's model for sand is one of the most accurate sediment transport formulas, it might not be the best choice for the MIKE 21C model that uses a non-equilibrium sediment transport description for the suspended sediment. The reason for this is that the transport relation gives no information on how the transport should be distributed between bed load and suspended load.

3.3.7 Yang's model for gravel transport

Yang (1984) adopted a transport equation of similar form for transport of gravel, but with modified coefficients. The model is specified by the following formula for the gravel concentration.

$$\log_{10}\left(c_{ppm}\right)=6.681-0.633\log_{10}\left(\frac{w_s d_{50}}{\nu}\right)-4.816\log_{10}\left(\frac{u_f}{w_s}\right)+$$
$$\left(2.784-0.305\log_{10}\left(\frac{w_s d_{50}}{\nu}\right)-0.282\log_{10}\left(\frac{u_f}{w_s}\right)\right)\log_{10}\left(\frac{VI-V_{cr}I}{w_s}\right) \quad (3.131)$$

Except from the modified coefficients the model is similar to the model for sand.

3.3.8 Wilcock & Crowe (2003) model

Wilcock & Crowe (2003) give the following non-dimensional bed-load:

$$W_i^* = \frac{(s_i-1)gq_{b,i}}{F_i\left(u_f'\right)^3} \quad (3.132)$$

Where:
W_i^* Non-dimensional bed-load of fraction i
s_i Relative density of fraction i
g Acceleration of gravity
$q_{b,i}$ Volumetric bed-load of fraction i
F_i Relative weight of the fraction (i) in the bed surface
u_f' Skin friction velocity

The non-dimensional bed-load is calculated from:

$$\mathrm{W}_i^*(\phi_i)=\begin{cases}0.002\,\phi_i^{7.5}, & \phi<1.35\\ 14\left(1-\frac{0.894}{\phi_i^{0.5}}\right)^{4.5}, & \phi\geq 1.35\end{cases} \quad (3.133)$$

Where φ_i is given by:

$$\phi_i=\frac{\tau'}{\tau_{ri}} \quad (3.134)$$

Where τ' is the bed shear stress (skin friction) and τ_{ri} a reference shear stress for fraction i. The reference shear stress for fraction i is given by:

$$\tau_{ri}=\tau_{rg}\left(\frac{d_i}{d_g}\right)^b \quad (3.135)$$

Where:
d_g Geometric mean grain diameter
d_i Grain size for fraction i
τ_{rg} Reference shear stress for the geometric grain size
b Exponent

The exponent b is calculated from:

$$b = \frac{0.67}{1 + \exp\left(1.5 - \frac{d_i}{d_g}\right)} \tag{3.136}$$

The reference shear stress for the geometric mean grain size is defined by:

$$\tau_{rg} = \theta_{rg}\left(s_g - 1\right)\rho g d_g \tag{3.137}$$

Where:

s_g Representative relative density for the geometric mean diameter

θ_{rg} Critical shields parameter for the geometric mean grain size

It is noted that the original model did not assume any variation in the s-values for the sediment fractions. In the present implementation we use the average s-value for the non-cohesive sediment fractions. The critical Shields parameter for the geometric mean grain size is calculated from:

$$\theta_{rg} = 0.021 + 0.015 \exp\left(-20F_s\right) \tag{3.138}$$

Where:

F_s Relative sand content in the bed surface.

F_s is calculated by summing the mass in the active layer of all fractions satisfying the two conditions:

- Fraction is non-cohesive
- Fraction has d_i<1 mm

This is divided by the total mass in the active layer.

Notes regarding Wilcock & Crowe

Wilcock & Crowe is only selectable for bed-load. The Wilcock & Crowe formula was developed for multi-fraction bed-load calculations. The F_i weights are already in the formula, and no other modifications apply.

Wilcock & Crowe can be used also for single fraction bed-load.

Egiazaroff does not apply to Wilcock & Crowe; it uses its own hiding function.

The GUI critical Shields parameter does not apply.

3.3.9 Parker (1990) model

The Parker (1990) bed-load formula is only appropriate for calculation of bed-load in gravel bed streams.

The non-dimensional bed-load is defined by:

$$W_i^* = \frac{(s_i - 1)g q_{b,i}}{F_i \left(u_f'\right)^3} \tag{3.139}$$

In the Parker formula the weight function F_i is renormalized to only include the gravel fractions.

The non-dimensional bed-load is calculated from the formula:

$$W_i^* = 0.00218\, G(\phi_i) \tag{3.140}$$

ϕ_i is calculated from:

$$\phi_i = \omega\, \phi_0 \left(\frac{d_i}{d_g}\right)^{-0.0951} \tag{3.141}$$

Where d_g is the geometric mean grain size, and ϕ_0 is calculated from:

$$\phi_0 = \frac{\theta_g{}'}{\theta_r{}'} \tag{3.142}$$

Where the skin friction Shields parameter θ_g' is based on the geometric mean diameter:

$$\theta_g{}' = \frac{(u_f{}')^2}{(s-1)g d_g} \tag{3.143}$$

And the reference Shields parameter:

$$\theta_r{}' = 0.0386 \tag{3.144}$$

The G-function is calculated from:

$$G(\phi) = \begin{cases} 5474\left(1 - \dfrac{0.853}{\phi}\right)^{4.5}, \phi > 1.59 \\ \exp(14.2(\phi-1) - 9.28(\phi-1)^2), 1 \le \phi \le 1.59 \\ \phi^{14.2}, \phi < 1 \end{cases} \tag{3.145}$$

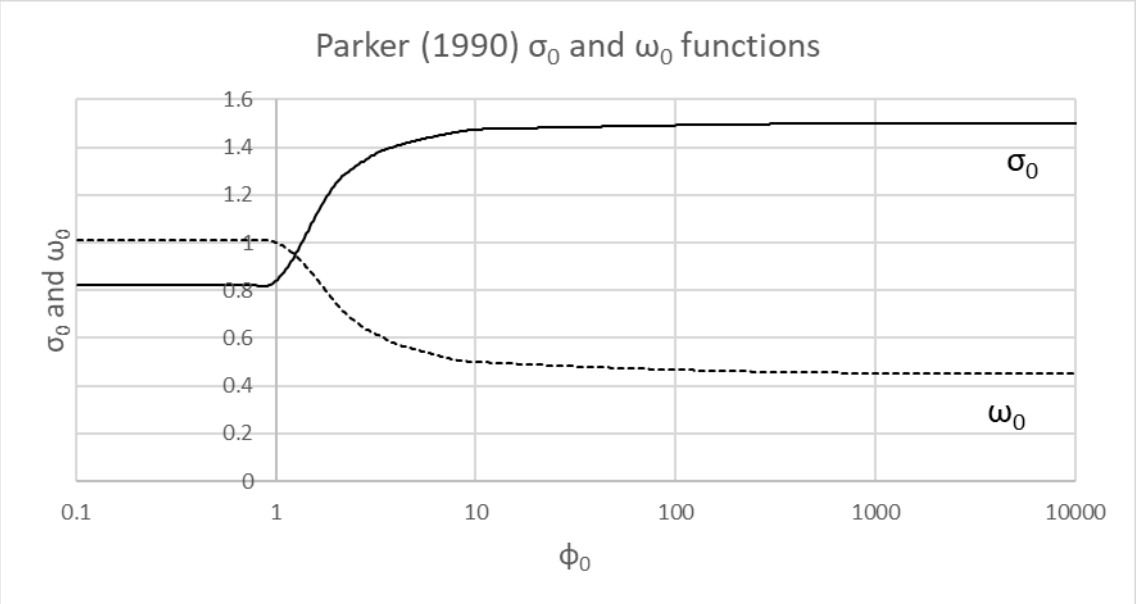

Figure 5 Parker (1990) σ_0 and ω_0 functions

The ω-function is given by:

$$\omega = 1 + \frac{\sigma_s}{\sigma_0(\phi_0)}(\omega_0(\phi_0) - 1)\theta_r' = 0.0386 \quad (3.146)$$

Where the two functions σ_0 and ω_0 are shown in the graph above.

Notes regarding Parker

Parker is only selectable for bed-load. The Parker formula was developed for multi-fraction bed-load calculations. The F_i weights are calculated separately and normalized for the gravel fractions.

Parker can be used also for single fraction bed-load.

Egiazaroff does not apply to Parker; it uses its own hiding function.

The GUI critical Shields parameter does not apply.

3.3.10 Lane Kalinske (1941) model

The concentration profile in Lane-Kalinske is calculated from a constant eddy diffusivity instead of the standard parabolic profile. The parabolic profile reads:

$$\nu_T(y) = \kappa u_f y \left(1 - \frac{y}{h}\right) \quad (3.147)$$

Here one will normally use the total friction (u_f) to determine the friction velocity because the total friction better represents the turbulence level compared to skin friction (u_f'). Lane-Kalinske in MIKE 1D is based solely on using total friction in agreement with the original publications.

The depth-averaged eddy viscosity is:

$$\epsilon = \frac{\kappa u_f}{h}\int_0^h y\left(1 - \frac{y}{h}\right)dy = \kappa h u_f \int_0^1 \frac{y}{h}\left(1 - \frac{y}{h}\right)d\left(\frac{y}{h}\right) = \kappa h u_f \int_0^1 s(1-s)ds = \frac{\kappa h u_f}{6} = \frac{h u_f}{15} \quad (3.148)$$

The concentration profile c(y) is found by solving the vertical advection-diffusion equation using this constant diffusivity:

$$w_s c + \epsilon \frac{dc}{dy} = 0 \quad (3.149)$$

With the boundary condition c(a) = c_a. The non-dimensional form is:

$$\frac{w_s h}{\epsilon} c + \frac{dc}{d\eta} = 0 \quad (3.150)$$

Or:

$$\frac{dc}{d\eta} = -\frac{w_s h}{\epsilon} c \tag{3.151}$$

With the solution:

$$c(\eta) = c_a \exp\left(-\frac{15 w_s}{u_f}(\eta - a)\right) \tag{3.152}$$

The velocity profile is given by:

$$u(\eta) = 1 + \frac{1}{\kappa}\frac{u_f}{V}(1 + \ln \eta) \tag{3.153}$$

It is noted that this does not accurately average to unity, and it gives unrealistic profiles for V/u_f'<5.

Lane & Kalinske (1941) do not provide the sediment concentration 5% of the water depth; it is given by Lane & Kalinske (1939):

$$C_a = 555\left(\frac{1}{2}\frac{u_f}{w_s}\exp\left(-\left(\frac{w_s}{u_f}\right)^2\right)\right)^{1.61} \tag{3.154}$$

Where:
C_a Near-bed concentration [ppm]

Note that [ppm] is approximated by [g/m3].

Originally the equation comes with a factor 5.55 and not 555, but the factor 5.55 is multiplied by a percentage (0-100) of the considered fractions. In MIKE 1D we use fraction weights (0-1) in the bed surface, and therefore the near-bed concentration should be multiplied by 100 to convert to the use of fraction weights.

It is noted that the skin friction is better for representing the near-bed concentration due to its entrainment nature. However, the work of Lane & Kalinske (1939) operates with turbulent fluctuations, which means the total friction is better than skin friction. Lane & Kalinske did not even mention skin friction in the 1939 or 1941 papers.

Vanoni (1953) notes that the analysis of Lane & Kalinske (1939) was not carried out to a point where the near-bed concentration was associated with some distance from the bed, and therefore the determined value is used as c_a MIKE 1D.

The suspended load capacity is calculated by:

$$q_s = \frac{q}{s\,\rho_w} C_0\left(\frac{w_s}{u_f}\right) P\left(\frac{w_s}{u_f}, \frac{V}{u_f}\right) \tag{3.155}$$

Where:
q Water flux
q_s Suspended load
ρ_w Water density 10^6 g/m^3
ss Sediment relative density

The P-function is given by:

$$P\left(\frac{w_s}{u_f},\frac{V}{u_f}\right)=\int_a^1\left(1+\frac{1}{\kappa}\frac{u_f}{V}\,(1+\ln\,\eta)\right)\exp\left(-\frac{15w_s}{u_f}\,(\eta-a)\right)d\eta \tag{3.156}$$

The P-function is tabulated internally in the code. In the original paper (Lane & Kalinske, 1941), the integral was done from η=0, but this cannot be done because the logarithmic velocity profile is not defined for η=0. Here we choose to integrate from η=a; it is also noted that the adopted logarithmic velocity profile becomes poorly defined for low η-values.

Here we note that the concentration profile is normalized to C(a)=Ca.

The suspended load capacity is translated to an equilibrium sediment concentration.

Notes regarding Lane-Kalinske

This is a suspended load formula, does not apply to bed-load.

Lane-Kalinske can be used in graded models, and indeed Vanoni (1953) gives that the near-bed concentration should simply be scaled with the percentage of the considered fraction in the bed surface. This is equivalent to the standard approach in MIKE 21C and MIKE 1D for multi-fraction models; scaling the near-bed concentration with the relative mass of the fraction in the bed surface is the same as scaling the capacity.

3.3.11 Ackers & White (1973) model

The Ackers & White sediment transport calculation starts with the non-dimensional grain diameter D*:

$$D^*=d\left(\frac{(s-1)g}{\nu^2}\right)^{1/3} \tag{3.157}$$

Three ranges of D* are considered in the formula:

- $D^*<1$: Fine sediment
- $D^*=1-60$: Transitional
- $D^*>60$: Gravel

Four coefficients derive from the non-dimensional grain diameter: n, A , C, m:

$$n=\begin{cases}1, & D^*<1\\ 1-0.56\log_{10}(D*), & 1\le D^*\le 60\\ 0, & 60<D^*\end{cases} \tag{3.158}$$

$$A=\begin{cases}0.37, & D^*<1\\ \frac{0.23}{\sqrt{D^*}}+0.14, & 1\le D^*\le 60\\ 0.17, & 60<D^*\end{cases} \tag{3.159}$$

$$C = \begin{cases} 2.95x10^{-4}, & D^* < 1 \\ 10^{2.86\log_{10} D^* - log_{10}^2 D^* - 3.53}, & 1 \le D^* \le 60 \\ 0.025, & 60 < D^* \end{cases} \quad (3.160)$$

$$m = \begin{cases} 11, & D^* < 1 \\ \frac{9.66}{D^*} + 1.34, & 1 \le D^* \le 60 \\ 1.5, & 60 < D^* \end{cases} \quad (3.161)$$

Ackers & White calculates a general sediment mobility number F_{gr}:

$$F_{gr} = \frac{u_f^n}{\sqrt{(s-1)gd}} \left(\frac{V}{\sqrt{32}\ \log_{10} \frac{10h}{d}} \right)^{1-n} \quad (3.162)$$

Where V is the flow speed.

From the general sediment mobility number, the general transport parameter G_{gr}:

$$G_{gr} = C \left(\frac{F_{gr}}{A} - 1 \right)^m \quad (3.163)$$

The general sediment mobility number relates to the sediment transport via:

$$C = G_{gr} \left(\frac{d}{h} \right) \left(\frac{V}{u_f} \right)^n \quad (3.164)$$

Where C is the volumetric sediment concentration. The volumetric sediment transport is hence:

$$q_t = Vh\, G_{gr} \left(\frac{d}{h} \right) \left(\frac{V}{u_f} \right)^n \quad (3.165)$$

Notes regarding Ackers & White

Ackers & White is a total load formula, which can be distributed to bed-load and suspended load by using constant factors. There is no requirement that the formula be used for both bed-load and suspended load, so it is allowed to e.g. use Ackers & White for suspended load and e.g. Meyer-Peter for bed-load.

Ackers & White was developed for single fraction sediment but can be adopted to graded models in which case the load is modified with the local relative weight function (F_i). No other modifications apply to Ackers & White for multi-fraction models.

3.3.12 Garcia & Parker (1991) model

Garcia & Parker is a true multi-fraction suspended load model. The advection-dispersion equation form used by Garcia & Parker is different from what we normally use in DHI's models:

$$Erosion - Deposition = w_s(E - c_b) \tag{3.166}$$

This is reformulated from near bed concentration to depth-integrated concentration by using:

$$c_b = \gamma C \tag{3.167}$$

Where γ is the ratio between near bed and depth-integrated concentration, and is calculated from a Rouse profile using b=0.05, i.e. the 5% of the depth used by Garcia & Parker (1991). This results in a function γ(Z), where Z is the Rouse number.

Now the source and sink have the generic form:

$$Erosion - Deposition = w_s(E - \gamma C) \tag{3.168}$$

Garcia & Parker (1991) provide the entrainment function for sediment mixtures:

$$E_i = F_i \frac{A\, Z_{ui}^5}{1 + \frac{A}{0.3} Z_{ui}^5} \tag{3.169}$$

Where:
E_i Entrainment rate for the fraction (i)
Z_{ui} Parameter calculated for each fraction (see below)
A Constant, A = 1.3x10^{-7}
F_i Fraction of (i) in the surface layer, i.e. surface supply modification

E_i is a volumetric concentration, which can be translated to the internally adopted mass concentration units [g/m^3] by multiplying by ρs$_i$, where:
ρ Water density ρ = 10^6 g/m^3
s_i Relative sediment density [-] for the considered fraction

The parameter Z_{ui} is calculated as:

$$Z_{ui} = \lambda_m \frac{u_f'}{w_{si}} Re_{pi}^{0.6} \left(\frac{d_i}{d_{50}}\right)^{0.2} \tag{3.170}$$

Where:
u_f' Skin friction velocity [m/s]
w_{si} Settling velocity for the considered fraction [m/s]
λ_m Parameter derived from the geometric grain size distribution [-]
Re_{pi} Grain Reynolds number for the fraction
d_i Grain size for the considered fraction [mm]
d_{50} Local median grain size [mm] in the bed surface

The grain Reynolds numbers for the individual fractions are given by:

$$Re_{pi} = \frac{\sqrt{(s_i - 1) g d_i^3}}{\nu} \tag{3.171}$$

The value of λ_m is given by Garcia and Parker (1991) as:

$$\lambda_m = 1 - 0.288\, \sigma_\phi \tag{3.172}$$

Where σ_φ is the standard deviation of the sediment mixture:

$$\sigma_\phi^2 = \sum \frac{m_i}{\sum m_i} (\phi_i - \phi_{mean})^2 \quad (3.173)$$

Where:
m_i Mass of each fraction in the bed surface [g/m^2]

with the geometric grain sizes φ_i defined using the phi scale (grain size in [mm]):

$$\phi_i = -log_2 d_i \quad (3.174)$$

and the mean geometric grain size (i.e. mean phi size) defined as:

$$\phi_{mean} = \sum \frac{m_i}{\sum m_i} \phi_i \quad (3.175)$$

Calculation of the γ-function

The derivation of γ is done from the Vanoni concentration profile:

$$c(y) = c_b \left(\left(\frac{y}{b} \right) \left(\frac{h-b}{h-y} \right) \right)^{-Z} \quad (3.176)$$

Where:
$c(y)$ Concentration profile
y Distance above the bed
h Water depth
b Reference level where b = 0.05h
Z Rouse number [-]

The Rouse number is calculated from the total friction velocity u_f to reflect turbulence:

$$Z = \frac{w_s}{\kappa u_f} \quad (3.177)$$

The function $\gamma = c_b/C$ is tabulated by numerically integrating the depth-integrated concentration:

$$C = \frac{1}{h-b} \int_b^h c(y)\, dy \quad (3.178)$$

The Vanoni profile now gives a tabulated function:

$$\gamma(Z) = \frac{c_b}{C} \quad (3.179)$$

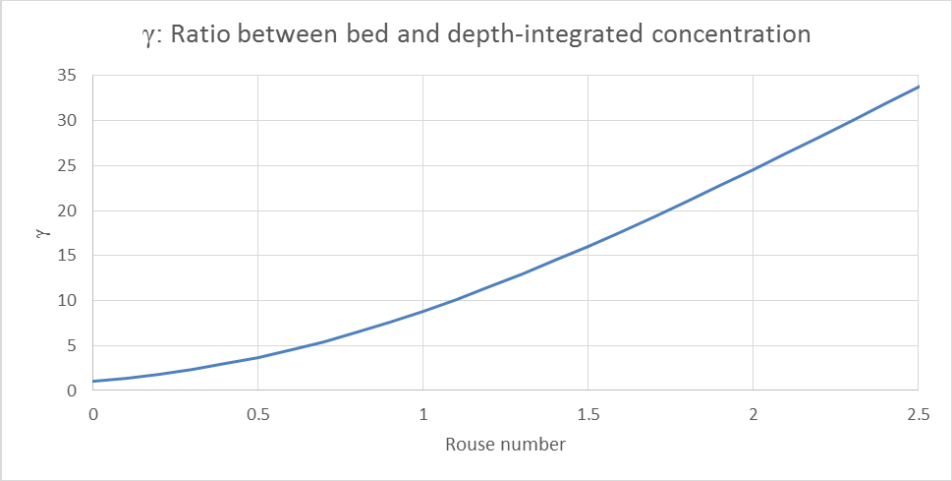

Figure 6 The γ-function

The numerically integrated γ(Z) function is shown graphically above. The parameter is unity for zero Rouse number (i.e. evenly distributed sediment has the same depth-integrated and bed concentrations) and increases quite fast with increasing Rouse number.

Notes regarding Garcia & Parker

Garcia & Parker is a suspended load formula, it does not apply to bed-load.

Garcia & Parker was developed from graded sediment data, and is a true multi-fraction suspended load model.

The model was originally developed for single fraction but was extended to multi-fraction. The single fraction form is imbedded in the presented formulation originally published by the authors.

Garcia & Parker does not use the critical Shields parameter, and therefore does not react to the Ashida & Michiue hiding function, and the formula already includes the surface weight function F_i.

4 Morphology

A morphological model is a combined hydrodynamic/sediment transport model. The hydrodynamic flow field is updated continuously according to changes in bed bathymetry.

Morphological models are traditionally divided into coupled and uncoupled models. In coupled models, the governing equations for flow and sediment transport are merged into one set of equations, which are solved simultaneously. In uncoupled models, the solution of hydrodynamics is solved at a certain time step prior to solution of the sediment transport equations. Subsequently, a new bed level is computed and the hydrodynamic model proceeds with the next time step. The latter approach is applied in the present modelling system. Other sub-models such as bank erosion, bank line update, alluvial bed resistance, bed forms, graded sediment are also included as described in this chapter.

4.1 Sediment Continuity Equation

Following calculation of sediment transport of bed material (bed load and suspended load), the bed level change can be computed from the equation:

$$(1-n)\cdot\frac{\partial z}{\partial t}+\frac{\partial S_x}{\partial x}+\frac{\partial S_y}{\partial y}=\Delta S_e \tag{4.1}$$

Where

S_x	Total sediment transport in x-direction
S_y	Total sediment transport in y-direction
n	Bed porosity
z	Bed level
t	Time
(x, y)	Cartesian coordinate system
ΔS_e	Lateral sediment supply from bank erosion

The total sediment transport is the sum of bed load and suspended load. For a curvilinear (s, n) grid, Eq. (4.1) is slightly different due to curving grid lines. This is handled numerically by using different Δs and Δn at inflow and outflow boundaries to each grid cell, see Figure 4.2.

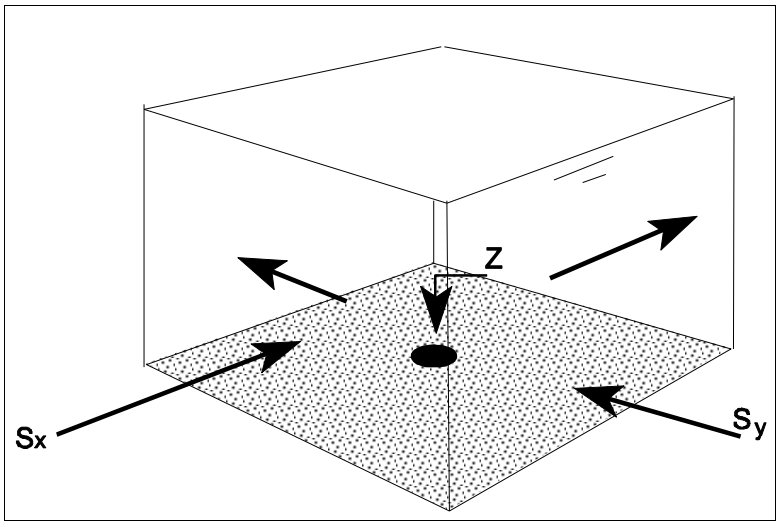

Figure 4.1 Solution of sediment continuity equation

A space centred - time forwarded difference scheme is applied. The time step is limited by the Courant criterion, i.e. that the Courant number should be less than 1. The wave celerity number can be estimated by considering the one-dimensional version of Eq. (4.1):

$$\frac{\partial z}{\partial t}+\frac{\partial S}{\partial x}=\frac{\partial z}{\partial t}+\frac{\partial S}{\partial z}\cdot\frac{\partial z}{\partial x}=0 \tag{4.2}$$

By assuming $\partial h/\partial t = -\partial z/\partial t$ and that sediment transport is a function of Shields stress (θ) only, the celerity c_{bw} of bed form waves is found to be:

$$c_{bw}=\frac{\partial S}{\partial z}=-\frac{\partial S}{\partial h}=\frac{\partial S}{\partial \theta}\cdot\frac{\partial \theta}{\partial h} \tag{4.3}$$

If the Chezy number is assumed constant, then θ is inversely proportional to h^2, i.e. $\partial\theta/\partial h = -2\theta/h$. For the transport formula of the Engelund and Hansen formula, we get:

$$c_{bw}=\frac{2.5\cdot S}{\theta}\cdot\frac{2\theta}{h}=5\cdot\frac{S}{h} \tag{4.4}$$

Where

S	Sediment transport rate
h	Water depth
c_{bw}	Roughly estimated bed form celerity

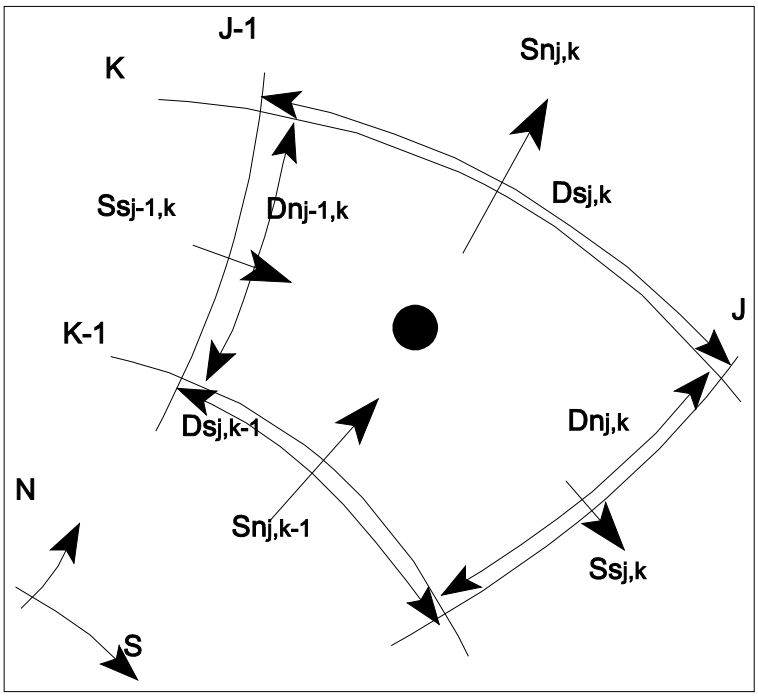

Figure 4.2 Sediment continuity equation defined in curvilinear grid

Based on the notations shown in Figure 4.2, the continuity equation for the sediment in a curvilinear grid can be expressed by the following difference equation:

$$(1-n)\frac{z_{j,k}^{n+1} - z_{j,k}^{n}}{\Delta t} + \frac{Ss_{j,k}\Delta n_{j,k} - Ss_{j-1,k}\Delta n_{j-1,k} + Sn_{j,k}\Delta s_{j,k} - Sn_{j,k-1}\Delta s_{j,k-1}}{0.25(\Delta s_{j,k} + \Delta s_{j,k-1})(\Delta n_{j,k} + \Delta n_{j-1,k})} = 0 \quad (4.5)$$

Where

S_s	Sediment transport rate in *s*-direction
S_n	Sediment transport rate in *n*-direction
n	Bed porosity
t	Time
(s, n)	Curvilinear coordinates
Δs	Space step in *s*-direction
Δn	Space step in *n*-direction
(j, k)	Grid coordinates

To close the system a boundary condition is required at the upstream boundary. Two options are possible: specification of the rate of bed level change ($\partial z/\partial t$), or simply the transport rate (S) into the system.

Theoretically, only upstream sediment transport boundary conditions are required. However, as the model allows change in the flow direction during a simulation, the sediment transport is specified at all boundaries. Each specific boundary condition becomes active only during inflow into the model domain.

4.1.1 Sediment transport boundary

The boundary condition can be specified in every single boundary point or as the sum over the whole boundary. If a width-integrated value is specified (either as a constant or a time series), model units are m^3/s. The model will automatically distribute the specified sediment transport proportionally to the local sediment transport capacity in the following manner:

$$q_{s,i} = Q_s \cdot \frac{q^e_{s,i}}{\sum_{i=1}^{n} q^e_{s,i} \cdot \Delta x_i} \tag{4.6}$$

Where

$q_{s,i}$ Actual sediment transport rate (m^2/s) at point *i* on the boundary line (i.e. equivalent to either S_s or S_n)

Q_s Integrated sediment transport (m^3/s) across the boundary

$q^e_{s,i}$ Sediment transport capacity rate (m^2/s) at point *i* on the boundary line

n Number of grid points on the boundary line

Δx_i Spacing between grid points along the boundary (equivalent to either Δs or Δn)

The sediment transport capacity (also called equilibrium sediment transport, because the sediment transport is in equilibrium with local hydraulic conditions) is calculated explicitly from the applied sediment transport formula. The specified sediment transport may be greater (or less) than the sediment transport capacity. If this is the case, erosion (or deposition) will take place just at the boundary line.

No distinction is made between suspended load and bed load when specifying the sediment transport boundary condition, as it is applied directly in Eq. (4.1) or Eq. (4.2). However, the suspended sediment model requires a separate boundary condition for concentration when solving the advection-dispersion equation describing the transport of suspended sediment.

This boundary condition for concentration is calculated automatically from the bed load and total sediment transport in the following way:

$$q_{s,sus} = q_s - q_{s,bed} \tag{4.7}$$

$$C = \frac{q_s - q_{s,bed}}{q} \cdot \rho_s \cdot 10^3 \tag{4.8}$$

Where

$q_{s,sus}$ Actual suspended sediment transport rate (m^2/s) at point *i*

$q_{s,bed}$ Bed load sediment transport rate (m^2/s) at point *i*

C Mass concentration of suspended sediment (g/m^3)

q Water flux (m^2/s) at point i

ρ_s Sediment bulk density (kg/m^3)

The actual bed load transport is the same as the bed load sediment transport capacity calculated from the local hydraulic conditions. Only suspended sediment can have over or under loading of sediment due to the time and space lag. This means that if a boundary

condition that exceeds the total sediment transport capacity is specified, the extra sediment will enter the model as additional suspended sediment.

4.1.2 Bed level change boundary

If the boundary condition is specified as a $\partial z/\partial t$ condition Eq. (4.2) is not solved, as the specified boundary condition can be used directly to calculate the new bed level at the boundary.

Also in this case, a separate boundary condition for mass concentration is required in order to solve the advection-dispersion equation for suspended sediment transport. The boundary condition is derived in the following way:

$$C = C^e + \frac{\partial z}{\partial t} \cdot \frac{\Delta y}{86400 \cdot q} \tag{4.9}$$

Where

C	Mass concentration of suspended sediment (g/m^3)
C^e	Equilibrium concentration of suspended sediment (g/m^3)
$\partial z/\partial t$	Specified rate for bed level change (m/day)
86400	Number of seconds per day
q	Water flux (m^2/s) at point *i*
Δy	Spacing (m) between grid points across the boundary

The relationship is based on the assumption that bed load transport is always in local equilibrium and that sediment continuity is preserved. A specified increase in bed level at the boundary therefore involves an overload of suspended sediment at the boundary. As with a sediment transport boundary condition, the specified value is used directly in the sediment continuity equation and the above formula is used only when specifying boundary conditions for the suspended load sub-model.

4.1.3 Flood and dry points

Points that are shallow and subject to flooding and drying require special treatment in the numerical model.

In the hydrodynamic model, a flooding depth and a drying depth are applied to handle hydraulic conditions with varying water stages and consequently different extents of flooded areas:

- Dry depth: When the local water depth becomes less than this, the point is land.
- Flood depth: When the local water depth becomes greater than this, the point is wet.

To ensure stability of the hydrodynamic model it is necessary to give a finite value of the dry and flood depth (normally between 0.2 and 0.6 m). Furthermore, it is usually necessary to have a small difference between dry depth and flood depth values to avoid alternating swapping, which can lead to instability.

In shallow water the characteristics of the morphological changes becomes slightly different to those in deeper water. Drainage channel forms are generally much smaller than the main

channels and therefore require more detailed model resolution. However, these have little influence on the overall morphology and are excluded.

The approach adopted is that no sediment transport occurs over dry grid cells, and that the bed level does not change unless grid cells are wet. The only restraint is that grid points along open boundaries must always be either constantly flooded or constantly dried. However, if the quasi-steady flow solver is used to solve the hydrodynamics, the model does allow open boundary cells to wet and dry during the simulation.

4.1.4 Availability of sediment

The model can be used for applications with reduced availability of sediment. An example of this is when scouring occurs down to bedrock.

For rivers with a normal sandy bed, there is no need to use this facility. If required, an initial layer thickness of the sediment on the bed is specified by a constant or a map.

4.2 Bank Erosion

The sediment transport model can include bank erosion in the continuity equation:

$$E_b = -\alpha \cdot \frac{\partial z}{\partial t} + \beta \cdot \frac{S}{h} + \gamma \tag{4.10}$$

Where

E_b	Bank erosion rate in m/s
z	Local bed level
S	Near bank sediment transport
h	Local water depth
α, β, γ	Calibration coefficients specified in the model

The extra sediment released when bank erosion occurs contributes to the sediment balance of Eq. (4.1). The contribution is obtained from the relation:

$$\Delta S_e = \frac{E_b \cdot (h + h_b)}{\Delta n} \tag{4.11}$$

Where

h_b	Height of the bank above the water level
Δn	Width of cell next to bank line

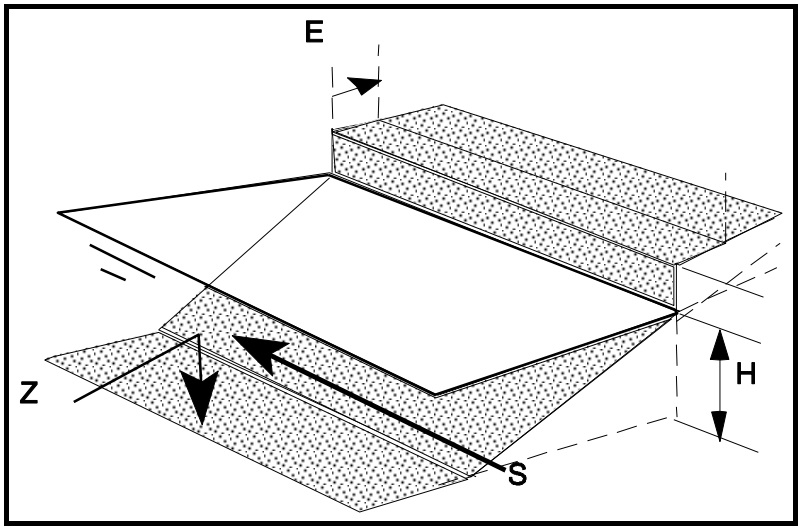

Figure 4.3 Sketch of bank erosion

The near bank slope dependency is included in the first term. The dependency upon the near bank shear stress exerted from the river flow is implicitly included in the second term. The last term γ, represents a constant erosion rate, which is independent of the hydraulic conditions.

The first term is based on the assumption that the shape of the transverse bed profile is preserved. Therefore, from geometrical considerations the bank erosion rate is proportional to the bed erosion. The α-coefficient corresponds to the transverse bed slope at the bank. Transverse bed slopes in natural rivers are typically of the order of 5-20 along eroding banks. This means that the α-coefficient should be chosen in the range from 0 to 20.

The second term is derived by considering that the eroded material E_b, is moved downstream by the flow determined sediment transport rate S, or at least a fraction β of it. This means that the β-coefficient should be chosen in the range from 0 to 1. Note that the bank erosion module assumes that the bank material is the same as the sediment on the river bed.

Observed bank erosion rates are used to calibrate the coefficients α and β. If no evidence for a relationship to $\partial z/\partial t$ or to S is found, it is possible to specify a constant bank erosion rate γ.

Bank erosion is computed at every time step, and the debris is included in the sediment continuity equation along the bank, see Eq. (4.1). If the accumulated bank erosion at a certain location exceeds a predefined critical width (related to the width of a computational grid cell along the bank), the curvilinear grid is updated with new bank lines. This implies the following steps in the model:

- Generation of a new orthogonal grid based on the new bank lines.
- Recalculation of grid parameters, such as space step Δs, Δn, and radius of curvature of grid lines R_s and R_n.
- Transformation of the model bathymetry from the old to the new curvilinear grid.

- Initialisation of accumulated bank erosion record, (which is being used to test, when grid updating is required).

Updating of the plan form can be excluded if bank erosion only influences the morphological development very close to the eroding bank and not the overall hydraulics.

4.3 Linear Stability Analysis

In order to understand the physical background for the output from the morphological model, it is useful to carry out a stability analysis on the flow and sediment transport equations. A very brief introduction is presented below. For more detailed information, see (among others) Olesen (1987).

The methodology is as follows:

- The length scale associated with the two-dimensional (depth-averaged) flow is derived.
- The length scale associated with the morphology of the riverbed is derived.
- In order to obtain length scales steady state flow conditions are assumed.
- Finally, the two approaches are combined to derive the overall morphological behaviour of the river from the linearised equations.

The momentum equation in the longitudinal direction is given by:

$$\frac{1}{\rho}\frac{\partial P}{\partial s} + u\frac{\partial u}{\partial s} + v\frac{\partial u}{\partial n} + \frac{g}{hC^2}u\,|\bar{u}| = 0 \tag{4.12}$$

Eq. (4.12) is linearised by considering all dependent variables as a sum of the mean value and a fluctuation (perturbation):

$$u = u_0 + u' \tag{4.13}$$

$$v = v_0 + v' \tag{4.14}$$

$$P = P_0 + P' \tag{4.15}$$

$$h = h_0 + h' \tag{4.16}$$

If Eqs. (4.13) - (4.16) are inserted into Eq. (4.12) we get:

$$\frac{1}{\rho}\frac{\partial(P_0+P')}{\partial s} + (u_0+u')\frac{\partial(u_0+u')}{\partial s} + (v_0+v')\frac{\partial(u_0+u')}{\partial n} + \frac{g}{(h_0+h')C^2}(u_0+u')\sqrt{(u_0+u')^2+(v_o+v')^2} = 0 \tag{4.17}$$

Ignoring terms of higher order than one and assuming that $v_0 = 0$ (we consider flow along a streamline), Eq. (4.17) yields:

$$\frac{1}{\rho}\frac{\partial(P_0+P')}{\partial s}+u_0\frac{\partial(u_0+u')}{\partial s}+u'\frac{\partial u_0}{\partial s}+v'\frac{\partial u_0}{\partial n}\frac{gu_0^2}{(h_0+h')C^2}+\frac{g}{h_0\,C^2}u_0u'=0 \tag{4.18}$$

The fifth term in Eq. (4.18) is made linear, by:

$$\frac{gu_0^2(h_0-h')}{(h_0+h')(h_0-h')C^2}=\frac{gu_0^2(h_0-h')}{h_0^2\,C^2} \tag{4.19}$$

If Eq. (4.19) is inserted into Eq. (4.18) and time-averaged, the sum of the zero order terms are equal to zero and can be cancelled. This yields the following linear differential equation for the perturbations:

$$\frac{1}{\rho}\frac{\partial P'}{\partial s}+u_0\frac{\partial u'}{\partial s}+\frac{2g}{h_0C^2}u_0u'-\frac{gu_0^2}{h_0^2\,C^2}\cdot h'=0 \tag{4.20}$$

Assume that pressure force is insignificant. This means that the derived equations are only valid for friction dominated flow controlled by flow inertia and bed resistance. Eq. (4.20) now yields:

$$\lambda_w\cdot\frac{\partial u'}{\partial s}+u'-\frac{1}{2}\frac{u_0}{h_0}h'=0 \tag{4.21}$$

Where the length scale λ_w is given by:

$$\lambda_w=\frac{h_0C^2}{2g} \tag{4.22}$$

The parameter λ_w is a measure of the length scale for adaptation of the flow field to changes in the bed topography, see the example sketched in Figure 4.4.

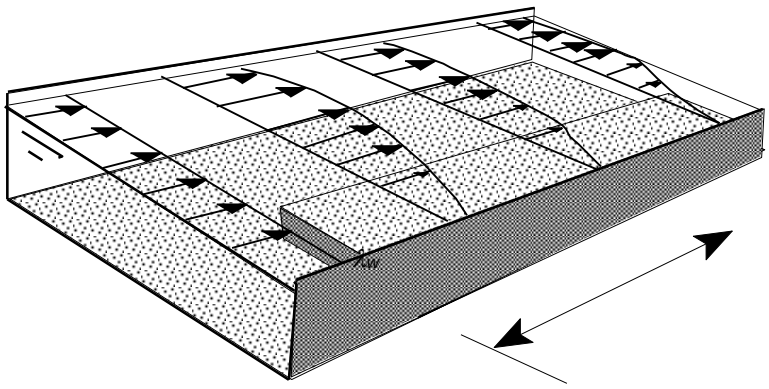

Figure 4.4 Adaptation of flow field due to changes in bed topography and definition of adaptation length λ_w

The length scale is important in different ways. If a shallow bar is developing, the inertia of the flow tends to smooth the riverbed, while the friction force enhances further growth of the bar. In numerical terms, the velocity over the shallow grid points can either increase because water depth is reduced and the same flux has to cross, or the velocity can decrease because flow is deflected away from the bar.

Not unexpected, the length scale for adaptation is proportional to the local depth. The bed resistance represented by the Chezy number also influences the length scale. In case of high bed resistance over a bar (low Chezy number), the length scale is small and flow is easily deflected. For the opposite case (low bed resistance), the adaptation length scale is much larger (or the intensity of flow deflection is much weaker).

Formations on the riverbed are governed not only by the flow hydraulics, but also of the sediment transport and the sediment continuity equation:

$$\frac{\partial S_s}{\partial s} + \frac{\partial S_n}{\partial n} = 0 \tag{4.23}$$

Eq. (4.23)is based on sediment transport rates defined in a curvilinear coordinate system that follows the stream line *s* of the fluid. The transverse sediment transport rate S_n is determined by the strength of the helical flow and the transverse bed slope, see Eq. (3.67) Section 3.2:

$$S_n = S_s \cdot \left(\frac{v}{u} + G \cdot \theta^{-a} \cdot \frac{\partial h}{\partial n} \right) \tag{4.24}$$

As an approximation the sediment transport along the streamline is now assumed to depend on the relation:

$$S_s = a_1 u^b \tag{4.25}$$

Where the proportionality factor, a_1 and the exponent, *b* is assumed constant. Taking the derivative of Eq. (4.25) with respect to the curvilinear coordinate *s*, we obtain:

$$\frac{\partial S_s}{\partial s} = b \cdot \frac{S_s}{u} \cdot \frac{\partial u}{\partial s} \tag{4.26}$$

If the influence of the Shields parameter θ in Eq. (4.24) is neglected, and Eqs. (4.23), (4.24) and (4.26) is combined and linearised the following equation can be obtained:

$$b \cdot \frac{\partial u'}{\partial s} + \frac{\partial v'}{\partial n} + u_0 G \frac{\partial^2 h'}{\partial h^2} = 0 \tag{4.27}$$

The continuity equation for the fluid, yields:

$$\frac{\partial h \cdot u}{\partial s} + \frac{\partial h \cdot v}{\partial n} = 0 \tag{4.28}$$

Rewritten in a linearised form Eq. (4.28) reads:

$$u_0 \frac{\partial h'}{\partial s} + u_0 \frac{\partial v'}{\partial n} + h_0 \frac{\partial u'}{\partial s} = 0 \tag{4.29}$$

Combining Eqs. (4.27) and (4.29) results in the following coupled differential equation:

$$\frac{\partial h'}{\partial s} - G \cdot h_0 \cdot \frac{\partial^2 h'}{\partial n^2} = \frac{h_0}{u_0} \cdot (b-1) \cdot \frac{\partial u'}{\partial s} \tag{4.30}$$

In addition to the differential of Eq. (4.30), there is a boundary condition. For the case with a sinusoidal variation of the depth across the upstream boundary, a solution can be written in the form:

$$h' = \exp\left[i \frac{\pi}{w} \cdot n \right] \cdot f(s) \tag{4.31}$$

Where

i	Imaginary number
w	Width of the river
n	Transverse coordinate
s	Longitudinal coordinate

By substitution Eq. (4.30) becomes:

$$\lambda_s \cdot \frac{\partial h'}{\partial s} + (h' - h_{h'd}) = 0 \tag{4.32}$$

Where the coupling to the hydrodynamics is defined through the parameter:

$$h_{h'd} = \lambda_s (b-1) \frac{h_0}{u_0} \cdot \frac{\partial u'}{\partial s} \tag{4.33}$$

While the length scale for changes of the bed disturbance is given by:

$$\lambda_s = \frac{1}{\pi^2} \left(\frac{w}{h} \right)^2 \frac{h_0}{G} \tag{4.34}$$

The solution of Eq. (4.32) is:

$$h' = \exp\left[\frac{i\pi}{w} n \right] \cdot \exp\left[-\frac{s}{\lambda_s} \right] \tag{4.35}$$

An example of the solution is sketched in Figure 4.5.

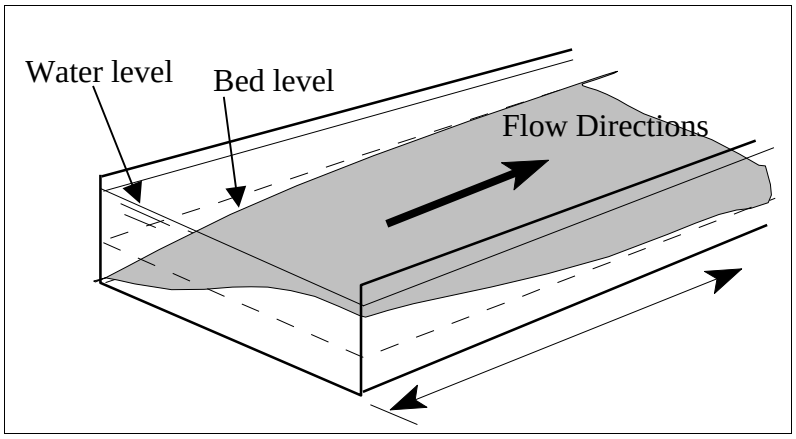

Figure 4.5 Adaptation of bed topography due to changes imposed on hydrodynamics

The adaptation length λ_s indicates the distance downstream that any disturbance can be felt, before it has been levelled out due to the sediment transport. The transverse bed slope factor *G* which, in combination with the strength of the helical flow, controls the bed shear stress deviation (and thus the sediment transport direction), is seen to be quite important for the adaptation length scale. In theory, the length scale would become infinite if the bed shear stress direction was unaffected by the transverse slope of the river bed. Without this, any disturbance would remain. For a large value of *G*, with strong deviation of bed shear stress mainly related to gravity effects on a transverse bed slope, the adaptation length will be short and disturbances will quickly disappear.

As seen from Eq. (4.34), the aspect ratio (width/depth ratio) is as well as the depth alone important to the value of the length scale. In fact, the imposed boundary condition of the present solution determines the importance of w/h.

If Eq. (4.33) is inserted into the equation for the response of bed topography to disturbances in flow field, Eq. (4.32), then differentiated with respect to *s*, we obtain:

$$\lambda_s \frac{\partial^2 h'}{\partial s^2} + \frac{\partial h'}{\partial s} - \lambda_s (b-1) \frac{h_0}{u_0} \frac{\partial^2 u'}{\partial s^2} = 0 \tag{4.36}$$

The equation for the response of flow field to changes in bed topography, Eq. (4.21), is also differentiated with respect to *s*:

$$\lambda_w \frac{\partial^2 u'}{\partial^2 s} + \frac{\partial u'}{\partial s} - \frac{u_0}{2h_0} \frac{\partial h'}{\partial s} = 0 \tag{4.37}$$

The $\frac{\partial u'}{\partial s}$ term is isolated from Eq. (4.32) (with Eq. (4.33) inserted) and the $\frac{\partial^2 u'}{\partial s^2}$ term from Eq. (4.36) substitutet into Eq. (4.37). We obtain the equation:

$$\lambda_w^2 \frac{\partial^2 h'}{\partial s^2} - \lambda_w \cdot \left(\frac{b-3}{2} - \frac{\lambda_w}{\lambda_s} \right) \cdot \frac{\partial h'}{\partial s} + \frac{\lambda_w}{\lambda_s} \cdot h' = 0 \tag{4.38}$$

The solution to Eq. (4.38) is complex, and given by:

$$\frac{h'}{h_0} = -\overline{h_j} \cdot \exp\left[i \cdot \left(\overline{k_j} \cdot s + \frac{\pi}{w} \cdot n \right) \right] \tag{4.39}$$

Where

j Solution number, for a second order differential equation two roots exists.

The complex wave number is divided into a real part representing the wavelength, and an imaginary part representing the damping of the wave:

$$\overline{k} = k_r + \cdot k_i \tag{4.40}$$

Substitution of Eq. (4.39) into Eq. (4.37) gives a polynomial equation to determine the wave numbers:

$$\left(\overline{k}\,\lambda_w\right)^2 + i \cdot \left(\overline{k}\,\lambda_w\right) \cdot \left(\frac{b-3}{2} - \frac{\lambda_w}{\lambda_s} \right) - \frac{\lambda_w}{\lambda_s} = 0 \tag{4.41}$$

The complex determinant is:

$$D = \lambda_w^2 \cdot \left(4\frac{\lambda_w}{\lambda_s} - \left[\frac{b-3}{2} - \frac{\lambda_w}{\lambda_s} \right]^2 \right) \tag{4.42}$$

Eq. (4.41) has the complex solution:

$$\overline{k}\,\lambda_w = -i \cdot \frac{1}{2} \cdot \left(\frac{b-3}{2} - \frac{\lambda_w}{\lambda_s} \right) \pm \sqrt{\frac{\lambda_w}{\lambda_s} - \frac{1}{4} \cdot \left(\frac{b-3}{2} - \frac{\lambda_w}{\lambda_s} \right)^2} \tag{4.43}$$

For $\frac{\lambda_w}{\lambda_s} > \left(\frac{b-3}{4} - \frac{\lambda_w}{2\lambda_s} \right)$ the real part of the wave number is determined by:

$$k_r\,\lambda_w = \sqrt{\frac{\lambda_w}{\lambda_s} - \left(\frac{b-3}{4} - \frac{\lambda_w}{2\lambda_s} \right)^2} \tag{4.44}$$

While the imaginary part of the wave number is:

$$k_i\,\lambda_w = \frac{\lambda_w}{2\lambda_s} - \frac{b-3}{4} \tag{4.45}$$

The solution is sketched in Figure 4.6.

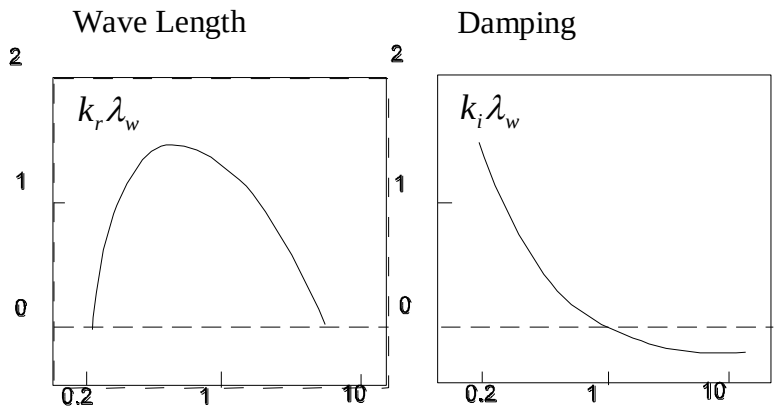

Figure 4.6 Sketch of wavelength, k_r and wave damping, k_i as function of the ratio between the length scales λ_w/λ_s

For $\lambda s/\lambda w$ greater than 1, the solution becomes unstable as the damping becomes negative, and the assumptions adopted during linearisation of the equations are no longer valid.

4.4 Alluvial Resistance

The Chezy number or the Manning number can be updated in two ways, either as a simple function of depth or as a function of computed dune dimensions.

The update according to depth is done in the following manner:

$$C = A \cdot h^b \tag{4.46}$$

Where:

A	Resistance coefficient
b	Resistance exponent

Application of varying bed resistance affects the simulated scour and deposition pattern. With resistance update included, flow is deflected more over shallow parts and sediment transport will increase due to the larger bed shear stresses. In general, this will reduce the overshoot effects of beginning bed scour and the topography of a point bar crest becomes more rounded, as reported by Talmon (1992).

4.5 Supply Limited Sediment Transport

Supply limited sediment transport means that the local sediment transport capacity is calculated as the product of local sediment layer thickness relative to an equilibrium layer thickness and the sediment transport capacity calculated from the selected formula. Supply limited sediment transport is activated when there is one bed layer of sediment instead of the default of zero. The sediment transport formula is altered to:

$$S = f\left(\frac{\Delta}{\Delta_{eq}}\right) S_{cap} \tag{4.47}$$

Which is a scaling of the sediment transport, S, relative to capacity, S_{cap}. The scaling is done by the function f and the sediment layer thickness Δ relative to the layer thickness that has been specified for full capacity, Δ_{eq}. When $\Delta < \Delta_{eq}$ the sediment transport will be below capacity, and the f-function is simply Δ/Δ_{eq}. There is no impact on the sediment load when the layer thickness is higher than the capacity thickness.

The equilibrium layer thickness is calculated as a fraction of the water depth, default being $\Delta_{eq} = h/12$. $h/12$ is used because dune height typically corresponds to 1/6 of the water depth. In addition to the equilibrium layer thickness relative to the water depth, a minimum and maximum value for the equilibrium thickness can be specified. By selecting the same value for the minimum and maximum, a constant layer thickness can be specified. Note that very thin layers of sediment can move very fast over a riverbed, and hence require low morphological time-steps.

The supply limited sediment transport model can be used for modelling a thin layer of sediment, such as in sewers, on top of an armoured riverbed, or of non-erodible features in a model area. The supply-limited model keeps track of the local layer thickness, and is thus able to reproduce thin sediment layers that facilitate transport in such cases. There are two main applications of the supply limited sediment transport model:

4.5.1 Local non-erodible areas

An example is a vegetation-covered island located in a river, which can be represented by using supply limited sediment transport. A map of initial sediment layer thickness can be specified, where layer thickness is zero on the island and has a very high number elsewhere, e.g. 100 m. This means that the island cannot be eroded, but additional sediment can deposit on the island (and be subsequently re-eroded).

4.5.2 Supply to the morphological system is lower than the sediment transport capacity

This is the most important application of the supply-limited model. Here the sediment will form a varying layer on an armoured riverbed (or concrete pipe). Layer thickness is determined by the incoming sediment supply. This is important in armoured rivers and can be used in such rivers for modelling of sandbars.

5 Quasi-Steady HD Solver

The theoretical background for the quasi-steady HD solver in MIKE 21C is described. The solver is a predictor-corrector algorithm that originates from methods for incompressible fluid flow.

Quasi-steady flow is where flow conditions vary slowly. An example is a long term flood (weeks to months), where relatively gradual changes in flow regime occurs. A dynamic solver has restrictions limiting the length of the timestep, which can make long term simulation computationally frightening. The quasi-steady solver is designed to perform simulations using a much longer timestep than a dynamic solver, thus reducing computational effort.

The solver uses a semi-implicit method for the continuity equation. Increasing the timestep means that surface wave celerity is substantially increased in the calculation.

The reason why the system reacts the way it does, is the dynamic term in the continuity equation. For a stationary solution we know very well that the term is zero, so why do we take the term into account at all? Well, the design of the MIKE 21 engine does not allow the removal of the dynamic term because it is the only link between the pressure and the continuity equation. If the term is removed, it becomes difficult to use the continuity equation for obtaining the pressure.

If the dynamic term is removed, it demands the use of a completely different solution strategy, namely one that allows the pressure to be determined from the continuity equation. In incompressible fluid flows, the continuity equation is actually exactly like how it would look for MIKE 21, if the dynamic term were removed. For incompressible flow, advanced solution methods have been developed and they include schemes such as SIMPLE, SIMPLER and PISO. Refer to Patankar (1980) for an overview and to Michelsen (1989) for details about the method applied herein.

5.1 Governing Equations

The depth integrated flow equations are given by:

$$\frac{dp}{dt} + gh\frac{\partial s}{\partial x} + \frac{gp\sqrt{p^2+q^2}}{C^2h^2} = \frac{\partial}{\partial x}\left(E\frac{\partial(p/h)}{\partial x}\right) + h\frac{\partial}{\partial y}\left(E\frac{\partial(p/h)}{\partial y}\right) \tag{5.1}$$

$$\frac{dq}{dt} + gh\frac{\partial s}{\partial y} + \frac{gq\sqrt{p^2+q^2}}{C^2h^2} = h\frac{\partial}{\partial x}\left(E\frac{\partial(q/h)}{\partial x}\right) + h\frac{\partial}{\partial y}\left(E\frac{\partial(q/h)}{\partial y}\right) \tag{5.2}$$

$$\frac{\partial h}{\partial t} + \frac{\partial p}{\partial x} + \frac{\partial q}{\partial y} = 0 \tag{5.3}$$

In Eqs. (5.1) and (5.2) the total time derivative is given by:

$$\frac{d}{dt} = \frac{\partial}{\partial t} + \frac{\partial}{\partial x}\frac{p}{h} + \frac{\partial}{\partial y}\frac{q}{h} \tag{5.4}$$

The original solver is based on the work of Michelsen (1989), and it was originally applied for incompressible flow. 2D depth-integrated flow is equivalent to compressible 2D flow, and the extension of the solver to compressible flow is fairly straightforward. In principle, one could omit the dynamic term already at this point and only work with the stationary continuity equation. However, for some cases, it is wise to have the dynamic term and by keeping it the solver is in principle also applicable for dynamic solutions.

The Smagorinsky viscosity formulation yields the viscosity from the following expression:

$$E = C_S^2 \Delta^2 \sqrt{\left(\frac{\partial u}{\partial x}\right)^2 + \left(\frac{\partial v}{\partial y}\right)^2 + \left(\frac{\partial u}{\partial y} + \frac{\partial v}{\partial x}\right)^2} \tag{5.5}$$

Otherwise the eddy viscosity is given as a constant or as function of space, i.e. $E(j,k)$. The Smagorinsky formulation can be useful in some cases, but for most applications in rivers, we have experienced that the eddy viscosity does not have a large role to play.

5.2 Curvilinear Transformations

Using scalar transformation rules does the transformation of the flow equations to curvilinear coordinates. In reality the velocity field is a vector, but if vector transformation is applied, the equations become more complex. The velocity field is simply kept in the Cartesian base also for the curvilinear equations. When the scalar transformation rules are applied, the transformed equation will not have any curvature terms, which is a major advantage because these tend to be difficult to handle due to their complexity. MIKE 21C uses vector-transformed velocities in its original engine.

When working with a Cartesian base velocity field, the staggering of the velocity field has to be omitted as it can never be guaranteed that the velocity will be pointing in the grid direction. All variables will be allocated in cell centres for the quasi-steady solver.

5.2.1 Transformation rules

The transformation between rectangular and general coordinates is quite simple to derive. Basically, the Cartesian values of the coordinates are functions of the general coordinates, i.e.:

$$x = x(\xi, \eta) \tag{5.6}$$

$$y = y(\xi, \eta) \tag{5.7}$$

A transported property is thus given as a function of:

$$\phi(x, y) = \phi(x(\xi, \eta), y(\xi, \eta)) \tag{5.8}$$

The differentiation of the dependent variable is thus:

$$\frac{\partial f}{\partial \xi} = x_\xi \frac{\partial f}{\partial x} + y_\xi \frac{\partial f}{\partial y} \tag{5.9}$$

$$\frac{\partial f}{\partial \eta} = x_\eta \frac{\partial f}{\partial x} + y_\eta \frac{\partial f}{\partial y} \tag{5.10}$$

This linear system of equations can be solved in order to obtain the expressions for the derivatives with respect to x and y, yielding:

$$J \frac{\partial}{\partial x} = y_\eta \frac{\partial}{\partial \xi} - y_\xi \frac{\partial}{\partial \eta} \tag{5.11}$$

$$J \frac{\partial}{\partial y} = x_\xi \frac{\partial}{\partial \eta} - x_\eta \frac{\partial}{\partial \xi} \tag{5.12}$$

Where J is the Jacobian (the cell volume, or the cross product of the direction vectors)

$$J = x_\xi y_\eta - x_\eta y_\xi \tag{5.13}$$

These can also be used in conservation form, i.e. with the derivatives under the parentheses. The conservative form is used in most cases, but in a few cases the non-conservative is applied. This holds for the inner derivative in the diffusion terms.

It is from the above expressions that all the terms in the equations are transformed.

The dynamic acceleration and bed friction terms are unaffected by the curvilinear transformation.

5.2.2 Transformed convection

The following operator describes the convection terms:

$$C(\phi) = \frac{\partial}{\partial x}\left(\frac{p}{h}\phi\right) + \frac{\partial}{\partial y}\left(\frac{q}{h}\phi\right) \tag{5.14}$$

If the conservative transformation rule is applied directly, we obtain:

$$J\,C(\phi) = \frac{\partial}{\partial \xi}\left[\frac{y_\eta p - x_\eta q}{h}\phi\right] + \frac{\partial}{\partial \eta}\left[\frac{x_\xi q - y_\xi p}{h}\phi\right] \tag{5.15}$$

It is noted that the terms in the parentheses are proportional to the velocities in the grid directions. They are in fact the discharges through the cell faces. The two terms are used internally in the code because they appear in many connections.

If we define the two fluxes *P* and *Q*, by:

$$P = y_\eta p - x_\eta q \tag{5.16}$$

$$Q = x_\xi q - y_\xi p \tag{5.17}$$

The convection terms can be written:

$$J\,C(\phi) = \frac{\partial}{\partial \xi}\left[\frac{P}{h}\phi\right] + \frac{\partial}{\partial \eta}\left[\frac{Q}{h}\phi\right] \tag{5.18}$$

Eq. (5.18) is a fundamental form for the convection terms. If the water depth is constant, the expression becomes:

$$Vol\,C(\phi) = \frac{\partial P\phi}{\partial \xi} + \frac{\partial Q\phi}{\partial \eta} \tag{5.19}$$

5.2.3 Pressure gradients

The pressure gradients do not yield the same logic forms as the transport terms do. The pressure gradients are found directly by using the non-conservative form of the transformation rule:

$$J\,gh\frac{\partial s}{\partial x} = gh\left(y_\eta \frac{\partial s}{\partial \xi} - y_\xi \frac{\partial s}{\partial \eta}\right) \tag{5.20}$$

$$J\,gh\frac{\partial s}{\partial y} = gh\left(x_\xi \frac{\partial s}{\partial \eta} - x_\eta \frac{\partial s}{\partial \xi}\right) \tag{5.21}$$

These cannot be reduced, because the flow in the Cartesian x-direction will necessarily depend on the pressure gradient in the x-direction, which in general will be a function of the pressure gradients in both grid directions. If a grid-aligned base had been used for the velocity field, the pressure gradients would be in the grid directions only, as is already the case in the original engine of MIKE 21C. It is the presence of both pressure gradients in both momentum equations that first of all prohibits the use of staggered grids. The staggered allocation only makes sense when the staggered velocity/flux can be directly tied to the pressure gradient over the cell face.

5.2.4 Transformed diffusion

A diffusion term looks in general like:

$$D(\phi) = h\frac{\partial}{\partial x}\left(E\frac{\partial(\phi/h)}{\partial x}\right) + h\frac{\partial}{\partial y}\left(E\frac{\partial(\phi/h)}{\partial y}\right) \tag{5.22}$$

The transformation is straightforward, though it requires some algebra. The inner derivatives are transformed by using the non-conservative form, while the outer derivatives are transformed using the conservative form. The transformed operator becomes:

$$D(\phi) = h\frac{\partial}{\partial \xi}\left(E\frac{y_\eta^2 + x_\eta^2}{J}\frac{\partial \phi/h}{\partial \xi}\right) + h\frac{\partial}{\partial \eta}\left(E\frac{x_\xi^2 + y_\xi^2}{J}\frac{\partial \phi/h}{\partial \eta}\right) \tag{5.23}$$

During the process of obtaining this expression, some terms have vanished due to orthogonality. Eq. (5.23) now expresses diffusion in the (ξ,η) system. It is seen that, it is much like the original expression. The geometric terms that appear are cell face lengths, so it is in fact a more fundamental form of the diffusion term, which is due to the general coordinates.

It is natural to introduce the diffusion coefficients:

$$D_\xi = E\frac{y_\eta^2 + x_\eta^2}{J} \tag{5.24}$$

$$D_\eta = E\frac{x_\xi^2 + y_\xi^2}{J} \tag{5.25}$$

By use of Eqs. (5.24) and (5.25) the diffusion term can be written:

$$D(\phi) = h\frac{\partial}{\partial\xi}\left(D_\xi\frac{\partial\phi/h}{\partial\xi}\right) + h\frac{\partial}{\partial\eta}\left(D_\eta\frac{\partial\phi/h}{\partial\eta}\right) \tag{5.26}$$

5.2.5 Momentum equations

The transformed momentum equations can now be written as:

$$J\frac{\partial p}{\partial t} + \left(\frac{Pp}{h}\right)_\xi + \left(\frac{Qp}{h}\right)_\eta + gh(y_\eta s_\xi - y_\xi s_\eta) = h\left(D_\xi\left(\frac{p}{h}\right)_\xi\right)_\xi + h\left(D_\eta\left(\frac{p}{h}\right)_\eta\right)_\eta \tag{5.27}$$

$$J\frac{\partial q}{\partial t} + \left(\frac{Pq}{h}\right)_\xi + \left(\frac{Qq}{h}\right)_\eta + gh(x_\xi s_\eta - x_\eta s_\xi) = h\left(D_\xi\left(\frac{q}{h}\right)_\xi\right)_\xi + h\left(D_\eta\left(\frac{q}{h}\right)_\eta\right)_\eta \tag{5.28}$$

5.2.6 Continuity equation

The transformation of the continuity equation is straightforward. The terms are simply transformed by using the conservation form of the transformation rule for the first order derivative, yielding:

$$J\frac{\partial h}{\partial t} + \frac{\partial P}{\partial\xi} + \frac{\partial Q}{\partial\eta} = 0 \tag{5.29}$$

Eq. (5.29) may also be seen as the cell volume changes according to how much enters the cell. This is a very simple and fundamental form of the continuity equation.

5.3 Discrete Equations

The discrete forms of the equations are obtained by performing an integration over the cells first.

5.3.1 Time derivative

For the time-derivative, which is written as $J\,\partial\phi/\partial t$, an implicit Euler scheme is applied, i.e.:

$$J\frac{\partial\phi}{\partial t}=\frac{J_P}{\Delta t}(\phi_P^{n+1}-\phi_P^n) \tag{5.30}$$

5.3.2 Convection

The first order upwind scheme will be applied in the present version. First, the operator is written in finite-volume form as:

$$\frac{\partial}{\partial\xi}\left[\frac{P}{h}\phi\right]+\frac{\partial}{\partial\eta}\left[\frac{Q}{h}\phi\right]=\left[\frac{P_e^n\phi_e^{n+1}}{h_e^{n+1}}-\frac{P_w^n\phi_w^{n+1}}{h_w^{n+1}}\right]+\left[\frac{Q_n^n\phi_n^{n+1}}{h_n^{n+1}}-\frac{Q_s^n\phi_s^{n+1}}{h_s^{n+1}}\right] \tag{5.31}$$

The scheme is semi-implicit. For the cell face discharges and water depth old values are used, while the convected variable is taken implicitly. The key in Eq. (5.31) is to find the four cell face values of ϕ. With the upwind scheme it is done by:

$$\phi_e=\begin{cases}\phi_P & P_e>0\\ \phi_E & P_e<0\end{cases} \tag{5.32}$$

and so forth.

5.3.3 Pressure gradients

The pressure gradients are written directly as:

$$S_p=gh\left(y_\eta\frac{\partial s}{\partial\xi}-y_\xi\frac{\partial s}{\partial\eta}\right)=gh_p y_{\eta p}(s_e-s_w)-gh_p y_{\xi p}(s_n-s_s) \tag{5.33}$$

$$S_q=gh\left(x_\xi\frac{\partial s}{\partial\eta}-x_\eta\frac{\partial s}{\partial\xi}\right)=gh_p x_{\xi p}(s_n-s_s)-gh_p x_{\eta p}(s_e-s_w) \tag{5.34}$$

Linear interpolation is used for the evaluation of the pressure at the four cell faces. A special procedure applies, when the neighbouring cell is not a water point.

Please note that the use of linear interpolation leads to central estimates for the pressure gradient. This will lead to instability if something special is not done. Here the so-called “momentum interpolation technique” will be applied. It will be described under the section about pressure correction.

The pressure gradient is calculated in more steps during a time-step. First, it is calculated with old values, and then it is calculated with corrected pressure values, which may continue in the PISO algorithm.

5.3.4 Diffusion term

The diffusion term is given by:

$$J\,D(\phi) = h\frac{\partial}{\partial \xi}\left(D_\xi \frac{\partial \phi / h}{\partial \xi}\right) + h\frac{\partial}{\partial \eta}\left(D_\eta \frac{\partial \phi / h}{\partial \eta}\right) \tag{5.35}$$

This is written in discrete form by using the standard approach of obtaining the fluxes over the cell faces, i.e.:

$$J\,D(\phi) = h_P\left[D\frac{\partial \phi / h}{\partial \xi}\right]_w^e + h_P\left[D\frac{\partial \phi / h}{\partial \eta}\right]_s^n =$$

$$h_P\left[D_e\left(\frac{\phi_E}{h_E} - \frac{\phi_P}{h_P}\right) - D_w\left(\frac{\phi_P}{h_P} - \frac{\phi_W}{h_W}\right)\right] + \tag{5.36}$$

$$h_P\left[D_n\left(\frac{\phi_N}{h_N} - \frac{\phi_P}{h_P}\right) - D_s\left(\frac{\phi_P}{h_P} - \frac{\phi_S}{h_S}\right)\right]$$

Please note that the reference to the diffusion coefficients, D_ξ and D_η, does not have to be done specifically. Whenever a diffusion coefficient is addressed on a cell face, it will be given automatically which one it is from the face.

The discrete diffusion can be written into the fundamental format that will be used for all equations:

$$J\,D(\phi) = a_W\phi_W + a_E\phi_E + a_S\phi_S + a_N\phi_N - a_P\phi_P \tag{5.37}$$

In which:

$$a_W = D_w\frac{h_P}{h_W} \tag{5.38}$$

$$a_E = D_e\frac{h_P}{h_E} \tag{5.39}$$

$$a_S = D_s\frac{h_P}{h_S} \tag{5.40}$$

$$a_N = D_n\frac{h_P}{h_N} \tag{5.41}$$

$$a_P = D_w + D_e + D_s + D_n \tag{5.42}$$

Please note that for a diffusion term in general, the identity $a_P = \Sigma\, a_{nb}$ will be fulfilled. It is a simple consequence of the diffusion only being able to redistribute. For the present case, the identity is not fulfilled because the diffusion does not redistribute flux; it redistributes

momentum. It is seen that, if the water depth is constant, the identity will be fulfilled. The above approach is also used in MIKE 21C, where it has been implemented implicitly. If the depth dependency is omitted, the so-called flux-based viscosity emerges. It is the experience with MIKE 21C that the flux-based eddy viscosity produces too unrealistic flow velocity distributions in rivers. Therefore use of the flux-based form should be avoided in general.

5.3.5 Bed friction

The discrete form of bed friction is very simple:

$$J\frac{gp\sqrt{p^2+q^2}}{C^2h^2}=\frac{gJ_P p_P^{n+1}\sqrt{\left(p_P^n\right)^2+\left(q_P^n\right)^2}}{C_P^2\left(h_P^n\right)^2}=Fp_P^{n+1} \tag{5.43}$$

$$J\frac{gq\sqrt{p^2+q^2}}{C^2h^2}=\frac{gJ_P q_P^{n+1}\sqrt{\left(p_P^n\right)^2+\left(q_P^n\right)^2}}{C_P^2\left(h_P^n\right)^2}=Fq_P^{n+1} \tag{5.44}$$

By expressing the term like this, we make sure that the dissipative effect of the bed friction gets to work implicitly. This is crucial for stability, and the implicit method ensures very fine stability as noted by Patankar (1980). The implicit description is also used in MIKE 21.

5.4 Solution Procedure

Having derived all the discrete terms of the momentum equations, we can now write the equations in a standard equation format:

$$\left(a_P+F+\frac{J_P}{\Delta t}\right)p_P^{n+1}=\frac{J_P}{\Delta t}p_P^n+\sum a_{nb}p_{nb}^{n+1}+S_p^n \tag{5.45}$$

$$\left(a_P+F+\frac{J_P}{\Delta t}\right)q_P^{n+1}=\frac{J_P}{\Delta t}q_P^n+\sum a_{nb}q_{nb}^{n+1}+S_q^n \tag{5.46}$$

Where:

a_p	Diagonal contribution from convection and diffusion
F	Implicit bed friction term
$J_p/\Delta t$	Dynamic change contribution
a_{nb}	Neighbour coefficients from convection and diffusion
$S_{p,q}$	Pressure terms, for the predictor step, the old pressure is used

Solving the momentum equations as they are shown above constitutes the predictor step of the present predictor-correct algorithm. The predictor step is simply: Advance the hydrodynamics according to the momentum equations, without taking the continuity equation into account.

5.4.1 Boundary conditions

There are only two types of momentum boundary conditions used in MIKE 21, and these are Dirichlet and homogenous von Neumann conditions. At a discharge boundary, the fluxes in the flow equations will receive Dirichlet conditions, and at a water level boundary, a standard zero gradient condition applies.

Since MIKE 21C uses grid aligned velocities, the direction of the flow at the inlet will also be grid aligned. This means that only one component of the velocity field will be assigned a value at the boundary, the other will be zero. This will not hold in general for a Cartesian base model. However, it is straightforward to derive how the boundary condition should be divided into p and q. The easiest way is to use the cell face discharge field, because it is grid aligned.

$$P = y_\eta p - x_\eta q \tag{5.47}$$

$$Q = x_\xi q - y_\xi p \tag{5.48}$$

When solving this system of equations to obtain p and q, we find:

$$p = \frac{x_\xi P + x_\eta Q}{J} \tag{5.49}$$

$$q = \frac{y_\eta Q + y_\xi P}{J} \tag{5.50}$$

Eqs. (5.49) and (5.50) are used to translate the discharge boundary condition into conditions for p and q. The derivation can also be more detailed.

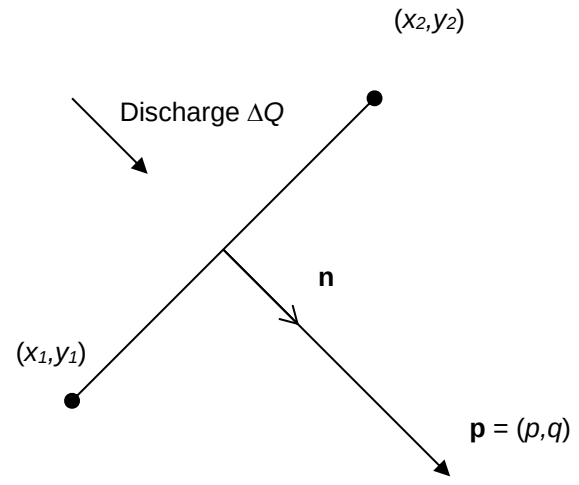

Figure 5.1 Flux through a west boundary cell, calculation of boundary conditions for the Cartesian fluxes from the discharge through the cell at the boundary

The unity normal vector can be expressed from the geometry as:

$$\vec{n} = \frac{(y_\eta, -x_\eta)}{\sqrt{x_\eta^2 + y_\eta^2}} \tag{5.51}$$

Since the direction of the unity normal vector is the same as the direction of the flux vector, we can write:

$$\vec{p} = \frac{\Delta Q \vec{n}}{\sqrt{x_\eta^2 + y_\eta^2}} \tag{5.52}$$

Hereby the two flux components becomes:

$$p = \frac{y_\eta \Delta Q}{x_\eta^2 + y_\eta^2} \tag{5.53}$$

$$q = \frac{-x_\eta \Delta Q}{x_\eta^2 + y_\eta^2} \tag{5.54}$$

5.4.2 Pressure correction algorithm

The power of the present solver lies in the pressure correction algorithm.

The first step in a primitive variable solver like the present is to advance the flux field (p, q) by solving the momentum equations, now written in the form that is used for the solution in the code itself:

$$a_p \, p_P^* = \sum a_{nb} p_{nb}^* + S_p^n + F_p^* \tag{5.55}$$

$$a_p \, q_P^* = \sum a_{nb} q_{nb}^* + S_q^n + F_p^* \tag{5.56}$$

Where

a_p	Diagonal coefficient for convection, diffusion, bed friction and the dynamic term.
a_{nb}	Neighbour coefficients of convection and diffusion
S_p, S_q	Source term, here only consisting of the dynamic term, i.e. no pressure included
F_p, F_q	Source term only containing pressure gradients

The superscript (*) refers to the predicted flux field that has been calculated by marching the momentum equations ahead in time using the pressure field (also superscript *) from the former time-step. The continuity equation will be used as a corrector, which is described in the following.

The (*) pressure terms are given by:

$$F_p^* = -gh_p y_{\eta p}(s_e^* - s_w^*) + gh_p y_{\xi p}(s_n^* - s_s^*) \tag{5.57}$$

$$F_q^* = -gh_p x_{\xi p}(s_n^* - s_s^*) + gh_p x_{\eta p}(s_e^* - s_w^*) \tag{5.58}$$

After having marched the momentum equations ahead in time, the equations are rewritten into a direct expression of the dependency of the flux field on the pressure gradient, i.e.:

$$p_P^{**} = \frac{\sum a_{nb} p_{nb}^{*} + S_p^n + F_p^{**}}{a_p} \tag{5.59}$$

$$q_P^{**} = \frac{\sum a_{nb} q_{nb}^{*} + S_q^n + F_q^{**}}{a_p} \tag{5.60}$$

Where the superscript (**) refers to corrected fluxes and pressure field. The (**) pressure field is found from the pressure equation, which is derived in the following. Before doing so, it is convenient to rewrite the corrector equation into a slightly different form:

$$p_P^{**} = p_p^0 + \frac{F_p^{**}}{a_p} \tag{5.61}$$

$$q_P^{**} = q_p^0 + \frac{F_q^{**}}{a_p} \tag{5.62}$$

Where the superscript (0) flux field denotes a provisory flux field that is basically the correct flux field without contributions from pressure gradients. The provisory flux field is thus likely to be very far from the correct flux field (the pressure gradient being the driving force), but it is convenient to introduce, which one will become apparent, when we insert it into the continuity equation.

The continuity equation is written in discrete form as:

$$J\frac{s_p^{**} - s_p^n}{\Delta t} + \left[y_\eta p - x_\eta q\right]_w^e + \left[x_\xi q - y_\xi p\right]_s^n = 0 \tag{5.63}$$

The expressions for the superscript (**) fluxes are given in the cell centres, whereas the continuity equations requires fluxes at the cell faces. The (**) fluxes on the cell faces can be written:

$$p_e^{**} = p_e^0 - g\left(\frac{h_P}{a_P}\right)_e \left(y_{\eta e}(s_E^{**} - s_P^{**}) - y_{\xi e}(s_{ne}^{**} - s_{se}^{**})\right) \tag{5.64}$$

$$q_e^{**} = q_e^0 - g\left(\frac{h_P}{a_P}\right)_e \left(x_{\xi e}(s_{ne}^{**} - s_{se}^{**}) - x_{\eta e}(s_E^{**} - s_P^{**})\right) \tag{5.65}$$

The pseudo flux has been interpolated directly between the cell centres, while the pressure gradient is written directly at the cell face instead of using interpolation, which gives the dependency of the flux through the cell face directly as a function of the pressure gradient over the cell face. This is termed “momentum interpolation” by Majumdar et al. (1992). On the north faces we find similarly:

$$p_n^{**} = p_n^0 - g\left(\frac{h_P}{a_P}\right)_n \left(y_{\eta n}(s_{ne}^{**} - s_{nw}^{**}) - y_{\xi n}(s_N^{**} - s_P^{**})\right) \tag{5.66}$$

$$q_n^{**} = q_n^0 - g\left(\frac{h_P}{a_P}\right)_n \left(x_{\xi n}(s_N^{**} - s_P^{**}) - x_{\eta e}(s_{ne}^{**} - s_{nw}^{**})\right) \tag{5.67}$$

The fluxes are now used to express the cell face discharges as a function of the cell face pressure gradient, yielding:

$$P_e^{**} = P_e^0 + (x_{\eta e}^2 + y_{\eta e}^2)\left(\frac{gh}{a_P}\right)_e (s_P^{**} - s_E^{**}) \tag{5.68}$$

$$Q_n^{**} = Q_n^0 + (x_{\xi n}^2 + y_{\xi n}^2)\left(\frac{gh}{a_P}\right)_n (s_P^{**} - s_N^{**}) \tag{5.69}$$

The terms involving the pressure gradients calculated from interpolated corner values have vanished, because of grid orthogonality. Due to the fact that the cell face discharges are grid-aligned, they will be dependent only on the pressure gradient across the cell face for orthogonal grids. Michelsen (1989) gives the expressions for the fluxes for non-orthogonal grids. The above equations are the discharge correction equations that express how the discharge should be corrected according to the corrected pressure field.

When the correction equations for the cell face discharges are inserted into the continuity equation, we obtain:

$$\frac{J}{\Delta t}(s_P^{**} - s_P^n) + (P_e^0 - P_w^0) + (Q_n^0 - Q_s^0) +$$

$$(x_{\eta e}^2 + y_{\eta e}^2)\left(\frac{gh}{a_P}\right)_e (s_P^{**} - s_E^{**}) + (x_{\eta w}^2 + y_{\eta w}^2)\left(\frac{gh}{a_P}\right)_w (s_P^{**} - s_W^{**}) + \tag{5.70}$$

$$(x_{\xi n}^2 + y_{\xi n}^2)\left(\frac{gh}{a_P}\right)_n (s_P^{**} - s_N^{**}) + (x_{\xi s}^2 + y_{\xi s}^2)\left(\frac{gh}{a_P}\right)_s (s_P^{**} - s_S^{**}) = 0$$

It is seen that this is a Poisson equation for the pressure correction. Eq. (5.70) is solved with boundary conditions, and the pressure updated. There are only two types of boundary conditions for the pressure equation: 1) water level, where there is a water level boundary and 2) zero flux elsewhere.

5.4.3 Under-relaxation and time-stepping

A dynamic term is kept in all the equations. Dynamic terms are equivalent of under-relaxation terms, which is shown here. The general equation in dynamic form can be written:

$$\left(A_P + \frac{J}{\Delta t}\right)\phi_P^{n+1} = \sum A_{nb}\phi_{nb}^{n+1} + S_P + \frac{J}{\Delta t}\phi_P^n \tag{5.71}$$

The steady form of the equation reads:

$$A_P\phi_P^{n+1} = \sum A_{nb}\phi_{nb}^{n+1} + S_P \tag{5.72}$$

Under-relaxation means that the new value of the transported property can be written as:

$$\phi_P^{n+1} = \omega\frac{\sum A_{nb}\phi_{nb}^{n+1} + S_P}{A_P} + (1-\omega)\phi_P^n \tag{5.73}$$

Hence, it is easily shown that the relation between under-relaxation and dynamic acceleration is:

$$\frac{J}{\Delta t} = \left(\frac{1}{\omega} - 1\right)A_P \tag{5.74}$$

5.4.4 Solution of the linear equations

The linear equations in the quasi-steady solver all have the following form:

$$A_P\phi_P^{n+1} = A_N\phi_N^{n+1} + A_E\phi_E^{n+1} + A_S\phi_S^{n+1} + A_W\phi_W^{n+1} + S_P \tag{5.75}$$

There are two linear equation solvers available in the quasi-steady solver:

- Line successive over relaxation (Line SOR)
- Stone's Strongly Implicit Procedure (SSIP)

In the Line SOR sweeping along lines solves the equations, while SSIP is a more powerful solver, see Stone (1968). The parameters used for the solution of the equations are:

- Solver (Line SOR or SSIP)
- Time-step, Δt
- Maximum number of iterations on the linear system of equations, N
- Stop criterion, ε

The procedure is to perform a single iteration on the system of equations with the linear equation solver. The residual is then calculated as the average error in the steady form of the equation, i.e.:

$$r = \frac{1}{n_{cells}}\sum_{n_{cells}}\left|\frac{A_N\phi_N^{n+1} + A_E\phi_E^{n+1} + A_S\phi_S^{n+1} + A_W\phi_W^{n+1} + S}{A_P} - \phi_P^{n+1}\right| \tag{5.76}$$

This is then compared with the specified stop criterion, and the iteration is stopped if one of the following two conditions is fulfilled:

- The residual becomes lower than the stop criterion, $r < \varepsilon$

- The amount of iterations becomes bigger than *N*

There are separate time-steps for the momentum and pressure equations.

The time-step for the momentum equations is limited by the non-linearity of the momentum equations. The time-step will usually be in the same order of magnitude as that for the standard HD solver.

The pressure time-step can, in most cases, be selected higher than the momentum time-step. The purpose of doing so is to speed up the speed of the surface waves to get quasi-steady solutions faster. Some experimentation is necessary to figure out how high the pressure time-step can be chosen. In some cases it can be chosen as high as an hour with a momentum time-step of 20 seconds, and in other cases it is not possible to set the pressure time-step much higher than the momentum equation time-step.

6 Planform Module

The Planform module of MIKE 21C allows the representation of lateral processes in morphological models. Bank erosion can be calculated and included in the riverbed sediment budget and the curvilinear grid can be updated to account for the movement in the bank line. This is handled by using the grid generator for a specified local area of the grid.

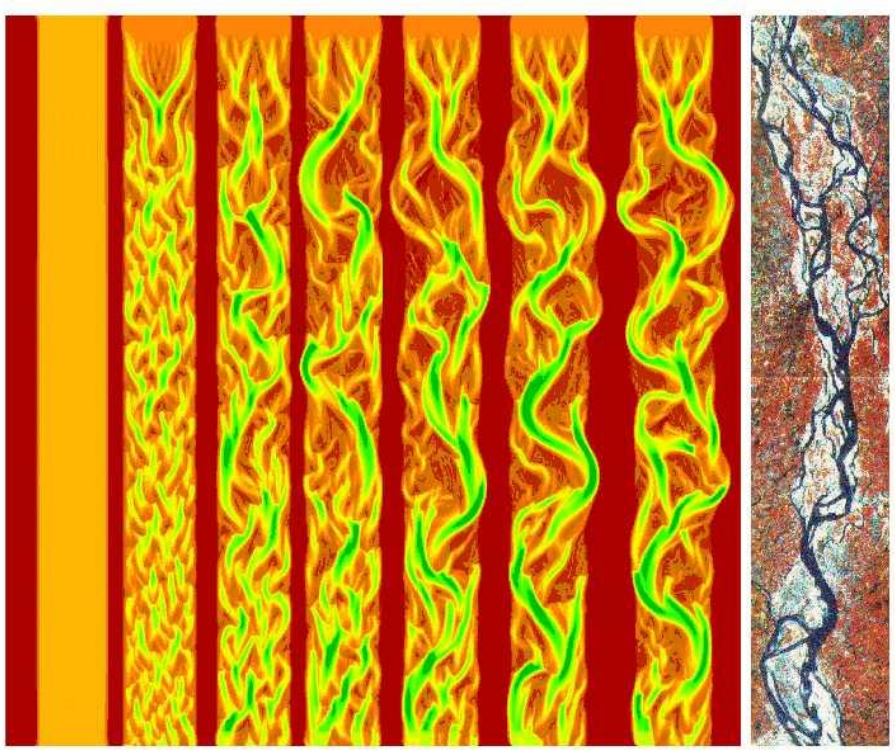

Figure 6.1 The long-term simulations of braiding were carried out with MIKE 21C. The model is capable of reproducing the chaotic behaviour of a braided river

Herein is described the principles that should be followed when using the module. The individual parameters are described in detail. The theoretical background for the grid generator is given in Chapter 1, and is not covered here.

6.1 Introduction

The Planform module (see Figure 6.2) of MIKE 21C has two elements:

- A bank erosion model
- A link to the MIKE 21C grid generator

In the bank erosion model the user specifies how many eroding banks are in the model. If there are no eroding banks, the specifications for the eroding banks as well as the update of the grid are not selectable.

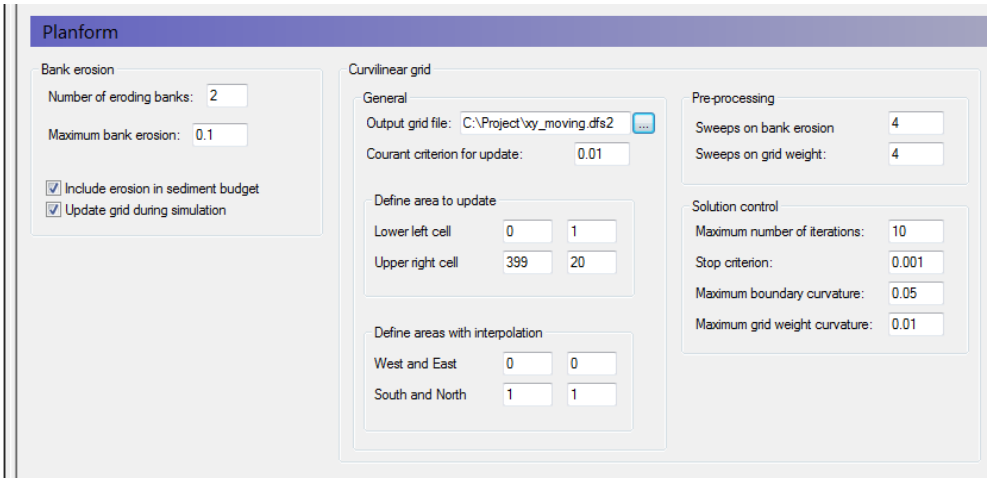

Figure 6.2 The dialogue window associated with the Planform module

The same “subroutine” (located in the dynamic link library “M21C_GridUpd.dll”) performs the generation of the grid in the grid generator and the update of the grid in the planform module of MIKE 21C. It is therefore strongly recommended to use the same key parameters for the generation of the grid and for the update of it. The stop criterion, boundary smoothness and weight smoothness should be the same, otherwise too large changes will occur in the grid during the first few updates. It is noted that the maximum number of iterations do not have to be as high as for the initial generation of the grid in the grid generator. The changes to the grid are usually very small and 10-20 iterations with the grid generator should normally capture the changes.

The update of the grid is designed to be able to capture moderate changes to the planform caused by bank erosion. It is not designed to handle things like occurrence of new channels, bifurcations etc. The module is basically designed to be able to account for bank line changes that can be represented with the same topology, as for the original grid.

6.2 Bank Erosion Model

The bank erosion model implemented in MIKE 21C uses the following model expression for the bank erosion rate [m/s]:

$$E = -\alpha \frac{\partial z}{\partial t} + \beta \frac{q_s}{h} + \gamma \tag{6.1}$$

Where separate values of the parameters α, β and γ can be specified for each eroding bank.

The α -term stems from the link between scour and bank erosion. In sandy rivers, it is often found that the transverse slope of an eroding bank remains constant when the bank line erodes. This means that the bank erosion and scour are directly proportional. The value of α is theoretically the transverse slope (1:α), but it should be calibrated for the particular application.

The β-term expresses that a certain fraction (β) of the sediment transport capacity is used for transporting the material eroded from a bank.

The γ-term is simply a constant bank erosion rate [m/s] that can be specified.

6.2.1 Specification of eroding banks

The eroding bank must be defined as a series of cells that all have the same j-value or the same k-value, i.e. a grid oriented line. The eroding bank cannot have both the same j-value and the same k-value (point).

All cells on one side of the line must be true land cells; this determines the orientation of bank erosion, and the direction of movement of the bank line. At least one cell on the other side of the line must have bed level below true land. It is allowed to let a bank line pass through an area with true land both in the line that is defined, and on both sides.

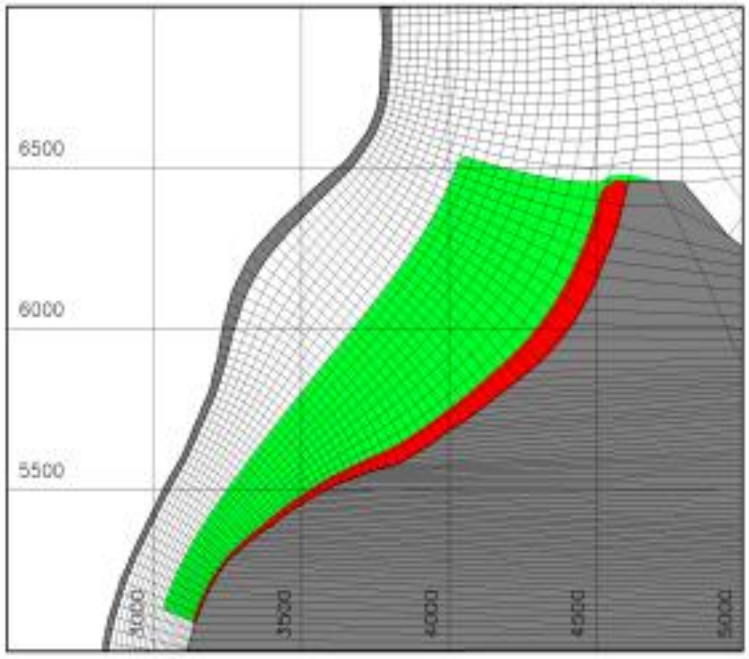

Figure 6.3 Specification of a series of cells that form an eroding bank (red). The series of cells go along a line that has true land. The example is from the Chaktomuk project (CPMU/DHI/Haecon NV, January 2002), and in that project the green part (including the red part) of the grid was updated during the simulation to account for the movement of the indicated bank line

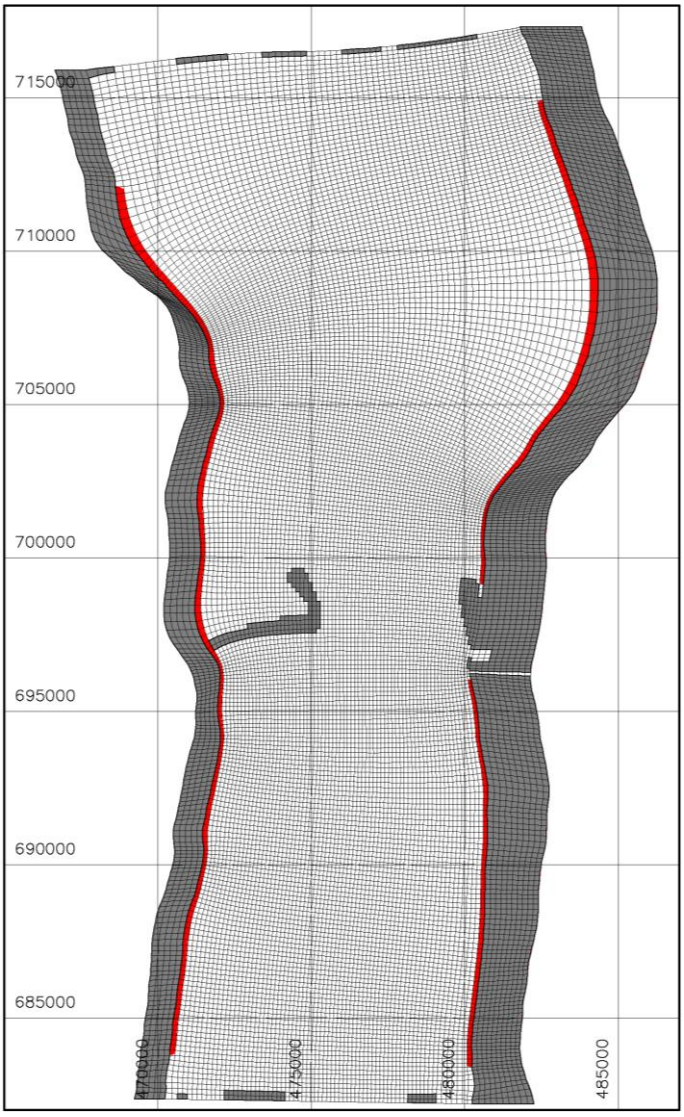

Figure 6.4 Specification of eroding banks (red cells) for the Jamuna Bridge model, DHI/SWMC (October 1999). The western bank is specified so it goes through the cross-dam of the bridge, which is accepted because the model can still identify the direction of erosion from the other cells. On the eastern bank the eroding bank has to be divided into two because of the work harbour. The whole internal part of the grid (all cells that are not dark) was updated for this project. Bank erosion in Jamuna River is substantial, typically up to 500-1000 meters during a monsoon season

6.2.2 Inclusion of erosion products

The inclusion of erosion products means that the erosion of the riverbank will supply sediment to the riverbed. In MIKE 21C calculating the sediment volume that is released when the bank is eroded is found from:

$$Volume = E(h + \Delta h)\Delta t \Delta s \tag{6.2}$$

Please note that here the porosity should not be taken into account, as the sediment comes from the riverbank, and not the water. The corresponding volume change on the riverbed is calculated from:

$$Volume = \Delta z \Delta s \Delta n \tag{6.3}$$

So we find that the bed level change in the cell adjacent to the eroding bank becomes:

$$\Delta z = \frac{E(h + \Delta h)\Delta t}{\Delta s} \tag{6.4}$$

Where

Δz	Change to the bed level due to the erosion products
Δt	Morphological time-step
E	Bank erosion rate [m/s]
h	Water depth in cell adjacent to the riverbank
Δh	Bank height above water, specified by the user
Δs	Length of cell adjacent to the eroding bank

The bank height above the water should be specified for each eroding bank to account for the fact that erosion usually releases more sediment onto the riverbed than the water depth would imply.

By default MIKE 21C will assume that eroding banks feeding sediment to the riverbed through the inclusion of erosion products will contain 100% sandy material with the same properties as the sand on the riverbed. Jamuna River in Bangladesh has such characteristics, and the inclusion of erosion products in the sediment budget is of paramount importance for the behaviour of this river.

Some sandy rivers have cohesive banks, which is quite often encountered in Europe. For such rivers one should not include erosion products, as the cohesive material that is eroded from the riverbank simply adds to the wash-load of the river, which does not participate in the morphological development. The eroded sediment should not be included in the sediment budget for a river with cohesive banks.

6.2.3 Fraction of sand in eroding bank

Some rivers have banks that are partly cohesive and partly sandy. For such riverbanks the “Bank_Fraction” option can be used for specifying that a certain fraction of the bank material is sandy, with the same properties as the sand on the riverbed. A riverbank that is composed of a mixture of sandy and cohesive material can be modelled by using this option.

6.2.4 Hints from the expert users

The following hints are given with respect to the bank erosion model:

- Avoid specifying eroding banks that come too close to the open boundaries. Bank erosion and its feedback to the hydrodynamics can cause problems at the open boundaries, especially when coupled with updating of the grid. If there is a lot of erosion on a riverbank that is close to your open boundary, you should consider moving the open boundary, if the erosion is important.
- The constant erosion should not be used for practical projects. It is mostly for testing purposes.

- The bank erosion model must be calibrated to match observed bank erosion rates. Bank erosion can be obtained from satellite imagery, aerial photographs, bathymetry data, maps etc. In some cases there are no firm data. Local observations from people living where bank erosion takes place can sometimes be the most important source.
- The α-term will usually be dominating in rivers with sandy banks. In that case use the bank slope as the initial estimate for the α-parameter. An α-value that lies very far from the bank slope should give rise to concern. Expect some deviation, but at least the value should be in the right order of magnitude.
- Likewise with the β-value. In the expression lies that a certain fraction of the transport capacity is allocated for erosion products, so a β-value that lies above unity should give rise to concern.
- Limit your application of bank erosion to banks where you are absolutely certain that erosion takes place, and where it is essential.

6.3 Automatic Updating of the Grid during Simulations

The updating of the grid during the simulation is handled by calling a “subroutine” located in a dynamic link library belonging to the MIKE 21C grid generator. It is the same subroutine that updates the grid in the m21gg grid generator.

Updating of the grid is essentially a matter of generating a grid based on an existing grid (“hot-start”) to account for the slow changes that are associated with bank erosion.

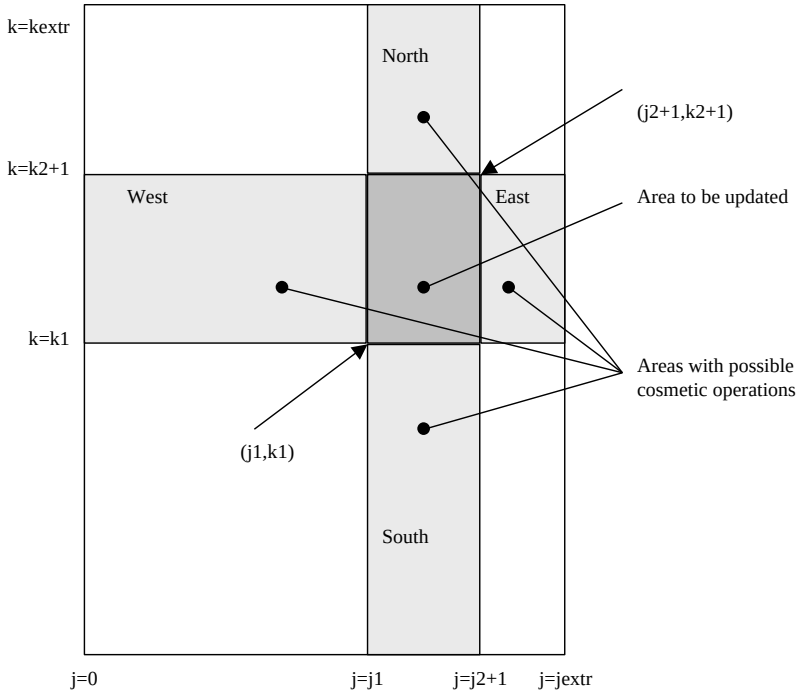

Figure 6.5 The specification of the local part of the grid to be updated and the up to four cosmetic areas around the grid

6.3.1 Definition of the local curvilinear grid

The Planform module is designed to be able to handle updating of a local part of the curvilinear grid. The first thing the user should do is to define this local part of the grid. The local part must be chosen such that the eroding banks are boundary lines in the local grid. Only by doing this can you ensure that the erosion on your banks will be accounted for in the grid.

Two cell coordinates define the local grid:

Lower left cell	(j_1,k_1)
Upper right cell	(j_2,k_2)

These are cell centre coordinates; i.e. refers to cells in the bathymetry. Remember that the grid coordinates are cell vertex allocated. The corresponding vertex coordinates can be calculated from

Lower left vertex	(j_1,k_1)
Upper right vertex	(j_2+1,k_2+1)

Example: For the Jamuna River model the whole grid except the two layers of land cells is to be updated. The Jamuna bathymetry is 0-233x0-84 in size. There are 5 land cells on the western bank and 10 land cells on the eastern. The local part of the grid to be updated will hence be:

Lower left cell	(0,5)
Upper right cell	(233,74)

6.3.2 Cosmetic issues

The update of the local part of the grid can cause the grid points in that part to migrate into the neighbouring areas due to bank erosion. The definition of areas with interpolation or extrapolation has been added to combat this. Note that it is purely cosmetic, but important for graphical presentation.

Up to four cosmetic areas can be defined, one in each direction from the local part that is updated. The areas are defined by an amount of cells in each direction from the local part, see also Figure 6.5.

The way this works is that the specified areas will be subjected to either interpolation or extrapolation.

If only one cell is specified, the area will be extrapolated. This is equivalent to extrapolation of one layer of land cells in the grid generator. This will be used in cases where one has a layer of land cells at a bank and needs to keep recalculating these, as the bank erodes.

If more than one layer of cells is specified, the model will interpolate the grid points in the specified area by using transfinite interpolation, see e.g. Thompson et al (1985). This was employed in the Jamuna Bridge model where the land cells around the main model were interpolated so the cells in those layers did not interfere with the main model area.

Example: For the Jamuna Bridge model there was a layer of 5 land cells at the western bank and 10 land cells at the eastern bank. The specifications for this model were:

Cells west and east:	(0,0)
Cells south and north:	(5,10)

The orientation of the Jamuna model was such that the topological south boundary was at the western bank, and the topological north boundary at the eastern bank.

6.3.3 Land cells in the local grid

Land cells are allowed in the local grid to be updated during a simulation. By default the model will freeze these land points in the grid generation process. This can be changed by the following setting in the pfs file, under the Planform section:

Freeze_Internal_True_Land = false

It is recommended to freeze internal true land, as internal true land will usually represent structures in the model area, and these do not move.

The model handles fixed land points the same way that the grid generator does, but it cannot yet update the grid weight during the grid generation process. This will usually not cause problems because the grid weight is updated each time the grid is updated anyway in the planform module.

6.3.4 The Courant criterion for updating the grid

The automatic update procedure for the grid operates on the largest time-scale in the model, i.e. the planform time-scale. Therefore it is not necessary to perform the update on every morphological time-step. At each morphological time-step the model will evaluate whether it is necessary to update the curvilinear grid. Comparing the accumulated bank erosion to the width of each cell at the eroding bank does this. A Courant number is calculated for the accumulated bank erosion:

$$Courant = \frac{\Delta b_i}{\Delta n_i} \tag{6.5}$$

Here Δb_i denotes the accumulated bank erosion in the cell and Δn_i the transverse width of the cell. The Courant number hence expressed how much the grid vertex point is going to move relative to the grid spacing. It is not allowed to move the grid vertex more than the transverse grid spacing, i.e. the Courant number should be below unity. The use of a Courant criterion here is an excellent way of achieving the optimal performance from the automatic grid updating procedure. As long as the bank erosion is small relative to the grid spacing, there will be no need for updating the grid.

The default value of the Courant criterion is 0.01. It is not recommended to use values larger than 0.1 for this criterion and too small values will waste a lot of time updating a grid that really does not need to be updated, as the accumulated changes to the grid are very small. The use of a Courant criterion is a full exploitation of the fact that the update of the grid takes place on the largest time-scale in the system, and still has to be handled

dynamically. The procedure adapts fully to the speed at which planform changes take place.

6.3.5 Pre-processing of the grid

Some pre-processing is carried out before the grid is passed to the grid generator. Two smoothing parameters are used for this:

- Sweeps on bank erosion
- Sweeps on grid weight

The sweeps on bank erosion simply means that the accumulated bank erosion since the last time the grid was updated will be subjected to a number of running-average sweeps, i.e.

$$b_i^{new} = \frac{b_{i-1} + b_i + b_{i+1}}{3} \tag{6.6}$$

This is subjected to restrictions in the form that fixed boundary points remain fixed. The smoothing pre-processing is not crucial. It is there to avoid irregularities that can arise due to the fast variations in the bank erosion rate. The limit on bank erosion (m/day) is also an important factor here, and probably more important than the filtering.

The procedure is the same for the grid weight, though the grid weight is a 2D field, i.e.

$$q_{i,j}^{new} = \frac{q_{i,j} + q_{i+1,j} + q_{i-1,j} + q_{i,j+1} + q_{i,j-1}}{5} \tag{6.7}$$

Again it is not crucial to perform this smoothing. It just adds extra security, which is good to have when performing an automated update of a curvilinear grid, which is not a straightforward procedure.

6.3.6 Arguments passed to the grid generator

The following parameters are passed to the grid generator:

- **Maximum number of iterations**. Exactly the same as is used in the grid generator. The default is 10 iterations, which is usually enough when the grid is to be updated to account for small changes.
- **Stop Criterion**. Exactly the same as used under the grid generator.
- **Maximum boundary curvature**. Also the same parameter as in the grid generator. It is strongly recommended to use exactly the same value as you did when the initial grid was generated.
- **Maximum grid weight curvature**. Also the same.

These parameters are also described in the scientific background for the grid generator.

6.3.7 Interpolation of the bathymetry when the grid moves

The updating of the grid means that the curvilinear coordinate system moves in the horizontal direction. The model bathymetry is a bed level value given in each computational cell. The cells will move when the grid is updated, and hence there will be a need for changing the bathymetry accordingly.

The updating of the bathymetry is handled automatically, but the user can deactivate the procedure by changing the pfs file in a text editor. The flag that signals the update of the bathymetry is simply not available in the GUI for MIKE 21C.

The bathymetry in MIKE 21C is an array with a value in each cell centre. The coordinates of the cell centres are changed when the grid is updated, and hence an error will be introduced into the representation of the topography in the model. To counteract this it is necessary to move the bathymetry in the opposite direction of the curvilinear cell centres when the grid is updated. The movement of the bathymetry is described by the following pure convection equation

$$\frac{\partial z}{\partial t} - \frac{dx}{dt}\frac{\partial z}{\partial x} - \frac{dy}{dt}\frac{\partial z}{\partial y} = 0 \tag{6.8}$$

The velocity field in this convection equation is the negative of the grid movement velocity field that is given by the change in coordinate relative to change in time, i.e.

$$\left(\frac{dx}{dt}; \frac{dy}{dt}\right) \tag{6.9}$$

The equation is further elaborated into a form without the time-step appearing:

$$\Delta z - \Delta x \frac{\partial z}{\partial x} - \Delta y \frac{\partial z}{\partial y} = 0 \tag{6.10}$$

What is stated now is that the local bathymetry changes according to how much the grid cells move and the gradient of the bathymetry, i.e. simple convection in the opposite direction of the grid.

Using a Second Order Upwind (SOU) scheme now solves this convection equation. The boundary condition is zero flux on all boundaries. If there is a convecting velocity at a boundary, it means that the boundary is moving, i.e. erosion takes place. The boundary conditions means that the bed level at the eroding bank will be assumed to also apply for the area into which the bank is moving. In other words the erosion is assumed to create a river channel with the same bed level as that adjacent to the eroding bank. In case there is no grid velocity at the eroding bank, the boundary condition really becomes irrelevant. The grid does not move in this case, and therefore the bathymetry will not change either.

6.3.8 Hints from the expert users

- Always use the same parameters for the update of the grid that you used when it was generated. If you apply very different values, i.e. demand a much smoother boundary for the grid, you will trigger large changes in the grid during the first update. This will cause problems for the procedure that performs interpolation of the bathymetry from the old to the new grid. Only the maximum number of iterations should be different, and preferably lower than when you generated the grid.

The automatic grid generation process is designed to be able to account for changes in the grid, which are not associated with completely new developments. In technical terms the procedure requires that the topology of the grid is unchanged, i.e. the fundamental structure of the geometry is unchanged due to the planform changes. The model cannot yet handle things like creation of new channels etc.

7 References

/1/ Ackers, P., and White, W. R. (1973). “Sediment transport: new approach and analysis,” Journal of Hydraulics Division, American Society of Civil Engineers, Vol. 99, No. HY11, pp. 2040-2060.

/2/ Bendegom, L. van (1947), “Some considerations on River Morphology and River Improvement”, De Ingenieur, 59, no. 4, p. B1-11

/3/ Booij, R. and Kalkwijk, J.P.T. (1982), “Secondary Flow in estuaries due to the curvature of the main flow and to the rotation of the earth and its development”, Report 9-82, Lab. Of Fluid Mech., Dep. Of Civil Eng., Delft Univ. of tech, Delft

/4/ Engelund, F. (1974), “Flow and bed topography in channel bends”, J.Hyd.Div, ASCE, Vol.100, no.HY11

/5/ Engelund, F. and Hansen, E. (1967), “A monographh on sediment transport in alluvial streams”, Teknisk Forlag, Danish Technological University, Copenhagen, Denmark

/6/ Engelund, F. and Fredsøe, J. (1976), “A sediment transport model for straight alluvial channels”, Nordic Hydrology, Vol. 7, no. 5

/7/ Fredsøe, J. (1979), “Unsteady flow in straight alluvial streams: Modifications of individual dunes”, J. Fluid. Mech., Vol.91, pp 497-512

/8/ Fredsøe, J. (1978), ”Sedimentation of River navigation channels”, J. Hyd. Div., ASCE, Hy2, February, pp.223-236

/9/ Fredsøe, J. (1978), “Meandering and Braiding of rivers”, J. Fluid Mech. Vol. 84, Part 4

/10/ Galappatti, R. (1983),”A depth-integrated model for suspended transport”, Report no. 83-7, comm. On hydraulics, Dept. of Civil Engineering, Delft Univ. of Technology

/11/ Galappatti, R. and Vreugdenhill, C.B. (1985), “A depth-integrated model for suspended transport”, Jour. Of Hyd. Research, Vol. 23, no. 4

/12/ Garcia, M., and G. Parker (1991) “Entrainment of bed sediment into suspension”, Journal of Hydraulic Engineering, 117(4): 414-435

/13/ Guy, H:P, Simons, D.B. and Richardson, E.V. (1966) "Summary of alluvial channel data from flume experiments, 1956-1966", U.S. Geological Survey Professional Paper 462-I, Washington D.C

/14/ Hickin, E.J, Nanson, G.C. (1984), “Lateral migration rates of river bends”, J. Hyd. Eng., ASCE, Vol. 110, no.11

/15/ Ikeda, S. (1980),”Incipient motion of sand particles on slopes”, Rep. Of Found. Eng. & Constr. Eng., Saitama Univ., Japan

/16/ Jansen, P.H., van Bendegom, L., van den Berg, J., de Vries, M., and Zanen, A. (1979), “Principles of River Engineering”, Pitman Publishing

/17/ Kalkwijk, J. P. T., and Booij, R. (1986), “Adaptation of secondary flow to nearly horizontal flow”, J. Hyd. Res, 24, no1. P18

/18/ Kalkwijk, J. P. Th, and de Vriend, H. J. (1980), “Computation of the flow in shallow river bends”, J. Hyd. Res., 18, no.4, p327

/19/ Kikkawa, H., Ikeda, J., and Kitagawa, A. (1976), “Flow and bed topography in curved open channels”, J. Hyd. Div., ASCE, Vol.102, No. HY9

/20/ Klaassen, G. J, Mosselman, E., Masselink, G., Brühl, H., Huisink, M., Koomen, E., Seymonsbergen, A.C. (1993), “Planform changes in large braided sand-bed rivers”, Delft Hydraulics, Publ. No. 480, Dec. 1993

/21/ Klaassen, G. J, Masselink, G. (1992), “Planform changes of a braided river with fine sand as bed and bank material, 5. Int. Symposium on River Sedimentation, April 1992, Karlsruhe, Germany

/22/ Koch, F.G. (1980), “Bed level computation for axis-symmetric curved channels”, Rep. R567-1X/W308 part1, Delft Hyd. Lab.

/23/ Lane, E.W. (1953), “Progress report on studies on the design of stable channels by the Bureau of Reclamation”, Proc. ASCE, Irr. And Drain, Div., Vol. 79

/24/ Lane, E.W and Kalinske, A.A. (1941) “Engineering calculations of References suspended sediment”, Trans.Am.Geophys.Union, vol.22, pp. 603-607.

/25/ Lane, E. W., and Kalinske, A.A. (1939) "The relation of suspended to bed material in rivers." Eos, Transactions American Geophysical Union 20.4 (1939): 637-641.

/26/ Luque, R. F. and van Beek, R. (1976), "Erosion and transport of bed-load sediment", Journal of Hydraulic Research, Vol. 14, No. 2, pp. 127-144.

/27/ Majumdar, S., Rodi, W., Zhu, J. (1992) “Three-dimensional finite-volume method for incompressible flows with complex boundaries”, Journal of Fluids Engineering, Vol. 114, pp 496-

/28/ Meyer-Peter, E. and Müller, R. (1948),”Formulas for bed load transport”, Proc. 2nd Congr. IAHR, Stockholm, Vol.2, paper 2

/29/ Michelsen, J.A. (1989), “Solution of the Navier-Stokes equations on general non-orthogonal meshes”, FTU/STVF pr J.nr. 95 83 02, Department of Fluid Mechanics, Technical University of Denmark, pp 1-45.

/30/ MIKE 21 Coastal Hydraulics and Oceanography, Hydrodynamic Module, Release 2.5, Users Guide and Reference Manual, Danish Hydraulic Institute (1995)

/31/ Mosselman, E. (1992), ”Mathematical modelling of morphological processes in rivers with erodible cohesive banks”, Comm. on Hydr. and Geotec. Eng., no.92-3, Delft University of Technology

/32/ Nouh, M.A. and Townsend, R.D. (1979), ”Shear stress distribution in stable channel bends”, Proc. ASCE, J. Hyd. Div., 105,HY10

/33/ Odgaard, A.J. (1981), “Transverse bed slope in alluvial channel bends”, J. Hyd. Div, ASCE, Vol.107, No.HY12

/34/ Olesen, K.W. (1987), “Bed topography in shallow river bends”, Faculty of Civil. Eng., Delft Univ. of Tech, Report 87-1

/35/ Parker, G. (1983), “Theory of meander bend deformation”, Proc. ASCE Conf. Rivers ’83, New Orleans

/36/ Patankar, S.V. (1980), “Numerical Heat Transfer and Fluid Flow”, McGraw-Hill.

/37/ Rijn, L. C. van (1984), “Part I: Bed load transport”, J. Hyd. Eng., 110, October, “Part II: Suspended load transport”, J. Hyd. Eng., 110, November

/38/ Rozovskii, I.L. (1957), “Flow of water in bends of open channels”, English translation: Israel Progr. For Scientific Transl. Jerusalem, 1961

/39/ Smart, G. M. and Jaeggi, M. N. R. (1983), "Sediment Transport on Steep Slopes", Mitteilung nr. 64 of the Laboratory for Hydraulics, Hydrology and Glaciology at the Federal Technical University, Zurich

/40/ Stone, H.L. (1968), “Iterative solution of implicit approximations of multidimensional partial differential equations”, SIAM Journal Num. Analysis, Vol. 5, No 3, pp 530-559.

/41/ Struiksma, N., Olesen, K.W., Flokstra, C., and de Vriend, H.J. (1985), “Bed deformation in curved alluvial channels”, J. of Hyd. Res., Vol. 23, No.1

/42/ Talmon, A.M. (1992), “Bed topography of river bends with suspended sediment transport”, Ph.D. Thesis, Delft Univ. of Tech.

/43/ Talmon, A.M., Struiksma, N. and van Mierlo, M.C.L.M. (1995), “Laboratory measurements of the direction of sediment transport on transverse alluvial bed slopes”, J. Hyd. Res., Vol.33, no4, 1995

/44/ Thompson, J.F., Warsi, Z.U.A. & Mastin, C.W. (1985) “Numerical Grid Generation - Foundations and Applications”, North-Holland.

/45/ Vanoni, Vito A. (1953) "A summary of sediment transportation mechanics.", 129-160.

/46/ Vanoni, V.A. (1975), “Sedimentation Engineering”, ASCE manuals and reports on engineering practice, No. 54, New York

/47/ Vanoni, V.A. (1984), “Fifty Years of Sedimentation”, J. Hyd. Eng. ASCE, Vol. 110, no. 8

/48/ Vriend, H. J. de (1981), “Steady flow in shallow channel bends”, comm. on Hydraulics 81-3, Dept. of Civil. Eng., Delft Univ. of Tech.

/49/ Vriend, H. J. de and Struiksma, N. (1983), “Flow and bed deformation in river bends”, Proc. ASCE Conference Rivers ’83, New Orleans, p. 810

/50/ Wilcock, P. R., & Crowe, J. C. (2003). Surface-based transport model for mixed-size sediment. Journal of Hydraulic Engineering, 129(2), 120-128.

/51/ Yang, C. T. (1983), "Rate of Energy Dissipation and River Sedimentation", 2nd International Symposium on River Sedimentation, Nanjing, China, pp. 575-585.

/52/ Yang, C. T. (1984), "Unit Stream Power Equation for Gravel", Journal of Hydraulic Division, ASCE, 110 (HY12), pp. 1783-1798

/53/ Zyserman, J.A. and Fredsøe, J. (1994) "Data analysis of bed concentration of suspended sediment", Journal of Hydraulic Engineering, ASCE, Vol. 120, No. 9, pp. 1021-1042